QUANTIFYING GRASSLAND NON-PHOTOSYNTHETIC VEGETATION BIOMASS USING REMOTE SENSING DATA

A Thesis Submitted to the College of
Graduate and Postdoctoral Studies
In Partial Fulfillment of the Requirements
For the Degree of Doctor of Philosophy
In the Department of Geography and Planning
University of Saskatchewan
Saskatoon, Canada

By

Zhaoqin Li

PERMISSION TO USE

In presenting this thesis in partial fulfillment of the requirements for a Postgraduate degree from the University of Saskatchewan, I agree that the Libraries of this University may make it freely available for inspection. I further agree that permission for copying of this thesis in any manner, in whole or in part, for scholarly purposes may be granted by the professor or professors who supervised my thesis work or, in their absence, by the Head of the Department or the Dean of the College in which my thesis work was done. It is understood that any copying or publication of use of this thesis or parts thereof for financial gain shall not be allowed without my written permission. It is also understood that due recognition shall be given to me and to the University of Saskatchewan in any scholarly use which may be made of any material in my thesis.

Requests for permission to copy or make to other use of material in this thesis in whole or part should be addressed to:

Head of the Department of Geography and Planning
117 Science Place
University of Saskatchewan
Saskatoon, Saskatchewan S7N5C8
Canada

OR

Dean
College of Graduate and Postdoctoral Studies
University of Saskatchewan
105 Administration Place
Saskatoon, Saskatchewan S7N 5A2
Canada

ABSTRACT

Non-photosynthetic vegetation (NPV) refers to vegetation that cannot perform a photosynthetic function. NPV, including standing dead vegetation and surface plant litter, plays a vital role in maintaining ecosystem function through controlling carbon, water and nutrient uptake as well as natural fire frequency and intensity in diverse ecosystems such as forest, savannah, wetland, cropland, and grassland. Due to its ecological importance, NPV has been selected as an indicator of grassland ecosystem health by the Alberta Public Lands Administration in Canada. The ecological importance of NPV has driven considerable research on quantifying NPV biomass with remote sensing approaches in various ecosystems. Although remote images, especially hyperspectral images, have demonstrated potential for use in NPV estimation, there has not been a way to quantify NPV biomass in semiarid grasslands where NPV biomass is affected by green vegetation (PV), bare soil and biological soil crust (BSC). The purpose of this research is to find a solution to quantitatively estimate NPV biomass with remote sensing approaches in semiarid mixed grasslands. Research was conducted in Grasslands National Park (GNP), a parcel of semiarid mixed prairie grassland in southern Saskatchewan, Canada. Multispectral images, including newly operational Landsat 8 Operational Land Imager (OLI) and Sentinel-2A Multi-spectral Instrument (MSI) images and fine Quad-pol Radarsat-2 images were used for estimating NPV biomass in early, middle, and peak growing seasons via a simple linear regression approach. The results indicate that multispectral Landsat 8 OLI and Sentinel-2A MSI have potential to quantify NPV biomass in peak and early senescence growing seasons. Radarsat-2 can also provide a solution for NPV biomass estimation. However, the performance of Radarsat-2 images is greatly affected by incidence angle of the image acquisition. This research filled a critical gap in applying remote sensing approaches to quantify NPV biomass in grassland ecosystems. NPV biomass estimates and approaches for estimating NPV biomass will contribute to grassland ecosystem health assessment (EHA) and natural resource (i.e. land, soil, water, plant, and animal) management.

Keywords: *non-photosynthetic vegetation, biomass, green vegetation, biological soil crust, bare soil, multispectral image, Landsat 8, Sentinel-2A, Radarsat-2, ecosystem health, vegetation phenology*

ACKNOWLEDGEMENTS

First of all, I would like to thank my supervisor, Dr. Xulin Guo, for her invaluable mentoring and encouragement during my Ph.D. study. Her constant guidance and support have been indispensable to the completion of my dissertation. I would also like to express my gratitude to my advisory committee members, Dr. Bram Noble, Dr. Dirk deBoer, and Dr. Longhai Li for their valuable comments on this research. I also want to thank Dr. Abraham Akkerman, who served as my committee chair, for his valuable assistance.

I would like to acknowledge the Natural Sciences and Engineering Research Council of Canada (NSERC), the Department of Geography and Planning, University of Saskatchewan, the Saskatchewan Innovation & Opportunity Graduate Scholarship, the Saskatchewan Environment Ministry, and the Canadian Federation of University Women (CFUW) Saskatoon Inc. for providing funding to support my study and life.

My gratitude goes to Mr. Adam Harrison, Dr. Eric Lamb, and Dr. Cherie Westbrook for providing facilities for drying my samples. Many thanks are also given to Dr. Xiaohui Yang, Dr. Dandan Xu, Carmen Finnigan and other field crew members for collecting some of the field data, and to the staff in Grasslands National Park (GNP) for their logistical support. I would like to thank MacDonald Dettwiler and Associates Ltd. - Geospatial Services Inc. (MDA GSI), the Canadian Space Agency (CSA), and Natural Resources Canada's Centre for Remote Sensing (CCRS) for providing Radarsat-2 data. Thank you to the United States Geological Survey (USGS) for distributing Landsat 8 and Sentinel-2A images and Advanced Spaceborne Thermal Emission and Reflection Radiometer (ASTER) Global Digital Elevation (GDEM) data. ASTER GDEM data are a product of the Ministry of Economy, Trade, and Industry (METI) of Japan and the United States National Aeronautics and Space Administration (NASA). I also want to thank the European Space Agency (ESA) for providing free software for processing Sentinel-2A images.

Finally, I would like to thank my colleagues and visiting professors in Dr. Guo's research group for their comments on my research and their help with field work. Special thanks are given to my husband (Dr. Zimu Yu) and my daughters (Hope and Frieda) for their unconditional love.

TABLE OF CONTENTS

LIST OF FIGURES

LIST OF TABLES

LIST OF ABBREVIATIONS

ALOS PALSAR	Array L-Band Synthetic Aperture Radar on Japan's Advanced Land Observing Satellite
BSC	Biological Soil Crust
MSAVI	Modified Soil-Adjusted Vegetation Index
$NDVI_{705}$	Red Edge Normalized Difference Vegetation Index
PAR	Photosynthetically Active Radiation
REP	Red Edge Position
AirSAR	Airborne Synthetic Aperture Radar
ALI	Advanced Land Imager
ASTER	Advanced Multispectral Sensor
ASTER	Advanced Spaceborne Thermal Emission and Reflection Radiometer
ATSAVI	Adjusted Transformed Soil-Adjusted Vegetation Index
AVHRR	Advanced Very High Resolution Radiometer
AVIRIS	Airborne Visible Infrared Imaging Spectrometer
BRDF	Bi-Directional Reflectance Distribution Function
CAI	Cellulose Absorption Index
DEM	Digital Elevation Model
EHA	Ecosystem Health Assessment
ENSO	El Niño/Southern Oscillation
ESA	European Space Agency
ETM+	(Landsat 7) Enhanced Thematic Mapper
EVI	Enhanced Vegetation Index
fAPAR	Fraction of Absorbed Photosynthetically Active Radiation
GDEM V2	Global Digital Elevation Model Version 2
GEOCOMP-n	New Geocoding and Compositing System
GNP	Grasslands National Park
GPP	Gross Primary Production
GPS	Global Positioning System
LCA	Lignocellulose Absorption Area
LCD	Lignocellulose Absorption Depth
LiDAR	Light Detection and Ranging
LUE	Light Use Efficiency
METI	The Ministry of Economy, Trade, and Industry of Japan
MICI	Terrestrial Chlorophyll Index
M-K	Mann-Kendall Test
$mNDVI_{705}$	Modified Red Edge Normalized Difference Vegetation Index
MODIS	Moderate-Resolution Imaging Spectroradiometer
MSACRI	Modified Soil-Adjusted Crop Residue Index

MSAVI	Modified Soil Adjusted Vegetation Index
MSI	Multispectral Instrument
MSS	(Landsat 1-3) Multispectral Scanner
NASA	National Aeronautics and Space Administration (United States)
NDI	Normalized Difference Index
NDII	Normalized Difference Infrared Index
NDSVI	Normalized Difference Senescent Vegetation Index
NDTI	Normalized Difference Tillage Index
NDVI	Normalized Difference Vegetation Index
NIR	Near-Infrared (700-1200 nm)
NOAA	National Oceanic and Atmospheric Administration (United States)
NPP	Net Primary Productivity
NPV	Non-Photosynthetic Vegetation
OLI	(Landsat 8) Operational Land Imager
PSRI	Plant Senescence Reflectance Index
PV	Photosynthetic Vegetation
r^2	Coefficient of Determination
RCM	Radarsat-2 Constellation Mission
RMSE	Root Mean Square Error
RVI	Radar Vegetation Index
SAR	Synthetic Aperture Radar
SATVI	Soil Adjusted Total Vegetation Index
SAVI	Soil Adjusted Vegetation Index
SD	Standard Deviation
SINDRI	Shortwave Infrared Normalized Difference Residue Index
SLC	Single-Look Complex
SMA	Spectral Unmixing Approach
SOC	Soil Organic Carbon
SVH	Spectral Variation Hypothesis
SWIR	Shortwave Infrared (1100-2500 Nm)
TM	Landsat Thematic Mapper
UAV	Unmanned Aerial Vehicle
USGS	United States Geological Survey
VIS	Visible (400-700 Nm)
VOG	Vogelmann Red Edge Index
VOG2	Vogelmann Red Edge Index 2
VOG3	Vogelmann Red Edge Index 3
WV-3 Imager	Worldview-3 Satellite Imager

CHAPTER 1:INTRODUCTION

1.1 Preface

This chapter introduces the ecological importance of non-photosynthetic vegetation (NPV) and summarizes the theory, methods, and research progress on quantifying NPV cover and biomass in diverse ecosystems using optical, radar, Light Detection and Ranging (LiDAR) data and their integration. More importantly, this chapter identifies research gaps evident from the literature and sets up the research hypothesis and objectives. Also, this chapter describes the study area and field data sampling and outlines the structure of this dissertation. Section 1.2 and 1.3 were published as a part of a review paper:

Li Z and Guo X. (2016) Remote sensing of terrestrial non-photosynthetic vegetation using hyperspectral, multispectral, SAR, and LiDAR data. Progress in Physical Geography 40 (2):276-304, *doi*: 10.1177/0309133315582005.

Zhaoqin Li reviewed the literature and wrote this manuscript. Dr. Xulin Guo provided valuable comments that greatly improved the manuscript. Re-use in the dissertation was granted by the Publisher (SAGE; Appendix A).

1.2 Ecological Importance of NPV

The classification of NPV and photosynthetic vegetation (PV) is based on vegetation photosynthetic function perspectives (Guerschman et al., 2009). NPV refers to the vegetation that cannot perform a photosynthetic function. Above-ground standing dead biomass and plant litter at the ground surface make up a large part of NPV. NPV also includes woody stems, below-ground dead biomass and dormant vegetation (Asner, 1998). However, below-ground dead biomass and dormant vegetation are not part of this research. NPV is a significant component of vegetation productivity in grasslands, savannas, shrublands, and dry woodlands (Asner, 1998) as well as wetlands (Schile et al., 2013).

NPV is ecologically important for controlling carbon, water, and nutrient uptake and natural fire frequency and intensity (Nagler et al., 2003; Guerschman et al., 2009), and serving as a wildlife habitat (Davis, 2005; Huang et al., 2009; Fisher and Davis, 2010). The presence of NPV exerts influence on ecosystem functioning by altering macro and micro environments (Figure 1-1). At a macro (or global) scale, NPV is a large carbon pool in natural ecosystems. Because of this, quantifying NPV is important for understanding carbon sequestration, a tool to lower atmospheric CO_2 concentration. Also, NPV as wildfire fuels (Kim et al., 2009; Newnham et al., 2011) has a potential impact on climate, as biomass burning has a substantial contribution to global greenhouse gas, aerosol, and black carbon emissions (Weise and Wright, 2013). Such effects of NPV on climate exert influence on ecosystems globally.

At a micro (or local) scale, the presence of NPV affects plant community structure and biodiversity by altering microenvironments (Facelli and Pickett, 1991). This further exerts influence on ecosystem functionality. NPV affects the transfer of light, heat, and water between the topsoil and the atmosphere. NPV intercepts light, which may negatively influence plant germination (Bonanomi et al., 2009) and seedling recruitment (Galvanek and Leps, 2012). NPV intercepts solar radiation and insulates the soil from air temperature that affects the near surface air and soil temperature (Facelli and Pickett, 1991). NPV-induced soil temperature change may exert direct and indirect effects on plant growth by modifying mineralization rates, and therefore nutrient availability (Facelli and Pickett, 1991). NPV accumulation may also increase soil water availability through trapping snow, reducing evaporation from the soil, decreasing runoff, and improving water infiltration (Guerschman et al., 2009; Donath and Eckstein, 2010; Deutsch et al., 2010; Wang et al., 2011). Thus, NPV may positively enhance productivity in semiarid ecosystems where plant growth is constrained by water availability (Deutsch et al., 2010; Wang et al., 2011). However, under some circumstances, large NPV accumulations may reduce water available to plants through retaining rainfall and reducing infiltration (Facelli and Pickett, 1991), consequently reducing ecosystem production (Jackson et al., 2006). NPV supplies nutritients to the soil (Yin and Huang, 1996; Henry et al., 2008; Hewins et al., 2013) through decomposition, and, in-turn, the amount, variety, and distribution of nutrients largely controls productivity and affects species composition (Eckstein and Donath, 2005; Patrick et al., 2008). Besides its contribution to climate warming agents, NPV as a wildfire fuel (Kim et al., 2009; Newnham et

al., 2011) has a profound influence on productivity and species composition. Finally, the presence of NPV is important for wildlife habitats (Davis, 2005; Huang et al., 2009; Fisher and Davis, 2010).

These factors suggest that NPV is important for the ecological functionality of grasslands (Jensen and Gutekunst, 2003; Rasran et al., 2007; Lamb, 2008; Ruprecht et al., 2010; Ruprecht and Szabo, 2012), savannah (Guerschman et al., 2009), forests (Huang et al., 2009), shrublands and dry woodlands (Asner, 1998), and croplands (Daughtry et al., 1996; Serbin et al., 2013). Accurate quantification of NPV and temporal and spatial variation of NPV is essential for ecosystem management (Guerschman et al., 2009; Serbin et al., 2013).

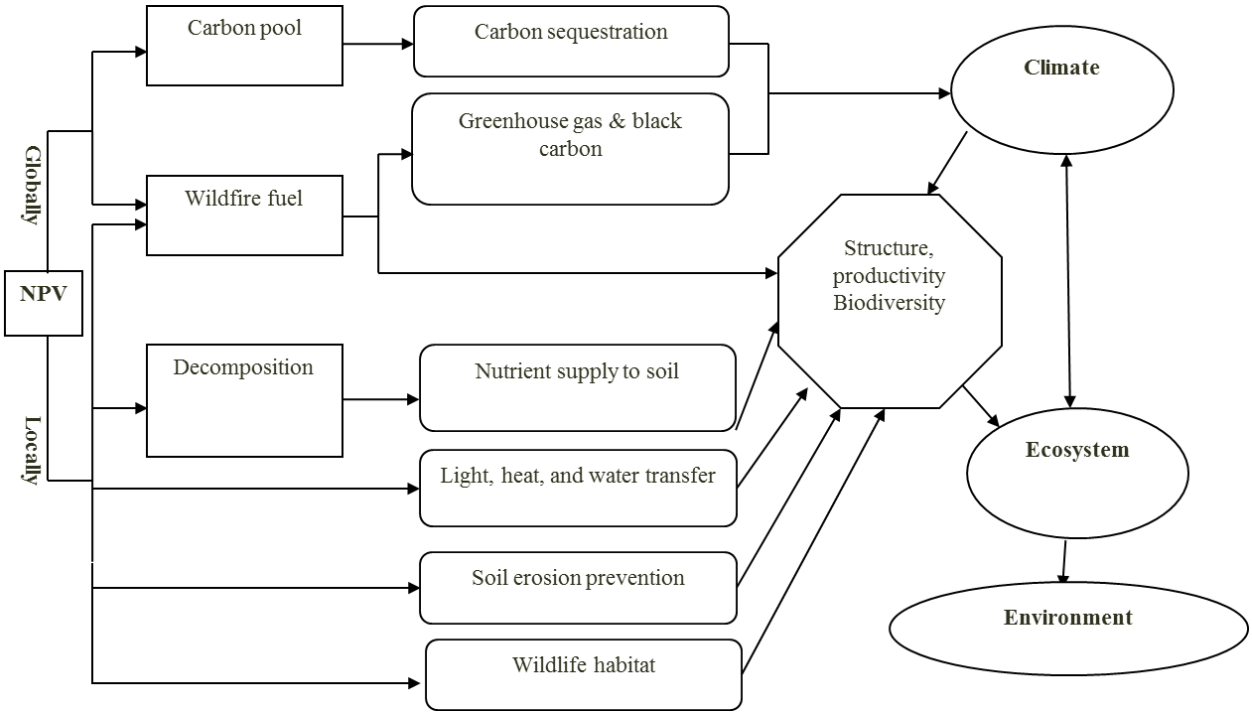

Figure 1-1 Ecological importance of non-photosynthetic vegetation (NPV) at global and local scales.

1.3 Remote Sensing of NPV

The ecological importance of NPV has driven many attempts to quantify it using traditional field sampling methods and remote sensing approaches. Traditional approaches, such as destructive harvesting (White et al., 2000) for NPV biomass and visual interpretation of NPV cover estimation, can provide accurate estimates. However, they are not suitable at large spatial scales due to being labor-intensive and time-consuming (Byrne et al., 2011). The use of remote sensing technology can provide an efficient way to estimate NPV at a range of spatial scales and to monitor spatial and temporal variations in NPV (Serbin et al., 2013).

Remote sensing techniques are grouped into passive and active categories based on energy sources used. Passive remote sensing is limited to collecting electromagnetic energy originating from the sun or the earth. This includes passive optical and passive microwave remote sensing. Passive optical remote sensing, including hyperspectral and multispectral sensors, have been used to study terrestrial ecosystem attributes, including plant vigor (e.g., biomass), organization (vertical structure/leaf area index (LAI), etc.), and resilience (e.g. vegetation response to climate, grazing and burning, etc.). Passive microwave remote sensing is used in meteorology, hydrology, and oceanography. Active remote sensors emit their energy and receive the backscattered energy from the surface. They are represented by Synthetic Aperture Radar (SAR), and Light Detection and Ranging (LiDAR). Similar to optical data, SAR and LiDAR data have demonstrated great potential to quantify ecosystem attributes, especially in forests and croplands.

1.3.1 Passive optical remote sensing data for NPV estimation

1.3.1.1 Theory

Research on NPV estimation has been focused on differentiating NPV from PV and bare soil. In this context, passive optical remote sensing data have greater potential to estimate NPV as NPV has much lower chlorophyll and water content than PV (Asner, 1998; Numata et al., 2008; Serbin et al., 2013), and the high cellulose and lignin content in NPV is absent in bare soil (Asner, 1998; Serbin et al., 2009a). These differences create separation in their spectra (Figure 1-2) that may be used to distinguish NPV from PV and bare soil.

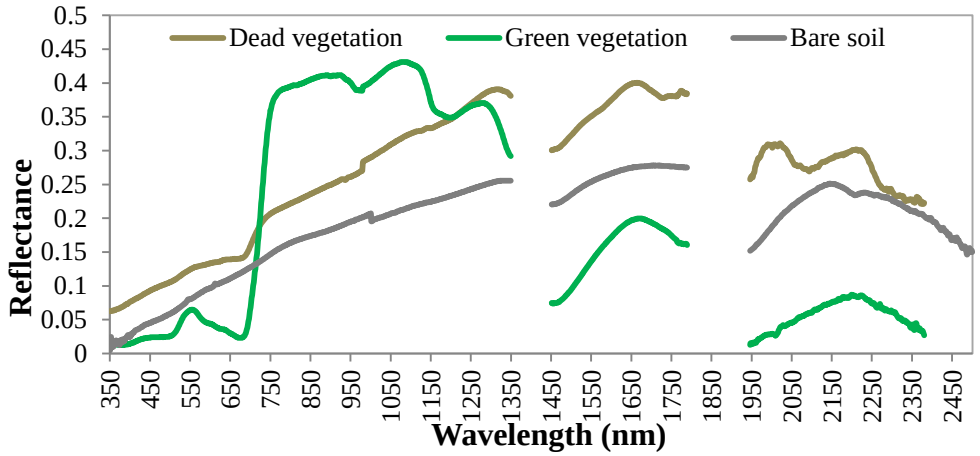

Figure 1-2 Spectral response curves of dead vegetation, green vegetation, and bare soil (samples were collected from Grasslands National Park (GNP), Canada in mid-June of 2004, and their spectra were measured in a laboratory with an ASD Spectroradiometer).

NPV can be separated from PV in the visible (VIS, 400-700 nm) and near-infrared (NIR, 700-1200 nm) wavelength regions because NPV reflectance in the VIS regions is generally higher than PV. This is due to a lack of absorption of pigments (especially chlorophylls a and b) (Asner, 1998; Cao et al., 2010). NPV reflectance is lower than PV in NIR due to the change in leaf structure (Figure 1-2). In the shortwave infrared (SWIR, 1100-2500 nm) region, leaf water content controls the absorption features of PV that blur absorption of cellulose and lignin in PV (Cao et al., 2010). Therefore, the absorption features near 2100 nm and 2300 nm of cellulose and lignin in the spectral range of NPV are usually not evident in the spectral range of PV (Daughtry et al., 2005).

NPV is difficult to separate from soil in VIS and NIR wavelength regions because they have similar featureless spectral reflectance curves (Aase and Tanaka, 1991; Daughtry et al., 1996; Nagler et al., 2000). However, NPV can be distinguished from soil in the SWIR wavelength region due to the unique absorption features of lignin and cellulose at 2090 nm and 2300 nm (Stoner and Baumgardner, 1981; Elvidge, 1990; Asner, 1998; Nagler et al., 2000). These unique absorption features have been used to develop spectral indices, such as the cellulose absorption index (CAI) (Daughtry et al., 1996; Nagler et al., 2000), to distinguish NPV from soil.

The VIS to NIR transition, also called red-edge (680-780 nm), is sensitive to variations in chlorophyll content. The red-edge chlorophyll index has demonstrated better performance than greenness indices, such as the Normalized Difference Vegetation Index (NDVI), for estimating chlorophyll content in semiarid mixed grasslands (Wong and He, 2013), green canopy cover in hyper-arid Atacama Desert (Chavez et al., 2013), and green leaf area index in croplands (Viña et al., 2011). These studies have demonstrated the potential of the red-edge position for identifying PV from NPV using the difference in chlorophyll content and structure. At the red-edge position, the slope of the reflectance spectra of NPV is greater than that in soils. Although the slope at the red-edge position is influenced by moisture conditions and age of NPV (Goward et al., 1994; Daughtry et al., 1996; Nagler et al., 2000), use of red-edge position for NPV estimation is worthy of further investigation.

Overall, the 400 to 2500 nm wavelength region contains sufficient information to separate NPV from PV and bare soil (Asner, 1998). However, the presence of water, soil minerals, and Soil Organic Carbon (SOC) makes distinguishing NPV from soils more difficult. Water content refers to both canopy water and surface soil water which can significantly alter the reflectance spectrum by reducing overall reflectance at all wavelengths (400-2500 nm) as well as broadening the water absorption feature at 1400 and 1900 nm (Nagler et al., 2000; Daughtry and Hunt, 2008). Despite the effects of water on the spectra, NPV could still be distinguished from soils because the cellulose absorption features of the NPV can be detected even in water-dominated spectra (Gao and Goetz, 1994). However, the concavity of the NPV cellulose-lignin absorption feature used for developing CAI becomes shallow in the presence of water (Nagler et al., 2000). Also, SOC and soil minerals affect the spectral absorption features in shortwave regions (Daughtry and Hunt, 2008; Serbin et al., 2009a; Serbin et al., 2009b), and thus increase the difficulty in estimating NPV.

1.3.1.2 Approaches

The approaches used for the NPV estimation using passive optical remote sensing data can be grouped into two categories: 1) empirical spectral indices–NPV cover/biomass relationships and, 2) linear spectral unmixing approach (SMA). The spectral indices for NPV cover estimation were originally developed based on the spectral contrast between NPV, PV, and bare soil. Based

on the spectral resolution of the sensors, the derived spectral indices are classified as hyperspectral and multispectral indices.

Spectral indices. Hyperspectral indices for NPV estimation were developed based on the absorption features of cellulose and lignin in shortwave wavelength regions. These indices include the most commonly used CAI, Lignocellulose Absorption Depth (LCD), and Lignocellulose Absorption Area (LCA). The CAI has demonstrated a strong correlation with NPV cover, including plant litter and crop residue (Serbin et al., 2009c; Cao et al., 2010; Serbin et al., 2013), and it outperformed LCD and LCA in previous studies (Daughtry et al., 2005; Numata et al., 2008; Serbin et al., 2009c; Ren and Zhou, 2012). However, the performance of these lignocellulose-based indices on NPV estimation is greatly affected by the presence of PV and soil minerals. The high water content of PV blurs the absorption features of cellulose and lignin in the shortwave wavelength regions. Research reveals that the CAI performance decreases when the fraction of green vegetation is greater than 30% (Daughtry et al., 2004; Daughtry et al., 2005). Although most common soil minerals will not affect the performance of CAI for crop residue cover estimation, the utility of CAI may be limited in high-cellulose soils (e.g. peat moss) because of the small variation in CAI in residue and soil (Serbin et al., 2009a). Additionally, the usefulness of LCA is constrained by common soil minerals, such as carbonates, epidotes, and chlorites (Serbin et al., 2009a), suggesting that information on soil composition may be beneficial to crop residue cover estimation (Serbin et al., 2009b). Although the effects of green vegetation and soil minerals on the hyperspectral indices developed for NPV estimation, hyperspectral data have a contiguous spectrum covering the 350-2500 nm optical wavelength and contain the most suitable wavelengths for discriminating NPV from bare soil and PV (Numata et al., 2008; Table 1-1). Additionally, Unmanned Aerial Vehicle (UAV) airborne hyperspectral cameras have provided a more recent solution to acquire hyperspectral reflectance.

Table 1-1 Hyperspectral remote sensing data that have been used or have a potential for NPV estimation

Name	Number of bands	Spectral Coverage (nm)	Spatial resolution (m)	Swath width (km)	Example citation	Availability
Airborne Visible InfraRed Imaging Spectrometer (AVIRIS)	224	400-2450	20[a]	10.6[a]	Asner et al., 2003; Asner et al., 2005	http://aviris.jpl.nasa.gov/
EO-1 Hyperion hyperspectral sensor (spaceborne)	220	400-2500	30	7.5 ×100	Roberts et al., 2003; Numata et al., 2008; Guerschman et al., 2009	http://eo1.gsfc.nasa.gov/Technology/Hyperion.html
Probe-1 (airborne)	128	400-2450	1-10	<1 to 6	Bannari et al., 2006	http://www.earthsearch.com/technology/about-probe-1/
Hyperspectral Mapper (HyMap) (airborne)	126	450-2500	3-5	0.13-2.3	potential	http://www.hyvista.com/

Note: [a] AVIRIS has a spatial resolution of 20 m at the nominal ER-2 aircraft altitude of 19.8 km.

Multispectral indices have been developed for Landsat Thematic Mapper (TM), such as the Normalized Difference Tillage Index (NDTI) (Van Deventer et al., 1997), the Normalized Difference Index (NDI) (McNairn and Protz, 1993), and the Normalized Difference Senescent Vegetation Index (NDSVI) (Qi et al., 2002). The NDSVI, based on the ratio between the difference and the sum of SWIR (1650 nm) and red (660 nm) bands, was more sensitive to senescent vegetation than green vegetation and soil (Marsett et al., 2006). To eliminate the soil effect from NDSVI, a soil adjustment factor was introduced to develop the Soil Adjusted Total Vegetation Index (SATVI) (Marsett et al., 2006). SATVI is sensitive to both green and senescent vegetation. However, it does not work when forbs cover more than 30% of the total vegetated area (Marsett et al., 2006). These multiband indices have successfully identified broad crop residue cover classes (McNairn and Protz, 1993; Biard and Baret, 1997; Van Deventer et al., 1997; Qi et al., 2002). Notably, they were less effective when used in agricultural regions with variable soil types (Daughtry et al., 2005) due to poor contrasts between crop residues and many soils (Serbin et al., 2009b), and because these indices were strongly affected by green vegetation (Gill and Phinn, 2008). These multispectral indices were generally inferior to the hyperspectral and spectral indices derived from Advanced Spaceborne Thermal Emission and Reflection Radiometer (ASTER), such as the Shortwave Infrared Normalized Difference Residue Index (SINDRI) (Serbin et al., 2009a; Serbin et al., 2009c; Daughtry et al., 2005). The limited capability of those multispectral sensors to discriminate NPV from PV and soils is due to the sensitivity, bandwidths and locations of SWIR, which are not ideal for effectively distinguishing NPV from soils (Asner and Lobell, 2000).

The linear spectral unmixing approach. The linear SMA relies on the hypothesis that reflectance within an image pixel is a linear combination of the spectral signatures of scene targets or endmembers (eq. 1.1 and 1.2) (Asner and Heidebrecht, 2002). The SMA is a popular method for estimating NPV cover when the ground cover is a mixture of PV, NPV, and bare soil. It had been used to map the cover of NPV, PV, and bare soil in semiarid shrublands, tropical forests, and along a vegetation gradient in Hawaii using Airborne Visible InfraRed Imaging Spectrometer (AVIRIS) (Asner et al., 2003; Asner et al., 2005). In addition to the AVIRIS data, the SMA has been applied to separate NPV from bare soil in shrublands using EO-1 Hyperion (Roberts et al., 2003) and in croplands using Probe-1 hyperspectral data (Bannari et al., 2006).

$$\rho\,(\lambda) = \sum(f_e \rho\,(\lambda)_e) = (\,f_{pv}\rho\,(\lambda)_{pv} + f_{npv}\rho\,(\lambda)_{npv} + f_{soil}\rho\,(\lambda)_{soil}) \quad (1.1)$$

$$\sum f_e = (\,f_{pv} + f_{npv} + f_{soil}) = 1 \quad (1.2)$$

where ρ (λ) is the reflectance of mixed canopies at wavelength λ within one pixel; f_e is the fractional cover of each ground cover endmember that is PV, NPV, and bare soil respectively; $\rho\,(\lambda)_e$ is the reflectance of each ground cover endmember at wavelength λ .

An alternative method of SMA was proposed (Daughtry, 2001) based on the hypothesis that NDVI and CAI values of PV, NPV, and bare soil form a triangle. On the triangle, PV has a high NDVI and an intermediate value CAI, NPV has a low NDVI and a high CAI, while bare soil has a low NDVI and a low CAI value (Figure 1-3). Any mixture of PV, NPV, and bare soil should be located within the triangle, and thus their cover can be resolved through the linear unmixing approach (eq. 1.2-1.6) when the positions of endmembers are known (Daughtry, 2001; Guerschman et al., 2009).

$$NDVI = {(\rho_{NIR} - \rho_{Red})}\Big/{(\rho_{NIR} + \rho_{Red})} \quad (1.3)$$

$$CAI = 100 \times \left(\frac{\rho_{2.0} + \rho_{2.2}}{2}\right) - \rho_{2.1} \quad (1.4)$$

$$N = \sum(f_e N_e) = (f_{pv}N_{pv} + f_{npv}N_{npv} + f_{soil}N_{soil}) \quad (1.5)$$

$$C = \sum(f_e C_e) = \left(f_{pv}C_{pv} + f_{npv}C_{npv} + f_{soil}C_{soil}\right) \quad (1.6)$$

Where ρ_{NIR} and ρ_{Red} are the reflectance at NIR and red wavelength regions respectively. $\rho_{2.0}$, $\rho_{2.1}$, and $\rho_{2.2}$ are the reflectance of the spectral bands centered at 2030, 2100, and 2210 nm respectively, and 100 is a scaling factor. N and C are the NDVI and CAI values in a given pixel of images or a given sampling qudarat of ground hyperspectral data, $N_{pv}, N_{npv}, and\ N_{soil}$ are the NDVI values of endmembers and $C_{pv}, C_{npv},\ and\ C_{soil}$ are the CAI values of endmembers. As in e.q. (1.1) and (1.2), $f_{pv}, f_{npv},\ and\ f_{soil}$ are the fractional covers of endmembers.

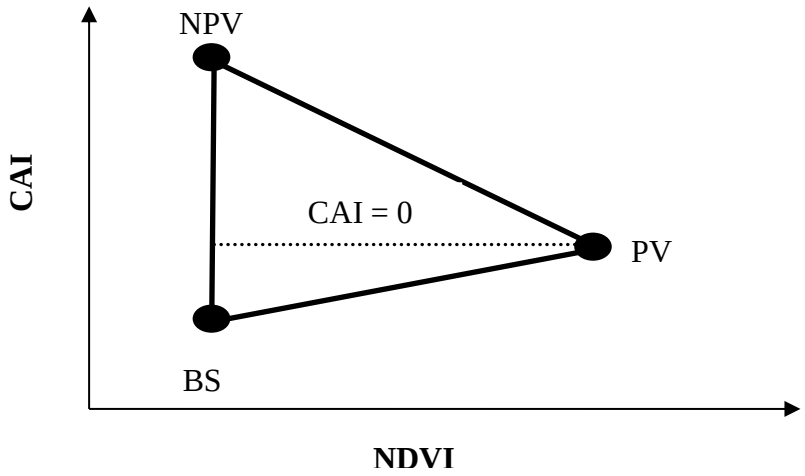

Figure 1-3 The triangular CAI-NDVI relationship of dead vegetation (NPV), green vegetation (PV), and bare soil (BS) (modified and combined from Guerschman et al. (2009) and Serbin et al. (2009b)).

The alternative SMA approach based on the NDVI-CAI triangle relationship of NPV, PV, and bare soil has been used for mapping tillage practices in agricultural areas (Daughtry, 2001; Daughtry et al., 2006) and estimating bare ground, NPV cover, and PV cover in Australian savannah (Guerschman et al., 2009). Typically, all soils have negative CAI values, NPV is CAI-positive, and CAI values of PV are approximately zero (Figure 1-2) (Serbin et al., 2009b). However, water content can significantly reduce the contrast between NPV and bare soil by decreasing the CAI of NPV towards zero (Figure 1-2) (Daughtry and Hunt, 2008; Serbin et al., 2009b), making this approach less useful. In addition, to use this alternative approach, NDVI can be replaced by other greenness indices if the variations of the indices for PV, NPV, and bare soil are easily distinguishable. LCA was used to replace CAI in the triangle relationship to estimate bare ground, NPV cover, and PV cover in Australian savannas (Gill and Phinn, 2009). However, unlike the CAI of soils, which is not affected by common soil minerals and compounds such as carbonates, chlorites, and epidotes, LCA values of soil could be increased to be above zero, complicating the application of the triangle relationship (Serbin et al., 2009a).

When using SMA models, hyperspectral data usually yield better NPV estimates than multispectral data, similarly to the spectral index approach. However, conclusions on the success of multispectral data are not consistent. Using SMA and multispectral data for NPV cover estimation was not successful in some studies (Arsenault and Bonn, 2005; Roberts et al., 1993;

Elmore et al., 2005), but successful in others, such as tropical savanna zones with Moderate-resolution imaging spectroradiometer (MODIS) data (Guerschman et al., 2009) and harvested croplands using Landsat and SPOT data without considering green vegetation (Pacheco and McNairn, 2010). In addition, tree mortality estimated from Landsat TM and ETM+ using the SMA approach in an Amazon forest demonstrated a strong relationship with field measurements (Negrón-Juárez et al., 2010).

1.3.1.3 NPV estimation with passive remote sensing data

Many efforts have been made to estimate NPV cover since the 1990's. The focus has been on distinguishing crop residue from bare soil (McNairn and Protz, 1993; Daughtry et al., 1997; Biard and Baret, 1997; Nagler et al., 2003; Daughtry et al., 2004; Roberts et al., 2003; Arsenault and Bonn, 2005; Bannari et al., 2006; Daughtry et al., 2006; Daughtry and Hunt, 2008; Serbin et al., 2009a; Serbin et al., 2009c; Pacheco and McNairn, 2010; Aguilar et al., 2012; Serbin et al., 2013; Zheng et al., 2013). In such studies, PV is not a significant contributor to the spectra. Efforts have been made to quantify NPV cover from a mixture of PV, NPV, and bare soil in grassland, savannah, and forest ecosystems (Roberts et al., 1993; Asner and Heidebrecht, 2002; Guerschman et al., 2009; Cao et al., 2010; Yue et al., 2010; Meyer and Okin, 2015; Smith et al., 2015; Jackson and Prince, 2016; Li et al., 2016). These studies have demonstrated the potential for using passive remote sensing data to obtain NPV cover estimates.

There have been far fewer attempts to estimate NPV biomass. The estimation of NPV biomass has been conducted in grazed pasture in the Brazilian Amazon (Numata et al., 2008) and semiarid steppe (Ren and Zhou, 2012) using hyperspectral data, as well as in semiarid mixed grassland (Cihlar, 2012) using multispectral data. These studies demonstrated that hyperspectral data have great potential for NPV biomass estimation (Numata et al., 2008; Ren and Zhou, 2012), while multispectral data were of far less use (Cihlar, 2012). The study in grazed pasture (Numata et al., 2008) was conducted in two grass dominated communities, and concluded that the relationship between spectral variables and NPV biomass was significantly influenced by species architecture and community heterogeneity. Ren and Zhou (2012)'s conclusion was drawn in a steppe ecosystem where PV cover is less than 30%. Whether conclusions of Numata et al. (2008) and Ren and Zhou (2012) are consistent in other herbaceous-dominated ecosystems, such

as semi-arid mixed grassland, needs further investigation. In addition, Cihlar's (2012) research may be improved by using other spectral indices, an SMA approach, or hyperspectral data. A summary of study sites, methods used, and accuracies of NPV cover and biomass estimation in the cited literature is presented in Table 1-2.

1.3.1.4 Optical remote sensing platforms

Although hyperspectral imagery and advanced multispectral ASTER imagery have demonstrated superiority over multispectral imagery such as Landsat, the limited spatial and temporal coverage of hyperspectral images constrains their applicability to monitoring NPV quantity at large spatial extents. Additionally, the ASTER sensor ceased functioning in April 2008 (http://asterweb.jpl.nasa.gov/latest.asp), and thus is no longer available for NPV estimates. Alternatively, spaceborne multispectral imagery with extended spatial coverage of the earth, temporal resolution, and much lower cost is worth investigation.

Active multispectral sensors with shortwave spectral bands that cover the cellulose absorption spectral regions include Advanced Land Imager (ALI), Land 7 Enhanced Thematic Mapper (ETM+), Landsat 8 Operational Land Imager (OLI), and MODIS. Zheng et al. (2014) asserted that MODIS imagery with 500 m spatial resolution in shortwave bands is too coarse to be used for mapping crop residues at the field scale. Nonetheless, Guerschman et al. (2009) concluded that MODIS could be used to estimate NPV cover in a tropical savannah based on the triangle relationship of NDVI and CAI between PV, NPV, and bare soil. ALI, ETM+, and OLI are all members of the Landsat family. The ALI sensor is not activated until requested and the imagery acquired has a very small footprint. Such limited temporal and spatial coverage hindered the application of ALI imagery in NPV estimation (Zheng et al., 2014). Landsat 7 ETM+ is still operational, while Landsat TM 4 and TM 5 are inactive. Imagery from ETM+ and TM has been used in many studies to estimate NPV, and it yields less accurate NPV estimation compared to hyperspectral or ASTER imagery as stated in the "Approach" section. Limited research has been conducted on the usage of OLI for NPV estimation so far, as it was only launched on February 11, 2013.

Table 1-2 A literature summary of non-photosynthetic vegetation (NPV) cover and biomass estimation using optical remote sensing data with respect to the study objects and sites, methods, and accuracy measured by coefficient of determination (r^2) and Root-mean-square error (RMSE).

Citations	**Study objects**	**Study sites**	**Remote sensing data**	**Methods**	**Accuracy**	
					r^2	RMSE
Roberts et al., 1993	NPV cover	Jasper Ridge Biological Preserve, California,USA	Airborne Visible/Infrared Imaging Spectrometer (AVIRIS)	spectral mixture analysis (SMA)	\	\
Biard and Baret, 1997	corn residue	corn field near Avignon, France	field measured hyperspectral and Landsat TM	linear regression with crop residue index multiband (CRIM)	0.91	0.1036
Asner & Heidebrecht, 2002	NPV cover	arid shrubland & grassland in Chihuahuan Desert, New Mexico, USA	AVIRIS, Landsat TM; MODIS; & ASTER	SMA	\	\
Nagler et al., 2003	crop residue; forest litter	corn, soybean, rice, and wheat fields in Tsukuba, Japan, & coniferous/ deciduous trees	lab measured hyperspectral reflectance	linear regression with CAI	0.72-0.94	\

Roberts et al., 2003	NPV in grasslands & chaparral	Grassland & Oak north of Santa Barbara, California, USA	field measured & EO-1 Hyperion hyperspectral reflectance; and AVRIS	SMA	*0.75	\
Daughtry et al., 2004	corn residue	corn, soybean, and wheat fields near Maryland, USA	field measured hyperspectral reflectance	linear regression with CAI	0.89	\
Arsenault & Bonn, 2005	corn residue	Sainte-Ange`le-de-Monnoir, Canada & Pays-de-Caux, France	simulated Landsat TM 5 reflectance	linear regression with CRIM & SMA	Regression (SMA): 0.96 (0.70) & 0.94 (0.68) in Canada & France respectively	\
Bannari et al., 2006	corn residue	wheat, canola, & pea fields, Saskatchewan, Canada	Field measured & Probe-1 (P) hyperspectral & IKONOS (IK) high spatial data	SMA	0.61 (P); 0.27 (IK)	0.12 (P); 0.24 (IK)
Daughtry et al., 2006	crop residue	corn & soybean fields, Iowa, USA	*EO-1 Hyperion	linear regression with CAI	0.77 in June & 0.85 in May	\

Daughtry & Hunt, 2008	crop residue	corn, soybean, & wheat fields near Beltsville, Maryland, USA	field measured hyperspectral	linear regression with CAI	0.813-0.933	0.089-0.165
Numata et al., 2008	NPV biomass	grazed pastures in the Brazilian Amazon	field measured hyperspectral and EO-1 Hyperion	multilinear regression with lignocellulose absorption depth (LCD) and normalized difference water index (NDWI)	0.70	\
Guerschman et al., 2009	NPV cover	tropical savanna, Australia	field measured hyperspectral data; EO-1 Hyperion, & MODIS	SMA based on the CAI-NDVI triangle relationship	***0.98	0.05
Serbin et al., 2009c	crop residue	corn, soybean, & wheat fields in Indiana, Illinois, Iowa, & Centreville, Maryland, USA	ground & airborne hyperspectral, & ASTER	linear regression with ASTER SINDRI index	0.640-0.868	0.088-0.159
Cao et al., 2010	dead fuel cover	Xilin Gole steppe, China	field measured hyperspectral data	linear regression with Dead Fuel Index calculated from simulated MODIS reflectance	0.96	\
Pacheco & McNairn, 2010	crop residue	corn, soybean, wheat and barley & pasture fields, Ontario, Canada	multispectral Landsat and SPOT data	SMA	0.45-0.98	**0.109-0.223

Yue et al., 2010	NPV cover	Karst ecosystem in Guizhou, China	field measured hyperspectral data	linear regression with karst rocky desertification synthesis index (KRDSI)	0.70	\
Aguilar et al., 2012	crop residue	malting barley, spring wheat durum, field pea, & fallow lands in the United States	field measured hyperspectral reflectance	linear regression with CAI	peas & fallow: 0.55; small grains: 0.41	peas & fallow: **0.149; small grains: **0.117
Cihlar, 2012	NPV biomass	semiarid mixed grasslands in Saskatchewan & Alberta, Canada	Landsat TM/ETM+; &MODIS	linear regression with normalized canopy index (NCI)	0.34	\
Ren and Zhou, 2012	NPV biomass	desert steppe, China	field measured hyperspectral data	linear regression with CAI	0.67	17.9 g m^{-2}
Zheng et al., 2013	crop residue	corn, soybean, & winter wheat lands near Iowa, Illinois, Indiana, & Maryland, USA	field measured & Airborne hyperspectral data; Landsat TM/ ETM+, & ASTER	Linear regressions of minimal values of Normalized Difference Tillage Index (minNDTI)	0.56-0.93	**0.084-0.151
Jacques et al., 2014	mass of dry herbaceous vegetation	rangelands in Sahel	MODIS	linear regression with soil tillage Index (STI)	0.66	280 kg DM/ha

Smith et al., 2015	NPV cover	semiarid mixed grasslands in Alberta, Canada	field measured hyperspectral &Landsat TM	Linear regression with CAI & SMA	\	\
Meyer and Okin, 2015	NPV cover	savannah in western Botswana	MODIS	SMA	0.75	\

Note: For studies that compared several methods or spectral indices, only the best method and highest accuracy are given in the Table. * r^2 was measured by Hyperion modeled NPV against AVRIS modeled NPV cover. ** The RMSE was converted from original % value to proportions to maintain consistency. *** r^2 measures the consistency between observed and predicted NPV cover.

The newly launched WorldView-3 (WV-3 Imager) satellite (August 13, 2014), and Sentinel-2A Multispectral Instrument (MSI) (June 23, 2015), provide new opportunities for NPV estimation. The Sentinel-2 mission includes twin satellites (2A and 2B) in the same orbit, ensuring continuity of SPOT- and Landsat-type multispectral data. The Sentinel-2B satellite is planned for launch in March 2017. It is collecting high spatial resolution (10 m, 20 m, and 60 m) multispectral imagery and is providing systematic global acquisitions with a high revisit frequency. The Sentinel-2A MSI sensors sample reflectance at two red-edge spectral ranges and two SWIR bands and provide a new opportunity for NPV estimation from space. The WV-3 Imager on the WorldView-3 satellite has eight multispectral bands in the VIS and NIR spectral ranges with one red-edge band and eight bands in SWIR regions. The red-edge and SWIR bands may greatly contribute to NPV estimation. In addition, it has a very high spatial resolution at 1.24 m for multispectral bands and 3.7 m SWIR resolution, which may also be an advantage for NPV estimation. However, like hyperspectral imagery, a small swath width (13.1 km) of WV-3 may hinder its application in large spatial extents. Information on WV-3 is from https://directory.eoportal.org/web/eoportal/satellite-missions/v-w-x-y-z/worldview-3. WorldView-3 imagery is not acquired until requested, further limiting its application.

Selecting an image for NPV estimation should take the spectral, spatial, and temporal resolution of the imagery into account. Most current research on NPV estimation has focused on the spectral resolution of the imagery, as low spectral resolution imagery has limited ability to differentiate NPV from PV and bare soil. Research on the spatial and temporal resolution of imagery on NPV estimation is limited. NDTI derived from a single Landsat image was not able to estimate crop residue cover (Daughtry et al., 2006). This is because the spectral resolution of band 7 (2080-2350nm) is too coarse to distinguish NPV from PV (Serbin et al., 2009b). A multi-temporal approach (minNDTI) that extracts minimum NDTI values from the spectral profiles of NDTI derived from time-series Landsat imagery was used to minimize the effects of PV on crop residue cover estimation (Zheng et al., 2013). The accuracy of crop residue cover estimation from the minNDTI approach is comparable to that of ASTER SINDRI and hyperspectral CAI in Central Indiana croplands. Nevertheless, less satisfactory results were observed in the other testing areas due to the effects of soil variation (Zheng et al., 2013). Whether a multi-temporal

approach works in other ecosystems including grasslands, and how spatial resolution of imagery affects NPV estimation, needs further investigation.

1.3.2 LiDAR for NPV estimation

A LiDAR device measures the distance between the sensor and a target surface. To do this, it emits a laser pulse towards the target surface and records the elapsed time between emission of the pulse and its reflection to the sensor (Lefsky et al., 2002). LiDAR sensors differ in the wavelength, power, pulse duration and repetition rate, beam size and beam divergence angle, the scanning mechanism, and the information recorded for each reflected laser pulse (Lefsky et al., 2002). LiDAR data can be classified as discrete return LiDAR and full waveform LiDAR. Discrete return LiDAR data can be further divided into single and multiple LiDAR returns. Single return records either the first or the last peak and multiple returns records a few peaks, while the full waveform LiDAR records the entire waveform of the reflected laser pulse (Jensen, 2009). LiDAR remote sensing can also be categorized as small and large footprint LiDAR according to the laser illumination area (Blanchard et al., 2011). Small footprint LiDAR typically has a laser illumination area of about 1 m^2 and is useful for detailed local mapping. Large footprint LiDAR can have tens of meters of illumination area and is more suitable for investigating interactions with multiple vertical structures and taking a complete ground sample (Jensen, 2009). LiDAR remote sensing can gather information returned from the ground as well as leaves, branches, and stems (or trunks) of vegetation in vegetated areas (Blanchard et al., 2011), and thus has the capability to measure the 3-D structure of both terrestrial and aquatic ecosystems at a range of spatial extents (Lefsky et al., 2002).

1.3.2.1 Current research on NPV estimation using LiDAR

LiDAR data have been widely used for measuring forest structure, aboveground biomass, and biodiversity in forest ecosystems (Lim et al., 2003; Lefsky et al., 2005; Hudak et al., 2008; Jaskierniak et al., 2011; Cho et al., 2012; Huang et al., 2013). Recently, efforts have been made to use LiDAR for NPV estimation or identification in forests. The application of LiDAR data on NPV estimation in forests relies on the fact that dead tree architecture is less complex than live tree architecture. This can help identify variation in distances and intensities of returned laser

pulses. The identification of NPV from living trees and the estimation of NPV volume (or biomass) were implemented at a tree or plot level. At tree level, full waveform LiDAR data have been used to distinguish standing dead trees from living ones in a forest using classification schemes (Yao et al., 2012). At a plot level, standing dead tree biomass and live tree biomass were estimated with LiDAR data with a correlation coefficient of predicted *versus* observed (from cross-validation with field data) of 0.79 and 0.85 respectively (Kim et al., 2009). Researchers concluded that LiDAR intensity alone is crucial for dead biomass estimation, while both LiDAR intensity and canopy volume are critical for live tree biomass estimation (Kim et al., 2009). The distribution of standing dead tree classes within forests has also been estimated based on extracted variables from LiDAR (Bater et al., 2009; Polewski et al., 2015). The cumulative proportion of dead tree stems within forest plots has been predicted using an ordinal regression approach with an r value of 0.61 and a Root Mean Square Error (RMSE) of 16.8% (Bater et al., 2009). LiDAR data have also demonstrated the capacity to estimate the volume of standing dead woody debris in natural forests with an RMSE 78.8% (Pesonen et al., 2008; Pesonen et al., 2010), and can provide auxiliary information for field sampling methods to assess coarse woody debris (Pesonen et al., 2009).

In addition to the application for measuring standing dead trees, LiDAR data have been used to delineate downed dead wood and dead basal area. The volumes of downed dead woody debris on naturally forested surfaces were estimated with an RMSE of 51.6%, which was more accurate than the estimation of standing dead tree volume (Pesonen et al., 2008; Pesonen et al., 2010). The dead basal area was analyzed using airborne LiDAR data in bark beetle affected coniferous forest canopies, and it was concluded that LiDAR-derived metrics can account for more variance in live areas than the dead basal area (Hudak et al., 2012). Downed dead wood was successfully identified using multiple-return airborne LiDAR data with an accuracy of 73% in a forested area (Blanchard et al., 2011). It was possible to identify downed dead trees with a correctness of 90% using full-waveform airborne LiDAR data. However, the accuracy was affected by the degree of decay, vegetation density, and laser penetration (Mücke et al., 2013).

1.3.2.2 LiDAR platforms for NPV estimation

Research discussed above demonstrated the potential of LiDAR remote sensing to determine the relative abundance of standing dead trees in forest stands and downed dead wood on the forested ground surface. LiDAR data used in previous research for identifying and estimating NPV in forest ecosystems are presented in Table 1-3.

Table 1-3 Summary of cited literature using LiDAR for NPV identification and estimation in forest ecosystems

LiDAR data	**Application**	**Citation**
full-waveform, airborne	downed tree identification	Mücke et al. 2013
discrete, multiple, airborne	downed dead wood delineation	Blanchard et al. 2011
full-waveform, airborne	dead tree discrimination	Yao et al. 2012
discrete, multiple, airborne	standing dead tree identification	Bater et al. 2009
discrete, multiple, ground	standing dead tree biomass estimation	Kim et al. 2009
discrete, multiple, airborne	dead basal area prediction	Hudak et al. 2012
discrete, multiple, airborne	downed and stand dead volume estimation	Pesonen et al. 2008

1.3.3 SAR for NPV estimation

Radar images are formed by backscattered microwave radiation sent to the earth by an energy generator and collected by a receiver on an aircraft or satellite platform. SAR imagery is advanced radar data that can be formed at fine spatial scales using the advanced SAR technology for acquiring imagery (Zheng et al., 2014). For orbital and suborbital imaging radars, the most commonly used bands are X-band (8-12 GHz), C-band (4-8 GHz), L-band (1-2 GHz), or P-band (0.3-1 GHz) with the corresponding free-space wavelength increasing from 2.4 to 100 cm (Jensen, 2009).

SAR data are useful for NPV estimation because they convey information on the physical structure and moisture status of NPV. NPV usually contains less moisture (Saatchi et al., 1995) and has a less complex canopy compared to PV. NPV, with low moisture content, typically has a very small dielectric permittivity, and thus less backscattering (Saatchi et al., 1995). In

addition, the less complex structure of NPV also causes a difference in backscattered radiation from PV (Liu et al., 2013).

1.3.3.1 Current research on NPV estimation using SAR data

Estimates for NPV cover have been made using SAR data. The sensitivity of crop residue to being measured by microwave backscatter has been shown in field experiments (McNairn et al., 2001). One X-band TerraSAR image was used to determine if a crop field had been tilled which is primarily determined by crop residue and surface roughness (Pacheco et al., 2010). Efforts have also been made to estimate NPV biomass using SAR data. Finnigan (2013) attempted to correlate canopy water content estimated from C-band Radarsat-2 imagery with NPV biomass in a semi-arid mixed grassland ecosystem with an r^2 value of 0.30. Phased Array L-band Synthetic Aperture Radar on Japan's Advanced Land Observing Satellite (ALOS PALSAR) data were used to determine standing dead tree biomass in the forests of West Africa (Carreiras et al., 2012). The most widely used method to estimate NPV using SAR data in these studies is to use regression models to establish the relationship between NPV and backscatter or variables derived from backscatter, such as canopy water content. These studies demonstrate that SAR data has great potential for estimating NPV. However, this potential is dependent on many factors, such as the characteristics of the instrument (frequency or wavelength, polarization, incident angle, look direction, and spatial resolution; Ghasemi et al., 2010), and the properties of the land surface including surface roughness, NPV type and size, and moisture content of the surface and NPV (Zheng et al., 2014).

Wavelength of SAR data on NPV estimation. The wavelength of a SAR system is critical for the effectiveness of SAR data for NPV estimation. Longer wavelength microwaves, such as L- and P- band SAR, can penetrate the tree canopy and reach NPV on the surface. Thus, they can be beneficial for identifying dead trees, coarse woody debris, and dead basal area in forested areas. However, in a sparsely vegetated or non-vegetated area (e.g., harvested cropland), longer wavelength signals tend to penetrate more deeply below the soil surface, and thus are less sensitive to the presence of NPV (McNairn et al., 2001). Consequently, SAR systems with shorter wavelength microwaves, such as X- and C-band, are potentially more effective for crop residue estimation (Zheng et al., 2014) and NPV estimation in grasslands or pastures.

Nonetheless, it is worth noting that these X- and C-band SAR data may not be applicable for NPV estimation in forest ecosystems due to their low penetration ability. SAR data with a suitable wavelength should be selected specifically for NPV estimation in different ecosystems.

Polarization of SAR data on NPV estimation. Polarization is another factor that needs to be accounted for when selecting SAR data for NPV estimation. Cross-polarized (HV and VH) backscatter is less sensitive to the look direction effects of a SAR system than co-polarized backscatter (HH and VV) (McNairn and Brisco, 2004). When SAR data were used for estimating crop residue, cross-polarized backscatter was more strongly correlated with crop residue than co-polarized scatter (McNairn et al., 2001). In addition, the other two polarimetric parameters, including co-polarized circular backscatter and pedestal height, that are related to multiple scattering and volume scattering were significantly correlated with crop residue (McNairn et al., 2002). However, the study conducted by McNairn et al. (2002) suggests these polarimetric parameters are more sensitive to surface roughness than crop residue. SAR data alone are difficult to use for crop residue estimation due to the high influence of surface roughness (Zheng et al., 2014). Nonetheless, how the polarimetric parameters of SAR data are related to NPV in forest and grassland ecosystems is poorly understood.

Incidence angle of SAR data on NPV estimation. Higher incident angle tends to reduce the penetration ability of SAR data. The reduced penetration of the soil surface increases the sensitivity of the signal to crop residue in harvested cropland (McNairn et al., 1996). However, the reduced penetration due to higher incident angles also makes SAR signals more sensitive to surface roughness (Baghdadi et al., 2002; Baghdadi et al., 2008). Whether a higher incident angle is beneficial for crop residue estimation requires further investigation. Additionally, how incident angle affects NPV estimation in forest and grassland ecosystems is also worthy of study.

Look direction of SAR data on NPV estimation. Look direction affects backscatter, especially co-polarized backscatter. When look direction is perpendicular to the row direction for croplands or farmed forests, much higher co-polarized backscatter is observed than when it is parallel to the row look direction (Beaudoin et al., 1990). However, look direction does not affect cross-polarization backscatter (McNairn et al., 2001). In this regard, how look direction affects NPV

estimation in croplands and farmed forests is dependent on the polarization of the SAR selected. Look direction effects may not be significant for NPV estimation in natural forest and grassland ecosystems.

Spatial resolution of SAR data on NPV estimation. Spatial resolution as an inherent property of one specific SAR data is an important factor affecting NPV estimation. The SAR sensors with coarse spatial resolution may result in mixed pixels that reduce the accuracy of NPV estimation. Some types of NPV with smaller size distributions may not be captured by SAR data with coarse resolution. In this regard, the integrated multi-resolution (or multi-sensor) data can be used to improve NPV estimation accuracy by reducing the amount of mixed pixels (Ghasemi et al., 2010).

Surface roughness effects on NPV estimation. Surface roughness may have significant effects on backscatter of SAR data. The effects of surface roughness are related to incidence angle, with greater effect at higher incidence angles (Baghdadi et al., 2002; Baghdadi et al., 2008). In addition, the effects of surface roughness on NPV estimation using SAR data are also related to the free-space frequency of SAR data. Lower frequency (longer wavelength) of SAR data may be more sensitive to surface roughness than NPV in harvested croplands (McNairn et al., 2002) and thus are not able to detect NPV.

Effects of NPV type and condition on NPV estimation. Backscatter of SAR data may have variable sensitivity to different types of NPV. Dead standing trees and dead woody debris in forests, plant residue in croplands, and standing dead grasses and plant litter on the surface in grasslands all affect backscatter differently. This is due to the different types of NPV differing in structure, decay status, and moisture content. The sensitivity of SAR C-band and L-band data to crop residue type and moisture content was investigated in field experiments where it was found that stronger backscatter was associated with higher moisture levels, especially with corn residue (McNairn et al., 2001). Limited research has been conducted on the sensitivity of SAR data with different free-space frequency and polarization to NPV in forest and grassland ecosystems. In addition, temporal and spatial variations of NPV properties may also play an important role in NPV estimation using SAR data (McNairn et al., 2001; Zheng et al., 2014).

Table 1-4 Current and future operational synthetic aperture radar (SAR) satellite systems for NPV estimation.

System	Dates of service	Wavelength/frequency band	Polarization	Spatial resolution (m)	Swath width (km)	Revisit interval	Incidence angles (◦)
Radarsat-2	2007-present	C	Full	9-100	25-170	24 days	49-60
TerraSAR-X*	2007-present	X	Full	16	100	2.5 days	15-60
COSMO-SkyMed Constellation	2007-present	X	Dual	30	100	1-15 days	25-50
SAR-Lupe (5 satellites)	2006-present	X	Full	<1	8 × 60[a]	11 h	Multiple
TanDEM-X	2010-present	X	Full	18	100-150	2.5 days	20-65
ESA Sentinel-1 A (1B)	2014 (2016)	C	Dual	5-100	80-400	12 days	Multiple
Radarsat Constellation	2018	C	Full	30	125	24 h	21-47
NovaSAR-S	2015	S	Full	6-30	22-750	<1-6 days	16-34**

Notes: X, C, and S denote 8-12, 4-8, and 2-4 GHz frequency bands respectively. * indicates the stripmap modes of TerraSAR-X, and ** means that the incidence angles of NovaSAR-S are for terrestrial application.

1.3.3.2 SAR platforms for NPV estimation

Current and future operational SAR satellite systems that demonstrate potential for NPV estimation are listed in Table 1-4. Selecting a suitable SAR data source should comprehensively take all the critical elements discussed above (section 1.3.3.1) into account. For example, to estimate NPV cover in croplands, full polarization, shorter wavelength (C- and X-band), and a large incidence angle are favorable (Zheng et al., 2014). However, for estimating downed logs

on the surface of forested ecosystems, X-band might not have enough penetration capability to reach the surface. Further research should be conducted on properties of SAR systems for NPV estimation in different ecosystems.

1.3.4 The integration of passive and active remote sensing data

Both passive and active remote sensing data have demonstrated potential for use in NPV estimation, but each data source has its own merits and drawbacks. Integrated multi-sensor data have significant advantages over each single source data (Hall and Llinas, 1997), and the maximum amount useful information can be retrieved from the fused images (Welch and Ehlers, 1987). Therefore, using the integrated passive and active remote sensing data for NPV estimation has the potential for excellent results, although currently only a few attempts have been made.

1.3.4.1 Integrated optical and LiDAR data

Optical remote sensing data contain biophysical and biochemical information of NPV, while LiDAR data can obtain physical structure information of NPV through measuring the distances and intensities of returned laser pulses to the sensors. Thus, integrated optical and LiDAR data are expected to provide better estimates of NPV. LiDAR data can provide horizontal and vertical structure information at very fine spatial scales with high vertical accuracy (Lim et al., 2003), and thus have the advantage of providing an estimate of total aboveground biomass. Visible and near-infrared wavelengths of passive optical systems are sensitive to vegetation leaf pigment structure and thus are beneficial for PV biomass estimation. NPV biomass thus can be estimated by subtracting PV biomass estimated from optical imagery from the aboveground total biomass quantified using LiDAR data.

Integrated passive optical and LiDAR data have seen limited use in NPV estimates. However, their integration has provided better results than independent data sources in many relevant fields, such as fuel type (Mutlu et al., 2008a; Varga and Asner, 2008; Erdody and Moskal, 2010; García et al., 2011), fuel quantity mapping (Mutlu et al., 2008b), tree crown metrics (McCombs et al., 2003; Popescu and Wynne, 2004; Buddenbaum et al., 2013), canopy height and biomass (Hyde et al., 2006; Swatantran et al., 2011), vegetation classification (Nordkvist et al., 2012) and

timber volume (Tonolli et al., 2011). The success of integrated passive optical and LiDAR in NPV relevant fields has demonstrated a potential for their application for NPV estimation, especially in forest ecosystems.

1.3.4.2 Integrated optical and SAR data

Optical remote sensing data contain biological information from NPV, while SAR data convey physical structure and moisture content information from NPV. In addition, better penetration of SAR than optical data is beneficial for estimating NPV on the surface. Therefore, the integrated passive optical remote sensing data and SAR data should provide better opportunities for NPV estimation.

Few studies have been focused on investigating integrated SAR and optical data on NPV estimation. The fusion of multi-frequency, multi-polarization Airborne Synthetic Aperture SAR (AirSAR) and AVIRIS optical remote sensing data have been used to estimate the quantity and quality of dead woody biomass in Yellowstone post-fire forest ecosystems, with partial success (Huang et al., 2009). The 500-m spatial resolution dual-polarization L-band ALOS PALSAR data cannot distinguish evergreen forest from standing dead trees, while the combination of ALOS PALSAR and MODIS imagery may provide an opportunity for monitoring deforestation in the Amazon region (Sheldon et al., 2012). In addition, attempts to use integrated SAR and optical data in NPV relevant fields have demonstrated potential for use in NPV estimation. For example, the fusion of AVIRIS and AirSAR data shows the potential for large-area rangeland monitoring in the context of estimating sagebrush, herbaceous, and bare ground cover in arid and semiarid sagebrush-grass ecosystems in Yellowstone (Huang et al., 2010). Incorporating optical and SAR images could provide more accurate land cover estimations (Peters et al., 2011; Pereira et al., 2013) and herbaceous biomass mapping (Svoray and Shoshany, 2003).

1.3.5 Advantages and disadvantages of remote sensing data for NPV estimation

Based on the above review, the accuracy of NPV estimates based on remote sensing data relies heavily on the type of data. Currently, remote images used for NPV estimation contain largely passive optical data. Multi-sensor approaches for NPV estimation based on polarimetric SAR,

LiDAR, and hyperspectral data have not been sufficiently developed (Koch, 2010). There is a need to develop more suitable approaches for integrating multi-sensor data. Selecting data is also important for NPV estimation, because each data source has advantages and disadvantages.

Advantages of passive remote sensing include its repeatability, lower acquisition cost, and greater spatial extent. The fact that optical remote sensing imagery is available for more than three decades into the past and has high spectral sensitivity for species identification is also important to consider (Koch, 2010). However, passive optical remote sensing data has constraints. In a dense canopy environment, passive optical remote sensing data are limited by their top-of-canopy characteristics and limited accessibility to objects below the canopy (Huang et al., 2009; Blanchard et al., 2011). The low penetration of optical data makes it difficult to estimate NPV where vegetation is dense and substantial surface plant litter is present. In an open canopy environment, the applicability of optical remote sensing is hindered by litter decay (Nagler et al., 2000; Daughtry, 2001; Nagler et al., 2003) and backgrounds that include bare soil and BSC. In arid and semiarid regions, moss and lichen contribute greatly to the canopy spectra. Although NPV is distinguishable from bare soil in the SWIR regions (Asner, 1998), the influence of BSC (e.g. moss) increases the difficulty of NPV estimation due to the similar cellulose and lignin absorption features of dry moss and NPV in the SWIR regions (Figure 1-3). In addition, optical data are easily affected by clouds, haze, and smoke (Avitabile et al., 2012) and saturation issues exist when such data are used to estimate terrestrial, particularly forest, densities (Song, 2013).

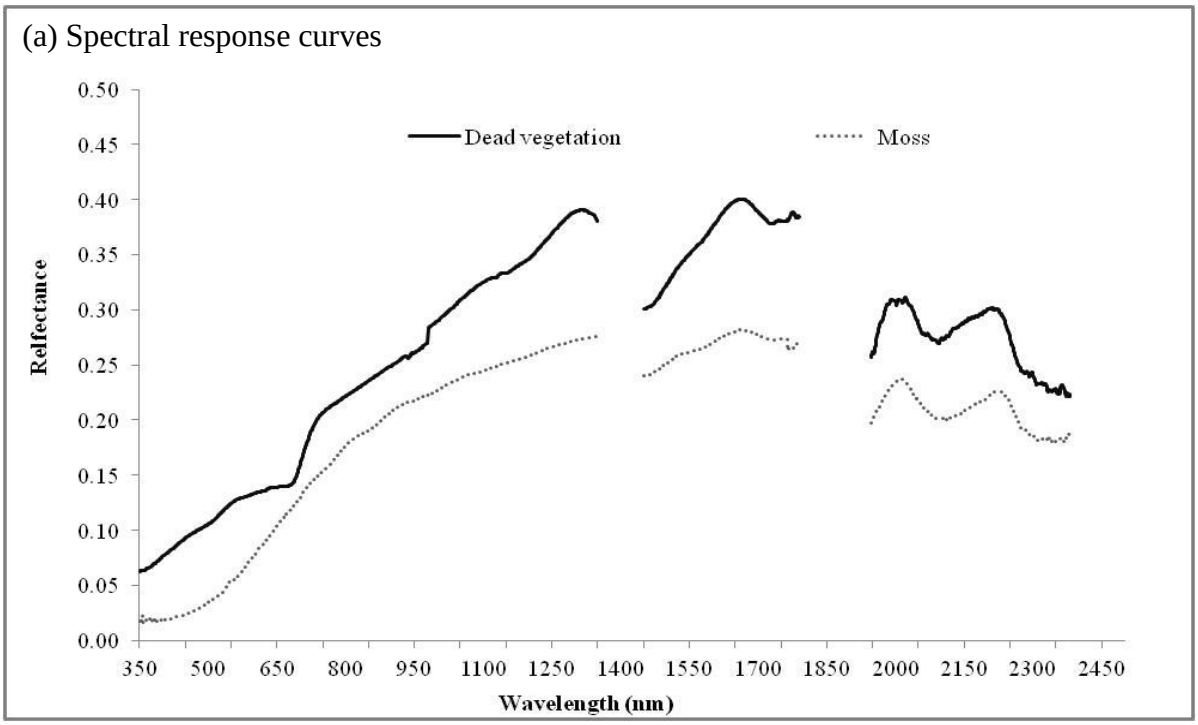

(b) Dead grass

(c) Dry moss

Figure 1-4 (a) Spectral response curves of dead vegetation and dry moss, (b) Photograph of dead grass, and (c) Photograph of dry moss (dead grass samples and moss samples were collected from Grasslands National Park (GNP), Canada, in the mid-June of 2004 and 2013 respectively, and their spectra were measured in laboratory with an ASD Spectroradiometer).

LiDAR has several advantages over passive optical sensors (Blanchard et al., 2011), especially in forests. The LiDAR pulse can penetrate a tree canopy to the forest floor, allowing the mapping of vertical and horizontal structures of both canopy and understory vegetation at a fine spatial resolution (Lefsky et al., 2002; Vierling et al., 2008; Guo et al., 2010). In addition, LiDAR can

be analyzed and used in different formats ranging from a collection of points, a derived raster layer, or a series of raster layers (Blanchard et al., 2011). However, compared to passive remote sensing, the application of LiDAR is limited by small spatial extent, complex data processing, and high acquisition costs (Blanchard et al., 2011). For terrestrial applications, LiDAR has a wavelength range of 900-1064 nm where healthy green vegetation has a high reflectance (Lefsky et al., 2002). Thus, just as for passive optical remote sensing, its application is affected by clouds (Lefsky et al., 2002). The use of both passive optical remote sensing and LiDAR were also affected by the decay of NPV (Nagler et al., 2003; Mücke et al., 2013). Whether LiDAR has advantages over optical sensors for NPV estimation in other ecosystems, such as grasslands and croplands, needs further investigation.

SAR data has a longer wavelength, meaning stronger penetration ability, and thus are not affected by clouds, haze, and rain that influence the quality of most optical images. The application of SAR remote sensing can also avoid issues of optical remote sensing for estimating NPV, such as decay mediated changes in the spectral reflectance features of NPV (Nagler et al., 2003). Polarimetric SAR data can provide better structural information than optical sensors, and this improved information can contribute to the separation of NPV from PV. However, just as with optical data, the direct application of SAR data for NPV estimation is restricted by saturation issues in high biomass vegetation areas (Koch, 2010). SAR data also have deficiencies resulting from antenna pattern calibration and the effects of local incidence angle, soil moisture, and surface roughness (Huang et al., 2010).

1.4 Summary and Research Gaps

The ecological importance of NPV has driven considerable research on quantifying NPV. Studies have demonstrated the potential of optical data, LiDAR, and SAR, and their integration for NPV estimation in diverse ecosystems, including croplands, savannah, grasslands, shrublands, and forests. However, no solution exists yet for quantifying NPV biomass with remote sensing approaches in Canadian mixed prairie grasslands with a considerable amount of PV, NPV, BSC, and bare soil (Cihlar, 2012).

1.5 Research Hypothesis and Objectives

The hypothesis of this research is that NPV biomass in Canadian mixed grassland can be quantitatively estimated with remote sensing approaches. The overall objective is to find a solution for quantifying NPV biomass with remote sensing approaches in Canadian mixed prairie grassland. The fractional cover of NPV, PV, bare soil, and BSC change as vegetation phenology changes, which means the degree of effects exerted by PV, bare soil, and BSC on NPV estimation change with vegetation phenology. Therefore, the first objective of this dissertation was to determine vegetation phenology. The second objective was to explore the potential of optical data for NPV biomass estimation based on the vegetation phenology. The third objective was to investigate the application of Radarsat-2 images for quantifying NPV biomass.

1.6 Study Area and Field Data Collection

1.6.1 Study area

This study was conducted in the west block of Grasslands National Park (GNP, 49.10°N, 106.89°W) in Canada (Figure 1-5). GNP, as a parcel of northern mixed-grass prairie, has been extensively studied because it is a genetic refuge for rare native and endangered species, and is at the northern edge of continental C_4 species (Li and Guo, 2014). GNP was established in 1984, and from then until 2006 it had no large herbivore grazing. In 2006, for conservation purposes, bison were introduced into the west block. Despite grazing, a substantial amount of dead vegetation is still observable, which is attributed to the low frequency of natural fire and prescribed burning.

GNP is in a continental semiarid climate region with hot summers and cold winters. The mean annual temperature is 3.8 ºC, and the average of the annual total precipitation is 347.7 mm, based on the 1971-2000 climate records from Environment Canada. Most of the annual precipitation comes from evening storms in May and June. Consequently, low soil moisture content is a typical climatic feature of GNP (Wang and Davidson, 2007). Moisture is the dominant factor limiting vegetation growth (Li and Guo, 2012), and the precipitation pattern in Canadian prairies

has been projected to change in the future according to climate modeling (Solomon et al., 2007). Under such circumstances, monitoring grassland ecosystems is important.

GNP has a rolling topography with elevation ranging between 750 and 905 m above sea level. Vegetation in GNP was classified into upland, valley, and slope communities based on topography with disturbed (invasive species) communities identified separately. The dominant upland vegetation species are speargrass and blue grama grass (Hesperostipa comata -Bouteloua gracilis) and western wheatgrass and sedge (Pascopyrum smithii-carex spp.) (Li and Guo, 2014). Valley vegetation communities mainly consist of western wheatgrass and sagebrush (Pascopyrum smithii-Artemesia spp.) with shrubs and occasional trees along the Frenchmen River (Li and Guo, 2014). Sloped communities have both upland and valley vegetation species. Main disturbed communities are occupied by crested wheatgrass (Agropyron cristatum) and smooth bromegrass (Bromus inermis). Typical vegetation in each community is shown in Figure 1-6.

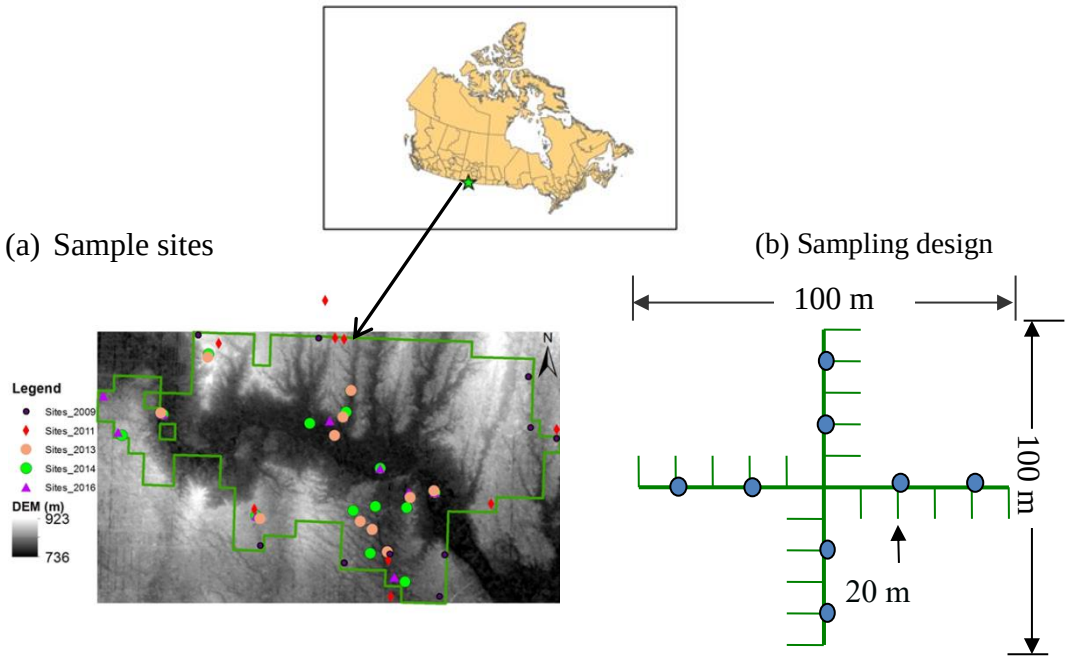

Figure 1-5 Location of the west block of Grasslands National Park and its surrounding pastures with (a) the sampling sites and (b) the sampling design (Background shows the elevation of the study area).

(a) Disturbed

(b) Slope

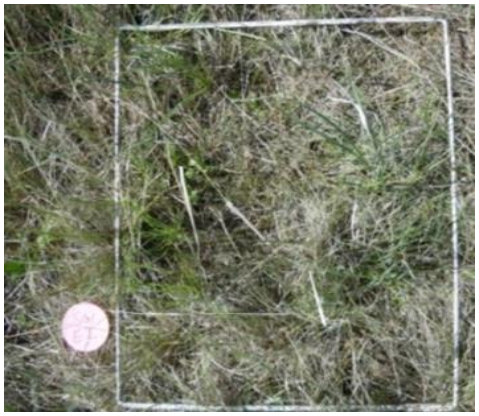

(c) Upland

(d) Valley

Figure 1-6 Typical vegetation communities in (a): disturbed grassland, (b): slope grassland (c): upland grassland, and (d): valley grassland.

The main soil type in GNP is Brown Chernozemic (Fargey et al., 2000) that developed from morainal parent materials. The morainal materials are mainly comprised of loams and clay loam derived from the underlying siltstone, shale, and sandstone (Pennock et al., 2011). Such soil has SOC storage of about 60 to 80 Mg ha^{-1} (Pennock et al., 2011). The soil mineralogy includes the clay mineral assemblage which is dominated by smectite and mica, with smaller quantities of chlorites, kaolinite, and vermiculite, and non-clay mineral fractions mainly consisting of carbonates, quartz, Mica, K-feldspar, Na-feldspar, and Ca-feldspar (Pennock et al., 2011). The SOC and soil mineralogy exert a certain influence on the soil spectra at shortwave wavelength regions (Daughtry and Hunt, 2008; Serbin et al., 2009a; Serbin et al., 2009b).

1.6.2 Field data sampling

Field data collected for this study are ground hyperspectral reflectance, vegetation biomass, and ground cover percentages for green grass, forb, shrub, standing dead, litter, bare soil, moss, lichen, and rock. Field seasons were from May 22 to May 31 in 2009, June 10 to June 25 in 2011, June 9 to June 17 in 2013, June 20 to July 2 in 2014, and July 2 to July 9 in 2016 at numerous sample sites (Figure 1-5 (a)). Stratified random sampling was used to locate sites. There were 10, 10, 12, 14, and 10 sampling sites in 2009, 2011, 2013, 2014, and 2016 respectively. The sample sites in 2009 and 2011 were randomly selected on the stratified grazed and ungrazed uplands. In 2013, 2014, and 2016, sample sites were randomly selected to represent upland, valley, slope, and disturbed communities and measurements were taken within one sampling plot at each site.

At each site, one sampling plot was set up in all sampling years except for 2009. In each plot, one 100 m × 100 m sampling transect was surveyed. Spectral measurements and biophysical parameters, except for biomass, were taken at 10 m intervals, while biomass was clipped at 20 m intervals (Figure 1-5 (b)). Thus, there were 20 total spectral and ground cover measurements, and 8 biomass samples within each site. At each site in 2009, measurements were taken within 5 sample plots. Within each plot, the same 100 m × 100 m sampling transect was surveyed, however, each arm was sampled at 2.5 m, 5 m, 10 m, 20 m, 30 m, and 50 m away from the central point for spectra and ground cover measurements (Yang and Guo, 2011). Biomass was clipped at 5 m and 20 m from the central point of the north and south arms and at 10 m and 50 m distance from the central point at the east and west arms, yielding 8 measurements within each plot and 40 samples at each site. The measurements within each sampling site were averaged over the site to avoid spatial autocorrelation in the analysis. The geocoordinates of each sampling site were recorded using a Global Positioning System (GPS).

Ground cover was visually estimated within a 50 cm × 50 cm quadrat. The general rule used for cover estimation is that cover was estimated at a 5% increment when the fractional cover is larger than 5% and smaller than 95%, or the cover was evaluated at a 1% increment.

Ground cover was visually estimated within a 50 cm × 50 cm quadrat. The fractional cover of grass, forbs, shrub, standing dead vegetation, plant litter on the surface, moss, lichen, rock, and bare soil were visually estimated at a sum of 100%. When the fractional cover is larger than 5% and smaller than 95%, cover was estimated at a 5% increment. When the fractional cover is smaller than 5% or larger than 95%, the cover was evaluated at a 1% increment.

Ground hyperspectral reflectance was measured using an ASD Spectroradiometer (Boulder, CO) with wavelength ranges from 350 to 2500 nm and a resolution of 3 nm at 700 nm and 10 nm at 1400 and 2100 nm. The hyperspectral reflectance was sampled near simultaneously when and where the biophysical data were sampled, yielding 20 spectra from each sampling plot. Spectra measures were taken between 10 am and 2 pm on sunny days during each field season. Prior to sampling and every 15 minutes while sampling, a white reference panel was used for calibration. While sampling, the sensor of the ASD instrument was pointed down from approximately 1 m above the ground, facing the canopy within the center of the sampling quadrats. The field of view of the probe was 25°, yielding a sampling area of 0.15 m2 that is slightly larger than the biomass sampling quadrat (0.10 m2). This difference would not cause large variations in NPV biomass estimation, because each sampling plot was set up in a relatively homogeneous area, and all the ASD measurements within one plot were averaged to represent the sampling plot.

The ground cover estimation is summarized in Table 1-5. The total dead vegetation coverage varies from 29% in 2013 to 50% in 2009 with 46% and 47% in 2011 and 2016, respectively. The mean green cover ranges from 19% in the early growing season of 2009 to 45% in 2013 and 47% in 2016. The averaged total NPV coverage is 38%. The BSC cover was 6% to 14% in the study years. The percentage of bare soil was as small as 1% and 2% in 2011 and 2016, respectively, while as high as 22% and 10% in 2009 and 2013, respectively.

Table 1-5 Biophysical data description in Grasslands National Park in 2009, 2011, 2013, 2014, and 2016 (BSC, biological soil crust including large amount of moss and small portion of lichen).

		% Green vegetation			% Dead vegetation			% Backgrounds		
Year	Description	Grass	Forb	Shrub	Standing dead	Litter	Total dead	Moss	Rock	Bare soil
2009	Average	12	5	2	40	10	50	6	3	22
	Max	17	8	8	73	20	83	13	10	56
	Min	10	3	0	10	0	24	4	0	14
	SD	2	1	3	19	7	18	2	3	12
2011	Average	28	14	0	18	28	46	10	1	1
	Max	44	22	3	31	45	55	17	4	3
	Min	18	9	0	4	12	33	1	0	0
	SD	7	4	1	9	10	7	5	1	1
2013	Average	33	11	1	11	18	29	14	2	10
	Max	73	25	3	37	32	61	29	15	36
	Min	18	2	0	0	4	4	0	0	3
	SD	16	7	1	13	9	17	9	5	10
2014	Average	33	10	4	19	19	38	7	2	5
	Max	49	48	14	32	39	71	25	15	22
	Min	9	0	1	7	3	10	0	0	0
	SD	12	13	5	10	13	23	8	4	8
2016	Average	34	4	6	18	29	47	6	1	3
	Max	51	8	15	28	50	63	17	3	6
	Min	27	1	0	7	9	29	0	0	0
	SD	7	2	5	7	12	8	6	1	2

1.7 Dissertation Structure

This dissertation was organized in manuscript format, and it consists of six chapters (Figure 1-7). Chapter 1 introduced the importance and rationale of this research. Chapter 2 fulfills Objective 1, estimating vegetation phenology under climate variation in the study area. Based on the vegetation phenology determined in Chapter 2, Chapter 3 (Objective 2) analyzes ground hyperspectral and multispectral Landsat 8 OLI and Sentinel-2A remote sensing data for NPV biomass estimation and Chapter 4 (Objective 3) explores the potential of fine Quad-pol Radarsat-2 data for NPV biomass estimation. Chapter 5 discusses the contribution of remote sensing of NPV to grassland ecosystem health assessment and monitoring, followed by Chapter 6 in which a general conclusion on this research is made, and contributions, limitations, and further research are also discussed.

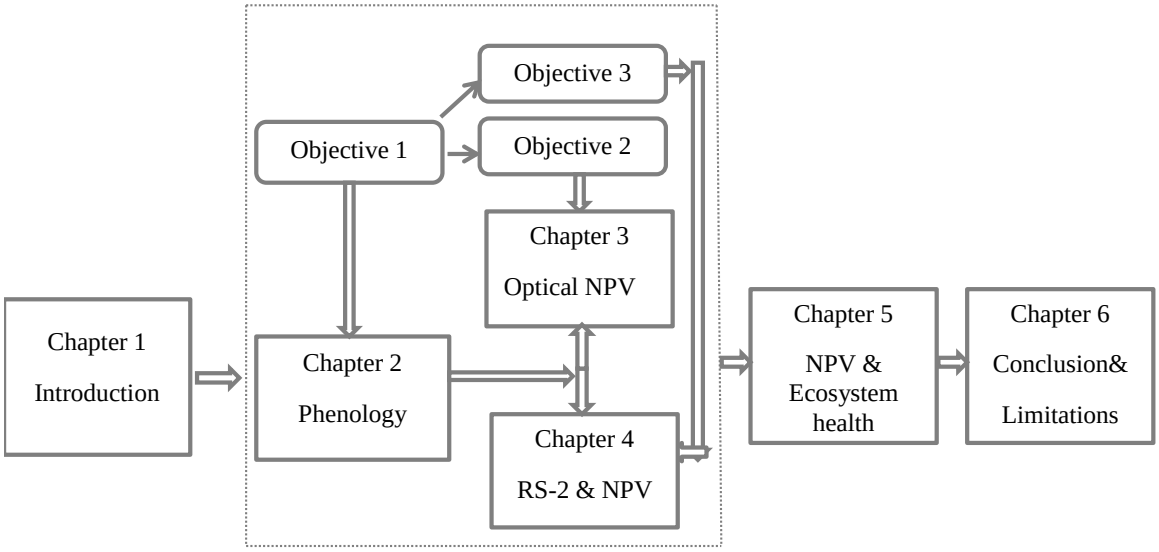

Figure 1-7 Flow chart and structure of this dissertation.

1.8 Addendum

To better organize this dissertation, Table 1 (the spectral indices used for NPV estimation in the selected literature) in the published paper was moved to Chapter 3 and titled Table 3-3 with the addition of new multispectral indices. Table 3 (a summary of the cited literature on NPV cover and biomass estimation) was updated with newly published research. Figure 1-1 was also updated. Information on the newly launched remote sensing platforms was updated. The last section of summary, challenges, and future direction in the paper was deleted from this chapter and moved to Chapter 5.

CHAPTER 2: VEGETATION RESPONSES IN SEMI-ARID NORTHERN MIXED GRASSLAND TO CLIMATE VARIATION

2.1 Preface

This chapter fulfills Objective 1- estimate vegetation phenology in the study area. In this chapter, vegetation phenology was estimated, effects of temperature and precipitation on vegetation were investigated, and temporal trend of vegetation productivity was explored. This work was published in the journal *Remote Sensing*.

Li Z and Guo X. (2012) Detecting climate effects on vegetation in northern mixed prairie using NOAA AVHRR 1-km time-series NDVI data. Remote Sensing 4: 120-134, *doi:*10.3390/rs4010120.

The initial idea for this paper came from my discussion with Dr. Xulin Guo. I analyzed and interpreted the data, and came up with the manuscript. Dr. Xulin Guo's comments dramatically enhanced the quality of the paper. It was published by MDPI – Open Access Publishing, and thus the authors retain the copyright.

2.2 Abstract

Percentage of canopy cover including PV, NPV, BSC, and bare soil changes with vegetation phenology. The performance of remote sensing data on NPV biomass estimation may change as vegetation phenology changes, because the contributions of PV, BSC, and bare soil to canopy spectra vary. Therefore, before seeking a solution to quantify NPV biomass with remote sensing tools, vegetation phenology in the study area is estimated. Because vegetation phenology and vegetation growth are highly dependent on climate variables, such as temperature and precipitation, this study also investigated grassland vegetation response to climate and established vegetation growth baseline using NDVI. The main findings were: (1) vegetation green-up generally started in mid-April to mid-May, peak growing season was reached in late June to mid-July, and senescence typically began in early to mid-July; (2) climate has significant effects on vegetation, and the growing season tended to increase in length indicated by earlier green-up and later senescence; and (3) vegetation productivity, reflected by the phenologically-

tuned annual NDVI, had an increasing trend from 1985 to 2007 and the baselines of annual NDVI range from 0.13 to 0.32, and only the NDVI in 1999 is beyond the upper bound of the baseline.

2.3 Introduction

Quantifying NPV biomass in a semiarid grassland with optical or SAR remote sensing approaches is made more challenging by the presence of PV, bare soil, and BSC (Smith et al., 2015; Li and Guo, 2016). Since the fractional cover of NPV, PV, bare soil, and BSC change as vegetation grows, the intensity of the influence of PV, bare soil, and BSC on remote sensing of NPV is expected to vary at different growing stages. Therefore, it is necessary to investigate the potential of remote sensing data for NPV biomass considering vegetation phenology.

Biotic elements including plants, animals, and abiotic elements including climate and soil, etc., and their interactions are important components of grassland ecosystems. In natural grassland ecosystems, climate is a dominant factor of vegetation growth and condition (Coupland, 1992). Weather has a moderate effect on the seasonal and annual variation of Net Primary Productivity (NPP), and spatial biological heterogeneity in GNP (Zhang et al., 2008). The results of the CENTURY model indicate that the stability of the vegetation community in GNP was affected by precipitation variability (Mitchell and Csillag, 2001). However, little work has been done to comprehensively investigate how vegetation phenology and productivity in GNP respond to climate change. In addition, climate variables, including temperature and precipitation, can be auxiliary data for measuring NPV biomass with remote sensing approaches if a significant relationship is found.

NDVI is a good indicator of various vegetation biophysical parameters, including biomass, LAI, green cover percentage (Amri et al., 2011), and NPP (Weiss et al., 2004), as well as fraction of absorbed photosynthetically active radiation (fAPAR) (Asrar et al., 1992). NDVI also demonstrates linear relationships with environmental variables, such as temperature and precipitation, under a variety of environmental conditions (Anyamba et al., 2001). Therefore, NDVI data have been widely used to estimate vegetation phenology (e.g., Balzarolo et al, 2016), study temporal responses (e.g. Anyamba et al., 2002; Lotsch et al., 2003) and spatial pattern of

vegetation to climate fluctuations (e.g. Nicholson and Farrar, 1994; Wang et al., 2001). NDVI data have also been used to explore vegetation trends (e.g. Tucker et al., 2001; Eklundh and Olsson, 2003; Nemani et al., 2003) under climate variation. In addition, previous studies have shown that NDVI could be quantified to measure the deviation of vegetation from normal conditions (Tucker and Sellers, 1986; Al-Bakri and Taylor, 2003; Piwowar, 2011). In summary, NDVI can be used to estimate vegetation phenology (Balzarolo et al., 2016), and study vegetation response to climate variation at a range of time and spatial scales (Anyamba et al., 2001).

In this chapter, using NDVI as a proxy, vegetation phenology in GNP was estimated, impacts of climate variation on vegetation phenology and vegetation productivity were investigated, and baselines for vegetation productivity were established. Before the analyses, the ability of NDVI to represent vegetation condition was evaluated based on the aboveground biomass data. Also, inter- and intra-annual relationships between NDVI and climate variables, including temperature and precipitation, were quantified.

2.4 Data

The NDVI data used were extracted from Canada-wide 10-day Advanced Very High Resolution Radiometer (AVHRR) 1 km spatial resolution composites. Composites were processed using the New Geocoding and Compositing System (GEOCOMP-n) (Adair et al., 2002; Cihlar et al., 2002), by the Manitoba Remote Sensing Centre, Canada. The GEOCOMP-n system produces higher level products with improvements on geocoding, inter-sensor calibration, atmospheric correction, Bi-directional Reflectance Distribution Function (BRDF) correction, and identification and removal of cloud contamination (Cihlar et al., 2002). NDVI composites used were from April 1st to October 31st during 1985 to 2007, and were produced from the imagery of AVHRR onboard the National Oceanic and Atmospheric Administration (NOAA) 9, 11,14,16,17, and 18 satellites. Some NDVI data within the range of -1~0 in a badland landscape area were removed after data retrieval, as they represent non-vegetation information. Finally, the inter- and intra-annual consistency of NDVI data was examined against dry green biomass data before data analyses.

Dried green biomass data were obtained by drying fresh green biomass, including green grasses, forbs, and shrubs, for 48 hours at 60 ˚C in the oven. Fresh aboveground biomass was collected in June and July of 2003 and 2005, as well as June of 2004, using the field methods described in Section 1.6.2 in Chapter 1.

Climate data used are daily temperature and precipitation from 1985 to 2007 in Val Marie, the weather station closest to the study area (approximately 1 km). Temperature data were averaged, and precipitation data were summed at different temporal scales (Section 2.5.3) to meet the requirements of analyses.

2.5 Methods

2.5.1 Applicability of AVHRR/NDVI data

Whether variation in NDVI responds to actual variation of vegetation cover in semiarid areas is debatable, due to seasonal variation in atmospheric water vapor (Justice et al., 1991), atmospheric aerosol content (Vermote et al., 1997), and large areas of bare soil (Farrar et al., 1994; Huete and Tucker, 1991). In addition, orbital drift and sensor changes also exert known effects on time series AVHRR/NDVI datasets (Kaufmann et al., 2000). Hence, the first step of this study is to verify the ability of AVHRR/NDVI data to estimate vegetation phenology and monitor vegetation condition in GNP. Nevertheless, the potential for using 10-day AVHRR 1 km NDVI data in GNP and the northern Great Plains has been shown (Zhang et al., 2008; Piwowar, 2011). Collected biomass data from all sample sites were averaged during a 10-day period to match the compositing period of AVHRR imagery. Also, NDVI data in the corresponding periods were extracted from sample sites and averaged. Finally, averaged aboveground biomass and NDVI data were plotted, and their relationship to the sampled sites was investigated through a comparison of the averaged NDVI of the sites from the mean NDVI of the entire study area.

2.5.2 Vegetation phenology

The curvature-change rate method developed by Zhang et al. (2003) was used to estimate vegetation phenology, namely green-up, peak growth, and senescence. This approach was chosen due to its ability to handle multiple growth cycles with no requirement to arbitrarily

define thresholds that identify phenological transition dates. Also, the method is ecologically meaningful.

2.5.3 Relationships between NDVI and climate variables

To investigate intra-annual NDVI-temperature and NDVI-precipitation relationships, temperature was averaged, and precipitation was accumulated based on the time intervals (Table 2-1), considering the lag effects of environmental variables on NDVI. The first and last NDVI data used in the correlation analysis were phenologically-tuned. While averaging temperature and summing precipitation, some values were removed because of continuous data missing on three out of 10 days. Finally, the effects of temperature and precipitation on NDVI were determined based on their correlation at various time intervals.

To find the period over which temperature and precipitation most affect vegetation growth in GNP, correlation of NDVI in the current 10 days (hereafter one period) was measured with respect to temperature and precipitation within different periods. This involved first, the current period, then the first, second, third, and fourth previous period, respectively (as shown in the first row in Table 2-1). Second, NDVI in the current period was measured with respect to temperature and precipitation within 20 day intervals, initially covering the previous period through to the current period, then two periods prior to one period prior, three periods prior to two periods prior, and five periods prior to four periods prior (second row in Table 2-1). This same approach was repeated for 30 day periods, 40 day periods and 50 day periods (row 3–5 in Table 2-1).

Table 2-1 The time intervals during which precipitation is accumulated, and temperature is averaged (0 indicates the current 10-day period, 1 indicates the first previous 10-day period, 0_1 indicates from current period to the first previous period, etc.) (adapted from (Wang et al., 2003)).

Duration	**Lag**				
	0	1	2	3	4
1	0	1	2	3	4
2	0_1	1_2	2_3	3_4	4_5
3	0_2	1_3	2_4	3_5	4_6
4	0_3	1_4	2_5	3_6	4_7
5	0_4	1_5	2_6	3_7	4_8

The impacts of temperature and precipitation on the inter-annual variation of NDVI were investigated by applying a multiple regression to annual NDVI, mean temperature, and total precipitation. Annual NDVI in this study refers to the phenologically-tuned averaged NDVI in the entire study area throughout the growing season. Mean temperature refers to averaged temperature, and total precipitation refers to the accumulated precipitation during each growing season. While calculating mean temperature and total precipitation, the time lags of their effects on NDVI determined by the intra-annual relationships were considered.

2.5.4 Trend detection

The non-parametric Mann-Kendall test (M-K) has been widely used for trend detection of normally or non-normally distributed time series in the environmental sciences (Hirsch et al., 1982). It can be applied to detect trends in vegetation phenology, annual NDVI, mean temperature, total precipitation, and monthly NDVI. For monthly NDVI trends, it was applied to every month from April to October.

Taking NDVI as an example, given the annual NDVI time series $NDVI_1$, $NDVI_2$ …, $NDVI_n$ are the sequential data values, n (23 in this study) is the data set record length, the M-K test statistic S is given by the formula:

$$S = \sum_{k=1}^{n-1} \sum_{J=k+1}^{n} sgn(NDVI_j - NDVI_k) \quad (2.1)$$

Where $NDVI_j$ and $NDVI_i$ are the annual values in years j and k, j > k, respectively, and

$$sgn\left(NDVI_j - NDVI_k\right) = \begin{cases} 1 & NDVI_j - NDVI_k > 0 \\ 0 & NDVI_j - NDVI_k = 0 \\ -1 & NDVI_j - NDVI_k < 0 \end{cases} \quad (2.2)$$

The variance of S is computed as:

$$VAR\ (S) = \frac{n(n-1)(2n+5)}{18} \quad (2.3)$$

The test statistic Z is calculated as below:

$$Z = \begin{cases} \frac{S+1}{\sqrt{VAR\ (S)}} & S > 0 \\ 0 & S = 0 \\ \frac{S-1}{\sqrt{VAR\ (S)}} & S < 0 \end{cases} \quad (2.4)$$

The statistical trend of mean NDVI is evaluated using the Z value. A negative (positive) Z value indicates a downward (upward) trend, and a zero Z value means that the time series data have no trend. The significance of the detected trend is tested based on 0.05 and 0.10 significance levels.

2.5.5 NDVI baselines

Statistically, values beyond two standard deviations of the mean can be defined as anomalies (Gliner et al., 2010). A 0.5 standard deviation value was used to define AVHRR NDVI baselines after Thaim (2003). However, this was too low to highlight sensitive areas (Li et al., 2004). A two standard deviation value was used to create NDVI baselines for the Northern Great Plains and define the NDVI anomalies (Piwowar, 2011). Thus, two standard deviations were also used in this study to establish NDVI baselines in GNP. Annual NDVI baselines were established by subtracting two standard deviations from mean NDVI value of 1985–2007. The same method was used to create monthly NDVI baselines from April to October.

2.6 Results

2.6.1 Applicability of AVHRR/NDVI

The averaged dry biomass and NDVI from sample sites and the mean NDVI in the study area are shown in Figure 2-1. Biomass and NDVI demonstrated clear inter-annual consistency indicated by the larger amount of dry biomass and the corresponding higher NDVI values in 2003 and

2004, and the smaller amount of biomass and reduced NDVI in 2005. Within each year, biomass variation is reasonably represented by the changes of NDVI. In addition, NDVI from the sampled area reasonably represents the mean NDVI in the study area. The seasonal and inter-annual consistency of NDVI and biomass supports the common use of NDVI to study vegetation response to climate variation (Anyamba and Eastman, 1996; Kogan, 1997).

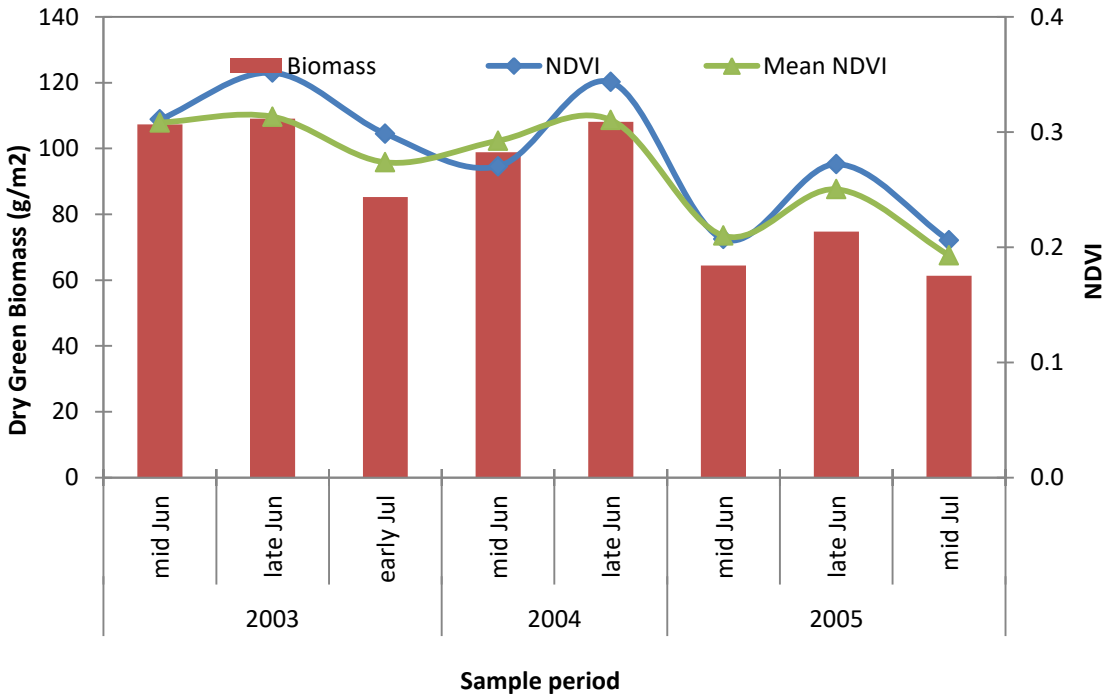

Figure 2-1 Biomass versus NDVI in the sampling sites and the mean NDVI in the west block of GNP from mid-June to mid-July in 2003, 2004, and 2005.

2.6.2 Relationships between NDVI and climate variables

The intra-annual relationships among NDVI, temperature and precipitation at various lags are shown in Figure 2-2. The mean temperature in the current period shows the most significant effect on NDVI with an r value of 0.63 (P = 0.000), followed by the mean temperature during the previous two periods (r = 0.62) (Figure 2-2(a)). Precipitation during the 50-day span ending with the current period ("4_0" in Table 2-1) has the strongest correlation with NDVI in the current period, indicated by an r value of 0.69 (P = 0.000) (Figure 2-2(b)).

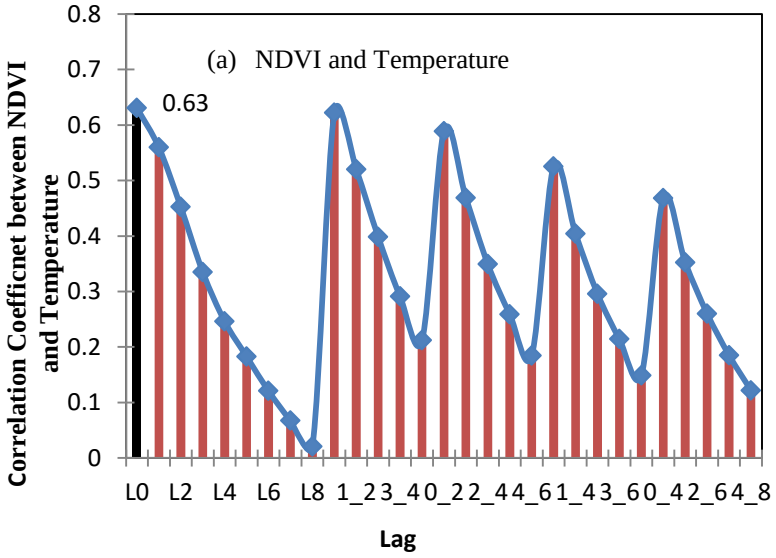

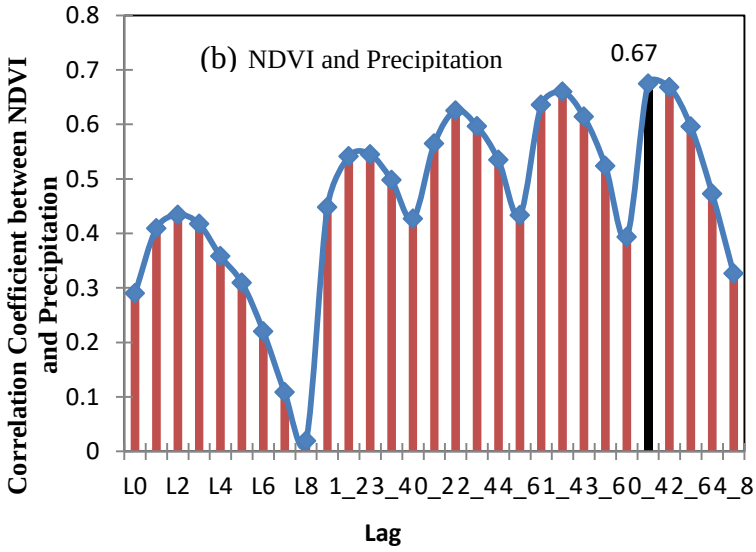

Figure 2-2 Intra-annual relationships between (a): NDVI and temperature and (b): NDVI and precipitation.

The multiple regression approach was applied to evaluate the impacts of temperature and precipitation on the inter-annual variation of NDVI, with the outcome shown in the following Equation:

$$V = -0.43 + 0.01 * T + 0.19 * Lg(P_r) \quad (r^2 = 0.30;\ n = 23;\ P < 0.05) \tag{2.5}$$

where V is phenologically-tuned annual NDVI; T is mean temperature (°C); P_r is the total precipitation (mm) throughout the growing season, considering the lag effects described above; $Lg(P_r)$ is the logarithm 10 transformed precipitation; n (23) is the number of years.

Multiple regression analysis indicates that the co-effects of temperature and precipitation on Inter-annual variation of NDVI in GNP is statistically significant. The r^2 value indicated that temperature and precipitation can account for 30% of the inter-annual variation of NDVI. Spearman correlation analyses were also performed to determine the effects of temperature and precipitation separately. The results show that the effect of temperature on interannual NDVI variation is not significant ($P > 0.10$), while the impact of precipitation is significant ($P < 0.05$).

2.6.3 Trends of phenology

The results of the trend analysis on green-up, peak growth and senescence are demonstrated in Table 2-2. The negative Z value of green-up indicates that vegetation in GNP tended to start growing earlier during 1985 to 2007. The positive Z values show that both peak growth and senescence were significantly delayed at the 0.10 significance level.

Table 2-2 The trends of green-up, peak growth, and senescence indicated by the Z values during 1985-2007 in GNP.

Phenology	**Green-up**	**Peak Growth**	**Senescence**
Z value	-0.79*	1.75*	0.16*

* indicates the significance at the 0.10 level

2.6.4 Trends of NDVI, temperature, and precipitation

The results of the M-K test on annual NDVI, mean temperature, total precipitation throughout the growing season, and monthly NDVI are shown in Table 2-3. During the 1985-2007 period, annual NDVI had an increasing trend indicated by the positive Z value (0.26). Both annual temperature and precipitation demonstrated a significant increasing trend indicated by the positive Z values of 0.03 and 0.08, respectively. The temperature trend is significant at the 0.05 level, while the precipitation is at the 0.10 level.

Positive Z values indicate that monthly NDVI in April, May, August, September, and October all show increasing trends, which are statistically significant at the 0.10 level. The slightly increased monthly NDVI can be explained by the earlier green-up and later senescence that was driven by increased temperature and precipitation.

Table 2-3 The trends of annual NDVI, temperature, and precipitation throughout the growing season, and monthly NDVI from April to October indicated by the Z values during 1985-2007 in GNP

Variables	Temperature	Precipitation	NDVI							
			Annual	Apr	May	Jun	Jul	Aug	Sept	Oct
Z values	0.03**	0.08*	0.18*	0.03*	0.08*	0.18*	0.13*	0.08*	0.03*	0.03*

Note: ** and * indicate significance at the 0.05 and 0.10 level, respectively.

2.6.5 NDVI baselines

Baselines of annual NDVI and monthly NDVI from April to October and the years in which NDVI were out of baseline are listed in Table 2-4. The baseline of annual NDVI ranges from 0.13 to 0.32. The largest baseline range (0.12-0.40) was observed in June, followed by July and August, while the smallest baseline range (0.06-0.20) occurred in October. In 1986 and 2000, monthly NDVI values in April are below the low limit of the baseline. 1999 was the only year in which monthly NDVI in May to July and annual NDVI are beyond the upper baselines. Other NDVI and monthly NDVI values were all within the baselines.

Table 2-4 Baselines of monthly and annual NDVI and years out of baselines from 1985 to 2007

	NDVI Baselines		Years out of baselines	
Time Period	**Low limit**	**Upper limit**	**Below low baseline**	**Above upper baseline**
April	0.02	0.22	1986, 2000	/
May	0.09	0.30	/	1999
June	0.12	0.40	/	1999
July	0.13	0.39	/	1999
August	0.08	0.34	/	/
September	0.07	0.27	/	/
October	0.06	0.20	/	/
Annual	0.13	0.32	/	1999

2.7 Discussion

2.7.1 Climate variables and NDVI

The significant effect of temperature on vegetation is consistent with the assertion of Mitchell and Csillag (2001) that seasonal temperature has a strong impact on grass productivity in GNP, based on prescribed temperature trends in the Century model. The finding of a significant relationship between precipitation and phenologically-tuned NDVI is consistent with the finding of Wang et al. (2003) that precipitation and NDVI in central Great Plains North America are strongly correlated at a particular temporal scale. The 40-day influence lag of precipitation and non-lag effect of temperature on NDVI indicate that the impact of precipitation lasts much longer than that of temperature in GNP. The statistically significant relationship between temperature, precipitation and vegetation productivity indicated that integrating them with remote sensing data may yield better NPV biomass estimation than using remote sensing data only.

Variation in climate is the major contributor to interannual NDVI variation because the effects of grazing and fire were negligible during the study period (Li and Guo, 2012). However, temperature together with precipitation, can only account for 30% of inter-annual NDVI variation. The unexplained portion of the inter-annual variation might be accounted for by variation in other environmental variables such as soil moisture that is controlled by precipitation

(Frank, 2003), wind (Magagi and Kerr, 1997), topography (Bindlish et al., 2008), soil type and humus in soil (Nicholson and Farrar, 1994).

Although co-effects of temperature and precipitation on the interannual variation of NDVI in GNP are statistically significant, these statistics indicate that the effect of temperature on the interannual NDVI variation is not significant ($P>0.10$), while the impact of precipitation is significant ($P<0.05$) at the 0.05 level. The finding that precipitation is more important than temperature on interannual variability of vegetation productivity in GNP agrees with the findings of Mitchell and Csillag (2001) based on the manipulated climate scenario in the Century model. It is also supported by the assertion of Coughenour (1985) that vegetation growth in northern semi-arid mixed grassland is primarily constrained by soil moisture, which is largely determined by precipitation (Kogan, 1997). Soil moisture or evapotranspiration data can be used to further investigate the impact of climate variation on vegetation condition in semi-arid mixed grassland, although these are not regular observational data reported by weather networks.

2.7.2 Trends of phenology, NDVI, temperature, and precipitation

A trend towards earlier green-up supports earlier conclusions that the growing season starts earlier at higher northern latitudes (Keeling et al., 1996; Randerson et al., 1999). Earlier green-up can be explained by increased winter temperature in southern Canada (Zhang et al., 2000). Delayed peak growth may be related to this increased annual maximum temperature (Zhang et al., 2000), which stunts vegetation development. Later senescence may be attributed to the increased minimum temperature that can delay the onset of frost (Zhang et al., 2000). Increased annual mean temperature and precipitation may increase the length of growing season (Li and Guo, 2012), and thus account for the delayed peak growth and senescence.

Increased mean temperature during the growing season is consistent with the fact that annual mean temperature has been increasing from 1900-1998 in southern Canada (Randerson et al., 1999). Also, the increasing trend of precipitation is consistent with the finding that precipitation in Canadian prairies has increased (Zhang et al., 2000, Akinremi et al., 1999). The increasing trend of annual NDVI can be accounted for by the increased temperature and precipitation.

2.7.3 Baselines of NDVI

Monthly NDVI anomalies in April of 1986 and 2000 may be explained by cold events in the winters of 1985–1986 and 1999–2000. The occurrence of NDVI anomalies in 1999 may be accounted for by the lag effect of anomalous warming associated with the largest El Niño/Southern Oscillation (ENSO) phenomenon observed last century during June 1997 to May 1998 (Anyamba et al., 2001; McPhaden, 1999). However, drawing a firm conclusion on the relationship between NDVI anomalies and ENSO events requires further study. Multiple temporal scales of the impact of temperature and precipitation, as well as extreme climate events (e.g., ENSO) on vegetation conditions, could be further investigated with longer data time series.

2.8 Conclusions

The comparisons between NDVI and biomass indicate that AVHRR 1 km spatial resolution NDVI data are suitable for monitoring vegetation condition in GNP. Estimates of the curvature-change rate of NDVI indicate that vegetation green-up started in mid-April to mid-May, peak growing season was reached in late June to mid-July, and senescence typically began in early to late July. Trend analyses indicated that vegetation growing season had a lengthening trend from 1985 to 2007 with an earlier green-up and later senescence. Concurrently, peak growth tended to be later.

The study of the effects of precipitation and temperature on intra-annual NDVI variation concluded that temperature has significant effects on NDVI variation with no time lag. At the same time, the mean temperature in the previous 10-day period has the second greatest impact on NDVI variation. Precipitation has stronger effects on NDVI than temperature with a lag of 40 days. Temperature and precipitation account for 30% of inter-annual NDVI variation. However, measured separately, the influence of precipitation is statistically significant, while the effect of temperature is not. Phenologically-tuned annual NDVI demonstrated an increasing trend. There was a significant increasing trend for both annual temperature and precipitation, which accounted for the increasing trend of annual NDVI. Monthly NDVI demonstrated an expanding trend in each month from April to October.

The annual AVHRR NDVI baselines range from 0.13 to 0.32. With climate variation, annual NDVI in most years of 1985-2007 are within the baselines. The only exception is 1999. Monthly NDVI baselines from April to October were also established, and most monthly NDVI are within the baselines. The exceptions are monthly NDVI in April of 1986 and 2000 that are below minimum baselines, and monthly NDVI in May to July in 1999 that are above maximum baselines.

This study measured vegetation phenology in GNP that is needed to remotely sense NPV biomass as studied in Chapters 3 and 4. It also demonstrates the successful application of AVHRR NDVI products on climate change studies in the northern mixed prairie. By comparing retrieved NDVI values from AVHRR composites to the created NDVI baselines, park managers can evaluate climatic effects on vegetation in every month for any year and thus adjust corresponding conservation plans (e.g., prescribed fire or grazing) to minimize these effects. The approaches used in this study can be applied to other areas to investigate vegetation response to climate variation.

2.9 Addendum

To allow this Chapter to better fit this dissertation, I have updated the abstract, replaced the first two paragraphs in the introduction, deleted study site information, and reorganized the original ‘results and discussion’ into two separate sections.

CHAPTER 3: GROUND HYPERSPECTRAL, LANDSAT 8 OLI, AND SENTINEL-2A DATA FOR NON-PHOTOSYNTHETIC VEGETATION BIOMASS ESTIMATION

3.1 Preface

This chapter was submitted as a manuscript to the International Journal of Remote Sensing (IJRS) on Dec 15, 2016. The IJRS is published by Taylor & Francis Group. If this research is published, the Group will allow me to reuse it as content for a thesis or dissertation at no cost as long as a permission request is submitted.

Li Z and Guo X. (2016) Quantifying non-photosynthetic vegetation (NPV) biomass in semiarid mixed grasslands using Landsat 8 OLI and Sentinel-2A images. International Journal of Remote Sensing (revison submitted in July, 2017).

Zhaoqin Li came up with the idea, analyzed the data, interpreted the results, and wrote the manuscript. Dr. Xulin Guo provided valuable comments to improve the quality of the paper.

3.2 Abstract

Research on quantifying Non-photosynthetic vegetation (NPV) with optical remote sensing approaches has been focusing on optically distinguishing NPV from green vegetation and bare soil. With a very similar spectral response curve to NPV, dry moss is a significant component in semiarid mixed grasslands and plays a large role in NPV estimation. However, limited attention has been paid to this role. We investigated the potential of optical remote sensing to distinguish NPV biomass in semiarid grasslands characterized by NPV, biological soil crust (BSC) dominated by moss and lichen, and bare soil. First, hyperspectral spectral indices were examined to determine the most useful spectral wavelength regions for NPV biomass estimation. Second, multispectral red-edge indices and shortwave-infrared indices were simulated based on Landsat 8 OLI and Sentinel-2A MSI band reflectance, respectively, to determine the most suitable multispectral indices for NPV estimation. Those multispectral indices were then applied to Landsat 8 OLI images and Sentinel-2A images acquired in early, middle, peak, and early

senescence growing seasons to investigate the potential of satellite images for quantifying NPV biomass. Our results indicated that red-edge hyperspectral indices, such as modified red-edge Normalized Difference Vegetation Index ($mNDVI_{705}$), Plant Senescence Reflectance Index (PSRI), and Normalized Difference Vegetation Index ($NDVI_{705}$), are better than shortwave-infrared hyperspectral indices (e.g., Cellulose Absorption Index (CAI)) for quantifying NPV biomass. Multispectral Landsat 8 OLI and Sentinel-2A MSI images demonstrated potential for NPV estimation in peak and (or) early senescence growing season using multispectral shortwave indices (NDI5) and multispectral red-edge indices ($NDVI_{red\text{-}edge}$). The performance of $NDVI_{red\text{-}edge}$ and NDI5 are similar in middle to early senesces seasons, while $NDVI_{red\text{-}edge}$ is better than NDI5 for NPV biomass estimation in early growing season.

3.3 Introduction

NPV plays an essential role in maintaining soil and site stability and affects nutrient, energy, and water cycling among air, vegetation, water, and soil (Facelli and Pickett, 1991). It also controls frequency and intensity of fires and grazing in grassland ecosystems (Nagler et al., 2003; Guerschman et al., 2009). These roles can directly and indirectly affect ecosystem functioning through influence on ecosystem vigor, organization, and resilience.

The ecological importance of NPV has driven considerable research on estimating its fractional cover using optical remote sensing data in croplands (Daughtry et al., 2006; McNairn and Protz, 1993; Serbin et al., 2013), savannah (Guerschman et al., 2009; Jackson and Prince, 2016; Li et al., 2016), shrublands (Asner and Heidebrecht, 2003), grasslands (Smith et al., 2015; Xu et al., 2014), forests (Roberts et al., 1993), and the Otindag Sandy Land of China (Li et al., 2016). Studies have also been conducted to quantify NPV biomass in grazed vegetation communities in the Amazon (Numata et al., 2008), the inner Mongolian steppe (Ren and Zhou, 2012), and pastoral Sahel in the Gourma region of East Africa (Jacques et al., 2014). These studies have demonstrated the potential of optical remote sensing data, especially hyperspectral data, for NPV estimation.

Studies of NPV estimation using optical remote sensing data have been focused on differentiating NPV from bare soil and green vegetation (Li and Guo, 2016), with little attention

to the effects of Biological Soil Crust (BSC). NPV can be separated from bare soil using shortwave-infrared (SWIR) spectral indices. This is because NPV has high lignin and cellulose content, showing strong absorption features in the shortwave wavelength regions of the NPV spectral response curve (Figure 1-2), unlike bare soil. Shortwave spectral indices, such as the Cellulose Absorption Index (CAI) (Daughtry et al., 1996), Lignocellulose Absorption Depth (LCD) (Numata et al., 2008) and Lignocellulose Absorption Area (LCA) (Numata et al., 2008) are commonly used for quantifying NPV (e.g., Daughtry et al., 2006; Ren and Zhou, 2012; Serbin et al., 2013). The lignin and cellulose absorption features in shortwave wavelength regions of green vegetation are obscured by the high water content of green vegetation (Figure 1-2). Therefore, optical remote sensing of NPV biomass using SWIR spectral indices becomes difficult where the fraction of green vegetation is greater than 30% (Ren and Zhou, 2012; Daughtry et al., 2004). In addition, the presence of considerable amounts of BSC, including moss and lichen in semiarid and arid grasslands, makes NPV estimation more challenging. This is because dry moss has very similar optical characteristics to NPV throughout the 400 to 2500 nm wavelength range (Figure 1-4) (Li and Guo, 2016; Smith et al., 2015). Consequently, in grasslands where there are large amounts of NPV and green vegetation with the presence of BSC and bare soil, such as Canadian mixed prairies, no solution has been found for quantifying NPV biomass using optical remote sensing data (Cihlar, 2012).

NPV can be distinguished from green vegetation by their different spectral responses in the visible (400-690 nm) and the near-infrared (NIR) (750-1200 nm) (Asner, 1998; Cao et al., 2010), and the red-edge position (690-750 nm). This is because NPV has much less chlorophyll content and less complex leaf structures (Asner, 1998; Nagler et al., 2003; Numata et al., 2008; Serbin et al., 2013). In this regard, spectral indices developed based on visible and NIR spectral bands, such as the Normalized Difference Vegetation Index (NDVI) and a difference index between green and red bands ((Green-Red)/(Green+ Red)), are useful for quantifying NPV. However, such spectral indices are highly influenced by the presence of bare soil (Colwell, 1974; Huete et al., 1985) and BSC (Karnieli et al., 1996).

The red-edge region is a chlorophyll absorption-to-leaf scattering transition zone (Clevers et al., 2002). The shape of the red-edge region is primarily controlled by the slope of the reflectance

curve (Filella and Penuelas, 1994), which is strongly affected by canopy vertical structure (e.g., Leaf Area Index) (Delegido et al., 2008; Lee et al., 2004). Red-edge position is also impacted by leaf chlorophyll content, meaning a decrease in chlorophyll content will shift it towards the shorter wavelength (Dash and Curran, 2004; Filella and Penuelas, 1994). These characteristics allow NPV to be distinguished from green vegetation, dry moss, and bare soil using the differences in structure and chlorophyll content. The slope of the reflectance curve of the red-edge region is the best wavelength region for separating NPV and dry moss (Figure 1-4). Hence, red-edge spectral indices are expected to have the most potential for NPV biomass estimation in grasslands where BSC is a considerable component.

The purpose of this study was to explore the potential of optical remote sensing data for estimating NPV biomass in Canadian mixed grass prairie where NPV estimation is not only affected by green vegetation and bare soil, but is also impacted by the availability of BSC. To achieve the objective, hyperspectral red-edge and SWIR spectral indices were used to investigate the potential of optical remote sensing data for NPV biomass estimation. Then, multispectral indices calculated from the simulated Landsat 8 OLI and Sentinel-2A MSI reflectance were examined to determine the most suitable multispectral indices for quantifying NPV biomass. Finally, the most suitable multispectral indices were applied to evaluate the potential of Landsat 8 OLI and Sentinel-2A MSI images for NPV biomass estimation.

3.4 Datasets

3.4.1 Field data

Field data used for this chapter are ground hyperspectral reflectance, dry vegetation biomass, and the ground cover data sampled in 2009, 2011, 2013, and 2016. Ground cover data include the fractional cover of green grass, forb, shrub, standing dead vegetation, plant litter on the surface, bare soil, moss, lichen, and rock. The ground cover estimation is summarized in Table 1-5.

3.4.2 Satellite images

Satellite data used in this study are the Landsat 8 OLI level 1T images from June 18, 2013, July 30, 2014, June 10, June 17, and July 3, 2016, and the Sentinel-2A level-1C images on May 3, June 12, and July 22 of 2016. Data were downloaded from the website of United States Geological Survey (USGS) (http://earthexplorer.usgs.gov/). The characteristics of the Landsat 8 OLI and Sentinel-2A images are summarized in Table 3-1. Both Landsat 8 OLI level 1T and Sentinel-2A level 1C products are geometrically corrected. Atmospheric correction was applied to all Landsat 8 OLI and Sentinel-2A images before surface reflectance retrieval. The Landsat 8 OLI images were atmospherically corrected using the ATCOR module in Geomatica PCI 2016. The Sentinel-2A images were atmospherically corrected using Sen2cor software provided by the European Space Agency (ESA) (http://step.esa.int/main/third-party-plugins-2/sen2cor/). At each ground sampling site, reflectance was retrieved within 3 × 3 pixels of the Landsat 8 OLI images, 9 × 9 pixels (Band 2, 3, 4, and 8) and 5 × 5 pixels (Band 5, 6, 7, 8a, 11 and 12) of the Sentinel-2A images to match the 100 × 100 m sample plot size. Retrieved reflectance within each sample site was averaged to represent the site.

Table 3-1 The characteristics of Landsat 8 OLI and Sentinel-2A imagery (only bands analyzed in this study are included).

Landsat 8 OLI			Sentinel-2A MSI		
Band	wavelength (nm)	spatial resolution (m)	Band	wavelength (nm)	spatial resolution (m)
Band 2 (Blue)	450-510	30	Band 2 (Blue)	458-522	10
Band 3 (Green)	530-590	30	Band 3 (Green)	543-577	10
Band 4 (Red)	640-670	30	Band 4 (Red)	650-679	10
			Band 5 (Red-edge 1)	698-712	20
			Band 6 (Red-edge 2)	731-747	20
Band 5 (NIR)	850-880	30	Band 8a (NIR plateau)	856-875	20
Band 6 (SWIR1)	1570-1650	30	Band 11 (SWIR 1)	1566-1655	20
Band 7 (SWIR2)	2110-2290	30	Band 12 (SWIR 2)	2101-2280	20

Note: only bands analyzed in this study are included.

3.5 Spectral indices

3.5.1 Hyperspectral indices

Red-edge and SWIR hyperspectral indices are potentially useful for quantifying NPV as discussed in the Introduction section. The commonly used red-edge and shortwave hyperspectral indices in the literature (Table 3-2) were calculated from ground hyperspectral reflectance and used to investigate the potential of optical remote sensing data for NPV biomass estimation.

3.5.2 Multispectral indices

Multispectral indices were developed mainly based on NIR and shortwave wavelength regions to estimate NPV (Table 3-3). Based on the justification on the usage of red-edge and visible bands, we came up with green-red index, red edge Normalized Difference Vegetation Index ($NDVI_{red-edge}$), and modified red edge Normalized Difference Vegetation Index ($mNDVI_{red-edge}$) (Table 3-3). These multispectral indices were calculated from the simulated Landsat 8 OLI and Sentinel-2A MSI band reflectance from ground hyperspectral data to determine the most suitable spectral indices for quantifying NPV biomass. The determined spectral indices were then used to estimate NPV biomass with Landsat 8 OLI and Sentinel-2A MSI images. The spectral bands used for deriving multispectral indices are shown in Table 3-1.

3.5.3 Analysis

Prior to analysis, the hyperspectral measurements and NPV biomass data sampled within each site were averaged over the site to avoid spatial autocorrelation in the analysis. Outliers of the biomass data of the 3 years (2009, 2011, and 2013) were checked at the site level using SPSS. Outliers were detected using an upper threshold (75% percentile + 2.20 × (75% percentile - 25% percentile)) and a lower threshold (25% percentile - 2.20 × (75% percentile - 25% percentile)) (Hoaglin and Lglewicz, 1987). Values larger than the upper threshold or smaller than the lower threshold were identified as outliers. Two outliers were statistically identified and were double-checked with the photos taken at the sites. After removing outliers, measurements made at 36 sampling sites of all 3 years were used for analysis.

Ordinary linear regression was applied to quantify NPV biomass using hyperspectral indices and the simulated multispectral indices of 2009, 2011, and 2013. The most suitable multispectral indices were then derived from Landsat 8 OLI and Sentinel-2A MSI images acquired in 2016 to investigate the potential of multispectral satellite images for quantifying NPV biomass in mixed prairie grassland. The coefficients of determination (r^2) and Root Mean Square Error (RMSE) were used to evaluate the performance of hyperspectral and multispectral indices for NPV biomass estimation. NPV biomass maps were also created using NDI5 derived from Landsat 8 OLI images acquired on June 18, 2013 and July 30, 2014.

Table 3-2 The hyperspectral indices used for NPV estimation (ρ is reflectance and BD is band depth at the corresponding wavelength)

Category	Spectral index name	Spectral index expression	Citation	Primary application
	Cellulose absorption index (CAI)	$100 \times \left(\frac{\rho_{2000} + \rho_{2200}}{2}\right) - \rho_{2100}$	Daughtry et al., 1996	Crop residue cover
	Lignocellulose absorption depth (LCD)	$\max(BD_{2015-2155})$	Numata et al., 2008	Senesced grass biomass
NPV indices				
	Lignocellulose absorption area (LCA)	$\sum_{i=2015}^{2155} BD_i$	Numata et al., 2008	Senesced grass biomass
	Normalized difference Lignin index (NDLI)	$\frac{\log\left(\frac{1}{\rho_{1754}}\right) - \log\left(\frac{1}{\rho_{1680}}\right)}{\log\left(\frac{1}{\rho_{1754}}\right) + \log\left(\frac{1}{\rho_{1680}}\right)}$	Serrano et al., 2002	Surface plant litter
	Plant senescence reflectance index (PSRI)	$\frac{\rho_{680} - \rho_{500}}{\rho_{750}}$	Merzlyak et al., 1999	Plant stress
Red-edge indices				
	Red edge normalized difference vegetation index ($NDVI_{705}$)	$\frac{\rho_{750} - \rho_{705}}{\rho_{750} + \rho_{705}}$	Gitelson and Merzlyak, 1994	Plant stress

Modified red edge simple ratio index (mSR_{705})	$\frac{\rho_{750} - \rho_{445}}{\rho_{705} - \rho_{445}}$	Datt ,1999	Plant stress
Modified Red edge normalized difference vegetation index ($mNDVI_{705}$)	$\frac{\rho_{750} - \rho_{705}}{\rho_{750} + \rho_{705} - 2\rho_{445}}$	Datt, 1999; Sims and Gamon, 2002	Plant stress
Vogelmann red edge index 1 (VOG1)	ρ_{740}/ρ_{720}	Vogelmann et al., 1993	Vegetation phenology
Vogelmann red edge index 2 (VOG2)	$\frac{\rho_{734} - \rho_{747}}{\rho_{715} + \rho_{726}}$	Vogelmann et al., 1993	Vegetation phenology

Table 3-3 The multispectral indices used for NPV estimation

Spectral index name	Spectral index expression	Citation	Primary application
Normalized Difference Index (NDI5)	$(NIR - SWIR_1)/(NIR + SWIR_1)$	McNairn and Protz, 1993	Crop residue
Normalized Difference Index (NDI7)	$(NIR - SWIR_2)/(NIR + SWIR_2)$	McNairn and Protz, 1993	Crop residue
Normalized Difference Tillage Index (NDTI)	$(SWIR_1 - SWIR_2)/(SWIR_1 + SWIR_2)$	Van Deventer et al., 1997	Tillage practices
Normalized Difference Senescent Vegetation Index (NDSVI)	$(SWIR_1 - Red)/(SWIR_1 + Red)$	Qi et al., 2002	Senescent vegetation density
the soil adjusted total vegetation index (SATVI)	$\frac{(SWIR_1 - Red) \times (1 + L)}{(SWIR_1 + Red + L)} - SWIR_2/2$ $L = 1$ for low vegetation	Marsett et al., 2006	Herbaceous vegetation cover
soil-adjusted corn residue index (SACRI)	$\frac{\alpha(NIR - SWIR_1 - \beta)}{\alpha NIR + SWIR_1 - \alpha\beta}$	Bannari et al., 1995	Crop residue
modified soil-adjusted crop residue index (MSACRI)	$C \times \frac{\alpha(SWIR1 - \alpha SWIR2 - \beta)}{\alpha NIR + SWIR2 - \alpha\beta}$	Bannari et al., 2000	Crop residue
Green-red index	$(Green - Red)/(Green + Red)$	Motohka et al., 2010; Tucker, 1977	NPV estimation

*Red edge NDVI ($NDVI_{red\text{-}edge}$)	$\frac{(\mathrm{Red}_{\mathrm{edge1}} - \mathrm{Red}_{\mathrm{edge2}})}{(\mathrm{Red}_{\mathrm{edge1}} + \mathrm{Red}_{\mathrm{edge2}})}$	Gitelson and Merzlyak, 1996	Vegetation stress
*modified Red edge NDVI ($mNDVI_{red\text{-}edge}$)	$\frac{(\mathrm{Red}_{\mathrm{edge1}} - \mathrm{Red}_{\mathrm{edge2}})}{(\mathrm{Red}_{\mathrm{edge1}} + \mathrm{Red}_{\mathrm{edge2}} - 2\mathrm{Band1})}$	Datt, 1999; Sims and Gamon, 2002	Vegetation stress

Note: α and β are the slope and intercept of the soil line. C = 5 (a multiplicative constant). * marks the spectral indices that are adapted from hyperspectral red-edge indices and are only derived from simulated Sentinel-2A band reflectance and Sentinel-2A images.

3.6 Results

3.6.1 Hyperspectral indices for quantifying NPV biomass

Potential of hyperspectral shortwave-infrared and red-edge spectral indices for NPV biomass estimation was evaluated using the r^2 values in Figure 3-1 and Figure 3-2, respectively. In terms of shortwave spectral indices, both CAI and Normalized Difference Lignin Index (NDLI) have an r^2 of 0.44 and RMSE of 69 g/m^2 for quantifying NPV biomass (Figure 3-1a & 3-1b), while LCD and LCA (Figure 3-1c & 3-1d) do not have a significant relationship with NPV biomass.

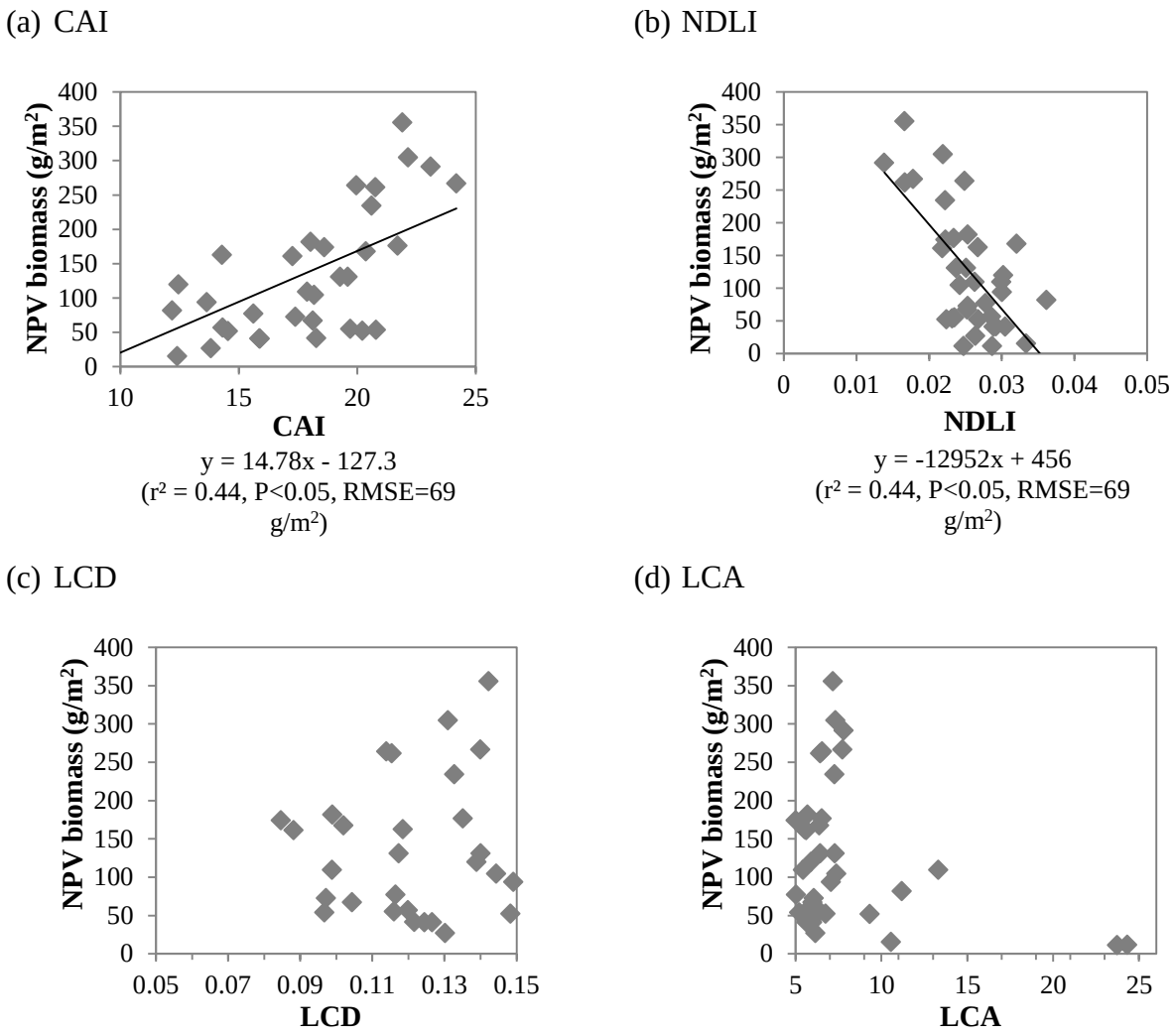

Figure 3-1 Shortwave-infrared spectral indices for Non-Photosynthetic Vegetation (NPV) biomass estimation in Grasslands National Park characterized by NPV, green vegetation, Biological Soil Crust (BSC), and bare soil.

Red-edge spectral indices can account for 41% to 65% of variations in NPV biomass with RSME values ranging from 54 g/m^2 to 70 g/m^2 (Figure 3-2). Plant Senescence Reflectance Index (PSRI) and mNDVI$_{705}$ have the best performance, with r^2 values of 0.64 and 0.65 respectively. Vogelmann red edge index (VOG1 and VOG2) with r^2 values of 0.46 and 0.41 respectively are inferior to other investigated red-edge spectral indices for NPV biomass estimation.

(a) PSRI

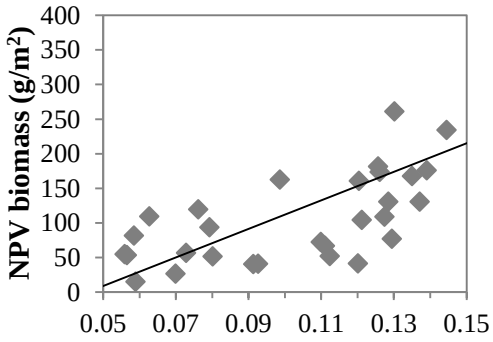

y = 2065.1x - 94.5
(r^2 = 0.64, P<0.05, RMSE=55 g/m^2)

(b) $NDVI_{705}$

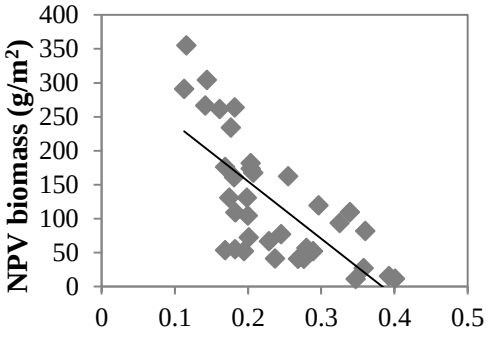

y = -845.8x + 323.9
(r^2 = 0.51, P<0.05, RMSE=64 g/m^2)

(c) mSR_{705}

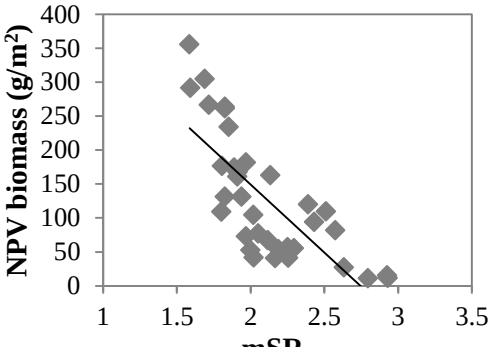

y = -200.2x + 549.4
(r^2 = 0.58, P<0.05, RMSE=59 g/m^2)

(d) $mNDVI_{705}$

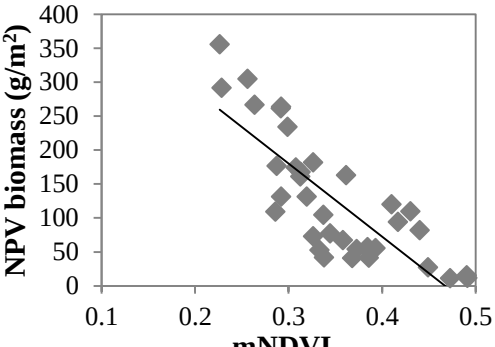

y = -1077.2x + 503.32
(r^2 = 0.65, P<0.05, RMSE=54 g/m^2)

(e) VOG1

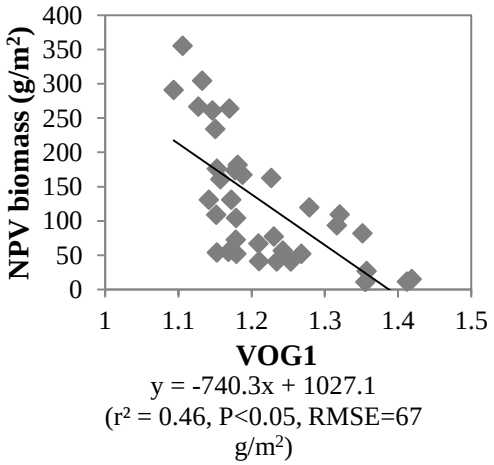

(f) VOG2

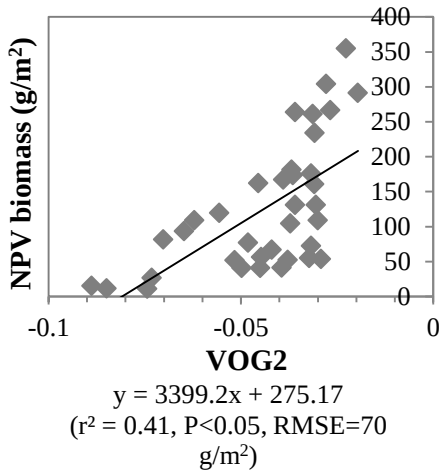

Figure 3-2 Red-edge spectral indices for Non-Photosynthetic Vegetation (NPV) biomass estimation in Grasslands National Park characterized by NPV, green vegetation, Biological Soil Crust (BSC), and bare soil (the sample number used for analysis is 36).

3.6.2. Simulated multispectral indices for quantifying NPV biomass

The r^2 values of the simulated multispectral indices of Landsat 8 OLI and Sentinel-2A MSI for NPV biomass estimation are presented in Table 3-4. Multispectral indices with good performance are determined. Then, the relationships between NPV biomass and the multispectral indices of Sentinel-2A are plotted as shown in Figure 3-3. The $mNDVI_{red\text{-}edge}$ has the largest r^2 value (0.67) and smallest RMSE (53 g/m^2), followed by Soil-Adjusted Corn Residue Index (SACRI) and Normalized Difference Index (NDI). Green/red index and $NDVI_{red\text{-}edge}$ also have fairly good performance indicated by a moderate r^2 value (0.51).

Table 3-4 The coefficient of determination (r^2) of the simulated multispectral indices for quantifying non-photosynthetic vegetation (NPV) estimation

Spectral indices	Landsat 8	Sentinel-2A
NDI5	0.61	0.62
NDI7	0.6	0.6
NDTI	0.35	0.36
NDSVI	0.1	0.12
SATVI	0	0
SACRI	0.64	0.64
MSACRI	0.22	0.25
Green/red	0.51	0.51
$NDVI_{red\text{-}edge}$	\	0.51
$mNDVI_{red\text{-}edge}$	\	0.67

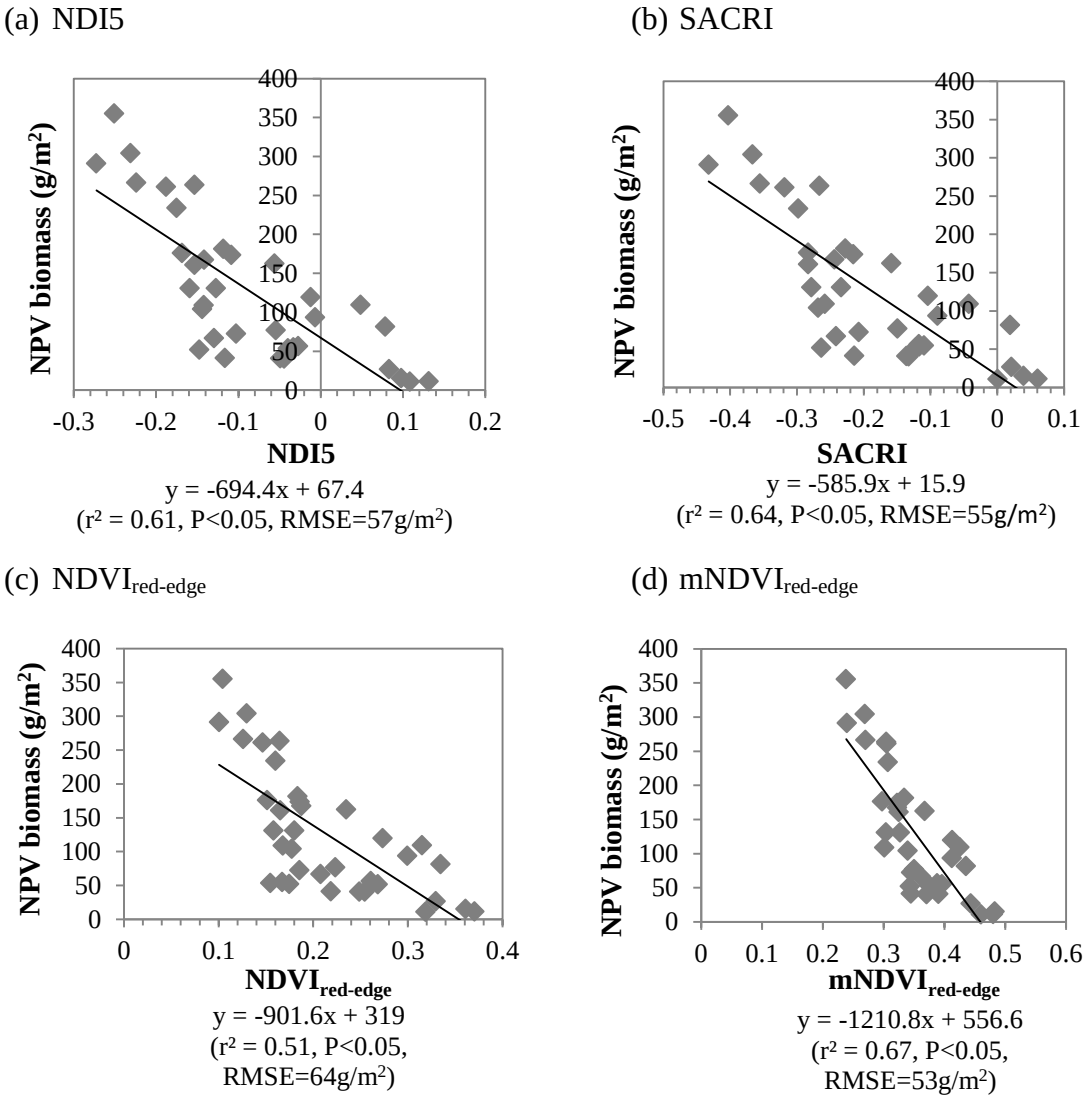

Figure 3-3 Simulated Sentinel-2A MSI multispectral indices for Non-Photosynthetic Vegetation (NPV) biomass estimation in Grasslands National Park characterized by NPV, green vegetation, Biological Soil Crust (BSC), and bare soil (the sample number used for analysis is 36).

3.6.2 Multispectral satellite images for quantifying NPV biomass

The multispectral NDI5, SACRI, and $NDVI_{red\text{-}edge}$ were selected to investigate the potential of multispectral satellite images for quantifying NPV biomass. Despite good performance, $mNDVI_{red\text{-}edge}$ was not used to investigate potential of Sentinel-2A images, because Band1 of Sentinel-2A images is designed for aerosol study. Potential of multispectral Landsat 8 images was explored using NDI5 and SACRI derived from the images acquired on June 10, June 17, and July 3, 2016 (Figure 3-4). In addition to NDI5 and SACRI, $NDVI_{red\text{-}edge}$ was also used for NPV estimation using Sentinel-2A MSI images acquired on May 3, June 12, and July 22, 2017 (Figure

3-5). The relationship between spectral indices and NPV biomass is highly affected by the disturbed community (the data marked by a triangle in Figures 3-4 & 3-5) where smooth brome grass is dominant (Figure 1−6a). The triangle point cannot be removed, as it is not an outlier.

Landsat 8 OLI images performed best in the peak growing season (July 3) with an r^2 value of 0.50 and RMSE of 69 g/m^2, achieved by NDI5 (Figure 3-4e). NDI5 has very similar performance to SACRI, and their performance was enhanced as percentage of green vegetation increased from June 10 to July 3.

(a) NDI5 June 10, 2016

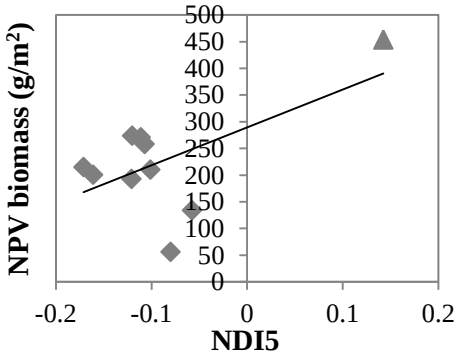

y = 709.1x + 289.4
(r^2 = 0.36, P<0.05, RMSE=78 g/m^2)

(b) SACRI June 10, 2016

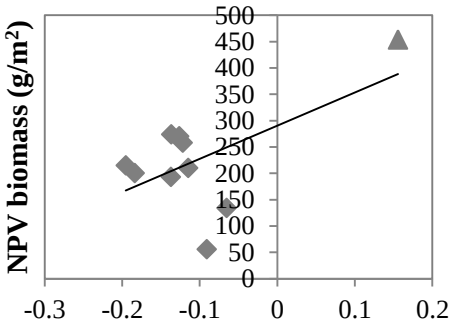

y = 628.6x + 290.4
(r^2 = 0.35, P<0.05, RMSE=78 g/m^2)

(c) NDI5 June 17, 2016

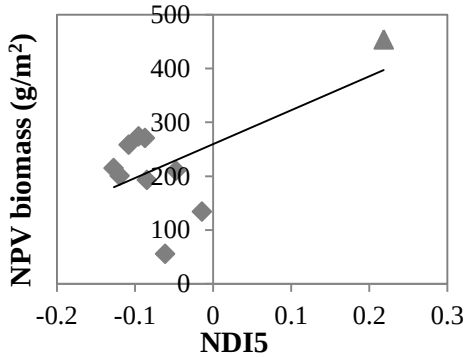

y = 628.1x + 259.5
(r^2 = 0.38, P<0.05, RMSE=77 g/m^2)

(d) SACRI June 17, 2016

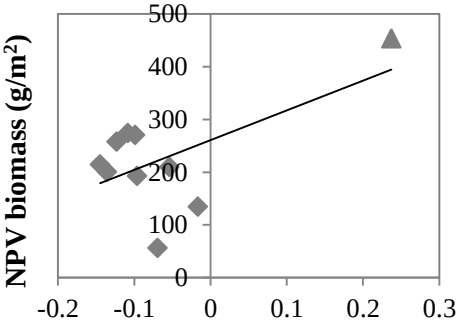

y = 563.7x + 260.9
(r^2 = 0.37, P<0.05, RMSE=78 g/m^2)

(e) NDI5 July 3, 2016

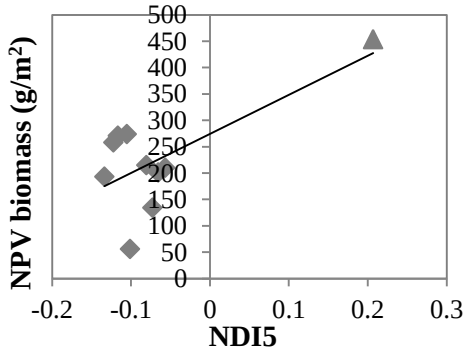

y = 741.3x + 274.5
(r^2 = 0.50. P<0.05, RMSE=69 g/m^2)

(f) SACRI July 3, 2016

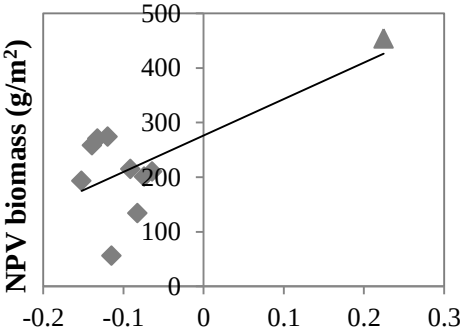

y = 668x + 276.4
(r^2 = 0.49, P<0.05, RMSE=70 g/m^2)

Figure 3-4 Normalized difference index (NDI5) and Soil-Adjusted Corn Residue Index (SACRI) of Landsat 8 OLI images acquired on June 10, June 17, and July 3, 2016 for quantifying NPV biomass (the sample number used for analysis is 10).

The best performance of Sentinel-2A MSI images was shown by NDI5 and $NDVI_{red\text{-}edge}$ with an r^2 of 0.43 and RMSE of 75 and 74 g/m^2 respectively using the image acquired on July 22, 2016 (the early senescence season). There are no Sentinel-2A MSI images available in the peak growing season for analysis. For all the three multispectral indices, NDI5, SACRI, and $NDVI_{red\text{-}edge}$, their performance was enhanced from early growing season (May 3), through middle growing season (June 12), to the early senescence season (July 22). In the early growing season, $NDVI_{red\text{-}edge}$ outperforms NDI5 and SACRI for NPV biomass estimation. In the middle growing season, NDI5 and $NDVI_{red\text{-}edge}$ have similar performance, which are better than that of SACRI. Like the application of Landsat 8 OLI images, the relationship between spectral indices of Sentinel-2A MSI images and NPV biomass is highly influenced by the triangle point (Figure 3-5) that is smooth brome community (Figure 1−6a).

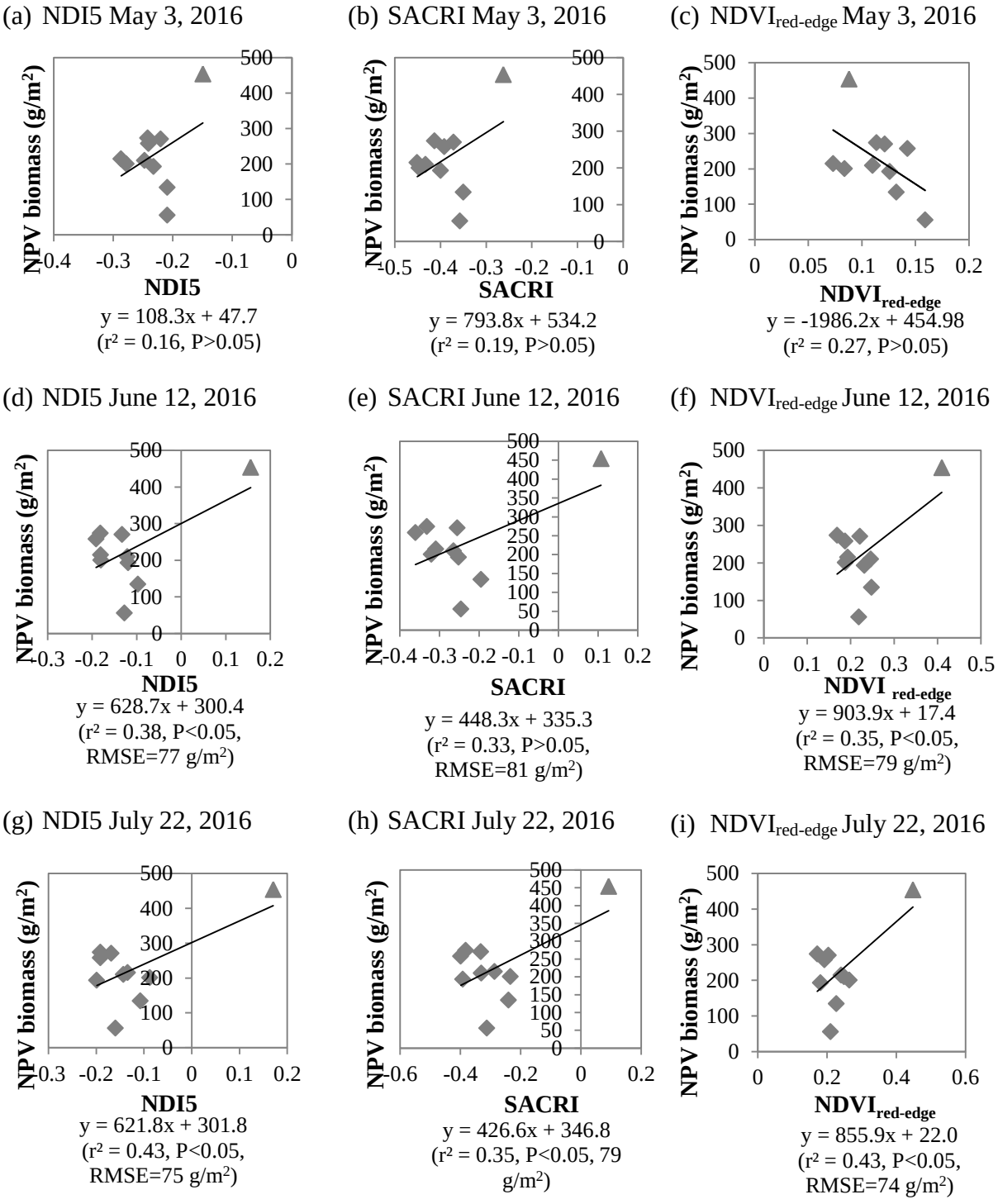

Figure 3-5 Normalized difference index (NDI5), soil-adjusted corn residue index (SACRI), and Red edge normalized difference vegetation index ($NDVI_{red-edge}$) of Sentinel-2A MSI images acquired on May 3, June 12, and July 22, 2016 for quantifying NPV biomass (the sample number used for analysis is 10).

1.1.4 NPV biomass maps

To further investigate if multispectral Landsat 8 OLI images can quantify spatial variations of NPV biomass, NPV biomass was estimated using NDI5 derived from the image acquired on June 18, 2013 (Figure 3-6). The relationship between NPV biomass and NDI5 was then applied to the Landsat 8 OLI images to create an NPV biomass map (Figure 3-7).

The NPV biomass can be quantified using NDI5 derived from the Landsat 8 OLI image with an r^2 of 0.42 and RMSE of 46.8 g/m^2.

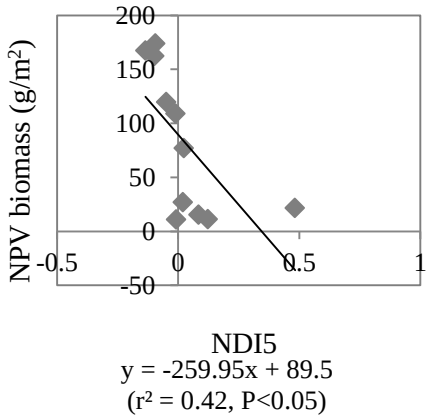

Figure 3-6 NPV biomass estimation using NDI5 derived from Landsat 8 OLI image acquired on June 18, 2013 (RMSE=46.8 g/m^2).

The NPV biomass map indicates low NPV biomass along the Frenchman River following the big wildfire in March 2013 that wiped out a large area along the valley. Spatial variations of NPV biomass generally correspond to land cover. However, extreme NPV biomass values were found in some areas, such as the Prairie dog town and disturbed community marked by the two red squares.

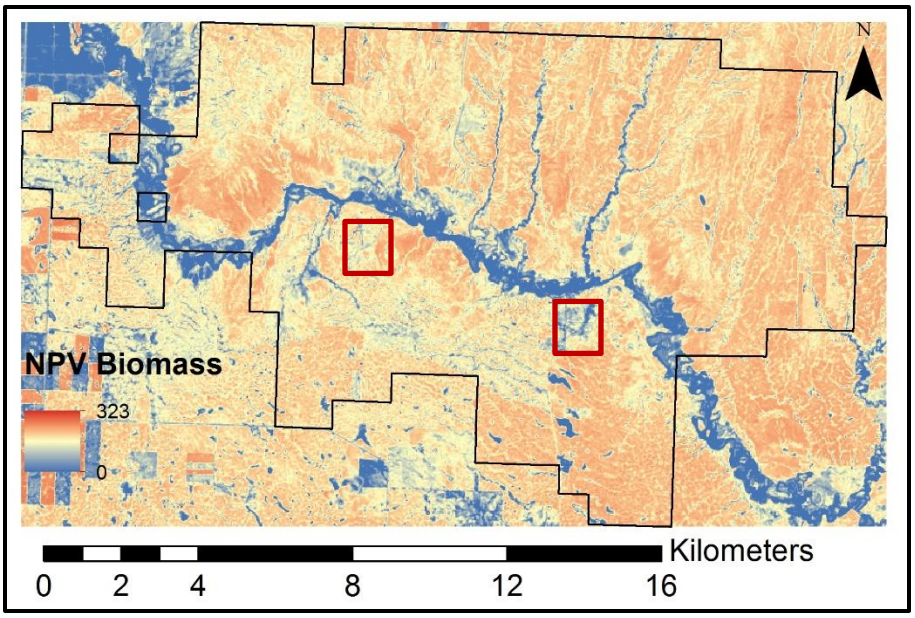

Figure 3-7 The NPV biomass estimation map using NDI5 derived from the Landsat 8 OLI image acquired on June 18, 2013 (RMSE=46.8 g/m^2).

NPV biomass was estimated using NDI5 derived from the image acquired on July 30, 2014 (Figure 3-8). The relationship between NPV biomass and NDI5 was then applied to the Landsat 8 OLI images to create an NPV biomass map (Figure 3-9). The NPV biomass can be quantified using NDI5 derived from the Landsat 8 OLI image with an r^2 of 0.50 and RMSE of 122 g/m^2. This map shows spatial variations of NPV biomass in the west block of GNP. It indicates high NPV biomass along the Frenchman River and low and high NPV biomass in the Prairie dog town and the disturbed alfalfa community marked by the two red squares on the map, respectively. The low NPV biomass in the Prairie dog town is accounted for by the exposed bare soil and the high NPV biomass of the alfalfa community is attributed to large biomass of alfalfa in previous years.

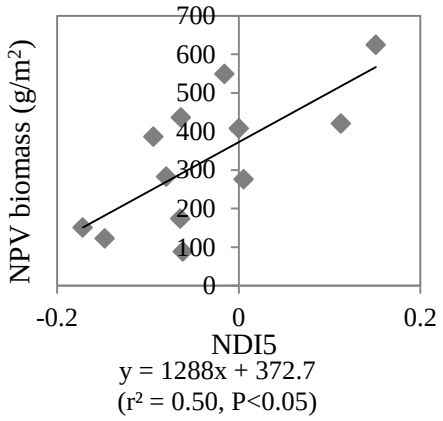

Figure 3-8 NPV biomass estimation using NDI5 derived from Landsat 8 OLI image acquired on July 30, 2014 (RMSE=122 g/m^2).

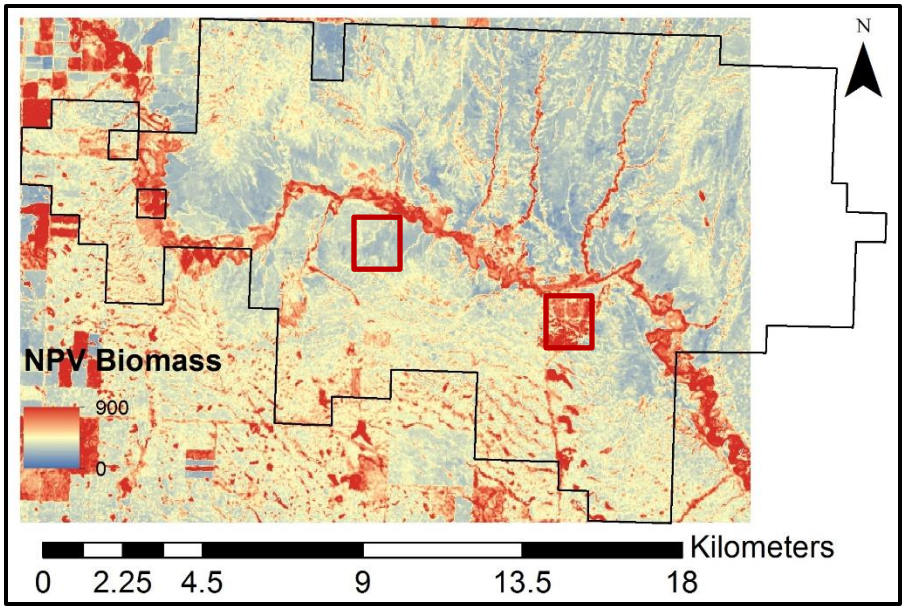

Figure 3-9 The NPV biomass estimation map using NDI5 derived from the Landsat 8 OLI image acquired on July 30, 2014 (RMSE=46.8 g/m^2).

3.7 Discussion

3.7.1 Spectral indices for NPV biomass estimation

Hyperspectral red-edge indices are generally superior to shortwave-infrared spectral indices for quantifying NPV biomass (Figures 3-1&3-2) in semiarid mixed grasslands, where ground cover consists of not only green vegetation, NPV, and bare soil, but also BSC. The best hyperspectral index for NPV biomass estimation is $mNDVI_{705}$, which incorporates reflectance at 445 nm that is sensitive to variations in caritinoid (Sims and Garmon, 2002). Generally, the good performance of hyperspectral red-edge indices is attributed to the sensitivity of red-edge position to the variations in chlorophyll content and structure (Filella and Penuelas, 1994; Lee et al., 2004; Delegido et al., 2008). However, the slope at the red-edge position may change as moisture content and age of NPV change (Daughtry et al., 1996), which affects the application of red-edge indices for NPV biomass estimation.

Despite inferiority to most hyperspectral red-edge indices investigated, hyperspectral shortwave-infrared indices have potential for quantifying NPV biomass because of the absorption features of cellulose and lignin in NPV. Nevertheless, such absorption features of cellulose and lignin can be obscured by water content of green vegetation when its fractional cover is larger than 30% (Daughtry et al., 2004; 2005). In addition, the similar spectra of NPV and dry moss in the shortwave-infrared regions also reduce the effectiveness of shortwave spectral indices. The r^2 value (0.44) of hyperspectral CAI for NPV biomass estimation is smaller than that ($r^2 = 0.67$) for Inner Mongolian desert steppes, where green vegetation cover is less than 30% (Ren and Zhou 2012). Hyperspectral CAI outperforms LCD and LCA for estimating NPV biomass in this study. This is inconsistent with the finding in a homogenous Amazon pasture (Numata et al., 2008). However, this does agree with the finding from the Inner Mongolian desert steppe that CAI outperformed LCD for NPV biomass estimation (Ren and Zhou, 2012). Notably, neither of these two studies considered the influence of both BSC and bare soil.

The simulated multispectral $mNDVI_{red\text{-}edge}$, followed by SACRI (normalized difference between NIR and SWIR1 with adjusting soil effects), NDI5 (normalized difference between NIR and SWIR1), and $NDVI_{red\text{-}edge}$, outperform the other investigated spectral indices for quantifying

NPV biomass. This highlights the importance of red-edge position. However, application of $mNDVI_{red\text{-}edge}$ to Sentinel-2A MSI images is difficult because Band 1 (Center wavelength: 443 nm; bandwidth: 20 nm) of Sentinel-2A MSI is very sensitive to aerosol. In addition, good performance of SACRI and NDI5 implies that the difference between NIR and SWIR1 bands is important for NPV biomass estimation. This finding is supported by our previous study in which NIR and SWIR were found to be very useful for fractional cover of NPV estimation in the study area (Xu et al., 2014).

The advantage of red-edge multispectral indices for quantifying NPV biomass was also demonstrated by the $NDVI_{red\text{-}edge}$ derived from Sentinel-2A MSI images. $NDVI_{red\text{-}edge}$ consistently has better performance than SACRI for NPV biomass estimation using Sentinel-2A satellite images. $NDVI_{red\text{-}edge}$ has very similar performance as NDI5 in middle growing season and early senescence season, but much better performance than NDI5 in early growing season (Figure 3-5). Although $NDVI_{red\text{-}edge}$ is the best index for NPV estimation in early growing season, the r^2 value is only 0.27. This indicates a need for hyperspectral images for quantifying NPV biomass in early growing season.

3.7.2 NPV biomass estimation at different vegetation growing stages

NPV estimation in grasslands needs to account for effects of fractional cover of NPV, green vegetation, bare soil, and BSC, and canopy structure. The best NPV biomass estimation was achieved in the peak growing season using Landsat 8 images acquired on July 3, 2016 (Figure 3-4). The increased green vegetation cover could mask NPV from nadir sensing in temperate grasslands where curing of green vegetation inconsistently and asynchronously occurs. Performance of each multispectral index for NPV biomass estimation changes at different vegetation growing stages (Figures 3-4&3-5). The amount of NPV is assumed unchanged from green-up until peak growing season. The change of performance of multispectral indices for NPV biomass estimation is mainly the consequence of change in ground cover from green-up to peak vegetation growing season.

In the early growing season when dead vegetation is dominant, the canopy is less dense compared to the peak and early senesces growing seasons. The less dense canopy increased

exposure of backgrounds including BSC, bare soil, and surface plant litter. Under such circumstances, NPV biomass is potentially overestimated because of the similar spectra of BSC and NPV. Presence of BSC and bare soil, and decay of surface plant litter (Serbin et al., 2013) contribute to canopy spectra. None of the investigated multispectral indices show a significant relationship with NPV biomass. Nonetheless, multispectral $NDVI_{red\text{-}edge}$ is superior to NDI5 and SACRI, because the red-edge wavelength region has the most potential to differentiate NPV from green vegetation, bare soil, and BSC (Figure 1-2 & 1-4a). In addition, SACRI is better than NDI5, because SACRI suppresses influence of bare soil.

From middle to peak and early senescence growing seasons, increased fractional cover of green vegetation, together with the pre-existing standing dead vegetation, form a denser canopy. A denser canopy decreases the exposure of BSC and bare soil. Thus, performance of NDI5, SACRI, and $NDVI_{red\text{-}edge}$ are all enhanced. However, the superiority of SACRI to NDI5 is no longer present (Figures 3-4 & 3-5). $NDVI_{red\text{-}edge}$ has very similar performance to NDI5.

This is the first study, to our knowledge, that has investigated the potential of red-edge spectral indices of optical remote sensing data in semiarid mixed grasslands characterized by large amounts of NPV, considerable amounts of BSC, and relatively low amounts of bare soil. This study explored the potential of multispectral Landsat 8 OLI and Sentinel-2A MSI images for quantifying NPV biomass, especially in peak and early senescence seasons. It indicated the potential to quantify spatial variations of NPV biomass using multispectral images, although performance of these multispectral images is highly associated with change of ground cover at different vegetation growing stages.

3.8 Further research

The relationships between spectral indices and NPV biomass change from negative to positive as fraction of ground cover changes. The hyperspectral $NDVI_{705}$ and simulated multispectral $NDVI_{red\text{-}edge}$ from hyperspectral reflectance decrease as NPV biomass increases (Figures 3-2 & 3-3). The relationship between multispectral $NDVI_{red\text{-}edge}$ calculated from Sentinel-2A MSI image acquired on May 3 and NPV biomass (Figure 3-5c) is also negative. However, the relationship changes to positive using the Sentinel-2A MSI images acquired on June 12 and July 22, 2016.

This transition of negative-to-positive relationship is controlled by fractional cover of NPV, green vegetation, BSC, and bare soil. When NPV cover is large, NPV cover is the dominant factor that influences $NDVI_{red\text{-}edge}$. An increase in NPV results in a decrease in $NDVI_{red\text{-}edge}$ (Figures 3-2, 3-3, & 3-5c). As green vegetation cover increases and NPV cover relatively decreases, green vegetation cover is the main factor that determines $NDVI_{red\text{-}edge.}$ For this reason, a positive relationship between NPV and $NDVI_{red\text{-}edge}$ was observed (Figure 3-5f & 3-5i). Our previous study has investigated the transition points of the negative-to-positive relationship between NDVI ((NIR-Red)/(NIR+Red)) and dead cover in the study area (Xu et al. 2014). Where the transition point from negative to positive $NDVI_{red\text{-}edge}$ and NPV relationship is, as well as what role BSC and bare soil play, need to further investigated.

The shortwave-infrared spectral indices NDI5 and SACRI are negatively correlated with NPV biomass using the simulated multispectral Landsat 8 OLI and Sentinel-2A MSI reflectance (Figure 3-2), while their relationships change to positive using Landsat 8 OLI and Sentinel-2A MSI images. As discussed on the relationship between $NDVI_{red\text{-}edge}$ and NPV biomass, the negative-to-positive relationship change of shortwave-infrared NDI5 and SACRI are also controlled by variations in fractional cover. The transition point of negative-to-positive relationship and the effects of BSC and bare soil on this relationship also need to be further explored.

3.9 Conclusions

Hyperspectral red-edge spectral indices, modified red-edge Normalized Difference Vegetation Index ($mNDVI_{705}$), Plant Senescence Reflectance Index (PSRI), modified Simple Ratio (mSR_{705}) and Normalized Difference Vegetation Index ($NDVI_{705}$), are better than shortwave-infrared hyperspectral indices, including Cellulose Absorption Index (CAI) for non-photosynthetic vegetation (NPV) biomass estimation. The best hyperspectral red-edge index is $mNDVI_{705}$ and the best shortwave-infrared index is CAI.

Multispectral Landsat 8 OLI and Sentinel-2A MSI images demonstrated potential for NPV estimation using shortwave-infrared multispectral indices (NDI5) and multispectral red-edge indices ($NDVI_{red\text{-}edge}$). However, performance of multispectral NDI5 and $NDVI_{red\text{-}edge}$ varies as

ground cover changes at different growing stages. The performances of NDI5 and $NDVI_{red\text{-}edge}$ are similar in middle to early senesces seasons, while $NDVI_{red\text{-}edge}$ is better than NDI5 for NPV biomass estimation in early growing season when the exposure of Biological Soil Crust (BSC) and bare soil is at the largest extent. The peak and (or) early senescence growing season, when the influence of BSC and bare soil is minimized, is the best time for NPV biomass estimation. The NPV biomass map shows potential of Landsat 8 OLI images for quantifying spatial variations of NPV biomass.

CHAPTER 4: NON-PHOTOSYNTHETIC VEGETATION BIOMASS ESTIMATION IN SEMIARID MIXED GRASSLAND FROM MULTI-ANGULAR, MULTI-TEMPORAL, AND MULTI-POLARIZATION RADARSAT-2 DATA

4.1 Preface

The main content of this chapter was accepted by Canadian Journal of Remote Sensing (CJRS) on August 1st, 2017. Like the IJRS, the CJRS is also published by Taylor & Francis Group which allows the published work to be reused as content of a dissertation with a request for permission.

Li Z and Guo X. (2017) Can Polarimetric Radarsat-2 images provide a solution to quantify non-photosynthetic vegetation biomass in semi-arid mixed grassland? Canadian Journal of Remote Sensing (accepted)

This manuscript was completed by Zhaoqin Li under the supervision of Dr. Xulin Guo, and the manuscript was improved by the valuable comments of Dr. Xulin Guo.

4.2 Abstract

Quantifying non-photosynthetic vegetation (NPV) biomass using optical remote sensing in semiarid mixed grassland is challenging. This is due to the combined effects of photosynthetic vegetation (PV), biological soil crust (BSC), and bare soil on the canopy spectra. Radarsat-2 provides a new way to quantify NPV biomass. This study investigated the potential of fine quad-pol Radarsat-2 images for quantifying NPV biomass and total aboveground biomass in semiarid mixed grasslands. The parameters used were Radar Vegetation Index (RVI), co-polarization ratio (HH/VV), cross-polarization ratios (VH/HH and VH/VV), de-Polarization ratio, the Cloude and Pottier decomposition component (Entropy and Alpha angle) and the Freeman-Durden decomposition components (volume, surface, and multiple scattering). The best NPV and total aboveground biomass estimations are achieved with an r^2 of 0.70 and 0.51 and relative Root Mean Square Error (rRMSE) of 9% and 8.4%, respectively, using the VH/VV cross-polarization ratio of the FQ23 (41.9°-43.3°) image in the middle growing season. The r^2 values are 0.65 and 0.70 and the rRMSE are 12.6% and 8.4%, respectively, for NPV and total biomass estimation using the depolarization ratio of the FQ3 (20.9°-22.9°) image in the peak growing season.

4.3 Introduction

Multispectral Landsat 8 OLI and Sentinel-2A MSI images have demonstrated the capability to quantify NPV biomass in the peak growing and early senescence seasons in semiarid mixed prairie grassland characterized by substantial amounts of NPV, PV, BSC, and bare soil (Chapter 3). However, the accuracy of NPV biomass estimation with Landsat 8 OLI and Sentinel-2A MSI images is highly affected the fractional cover of PV, BSC, and bare soil. Also, passive optical remote sensing data have limited ability to access objects below the dense canopy (Huang et al., 2009; Blanchard et al., 2011), which makes it difficult to estimate plant litter on the surface in valley grassland communities in GNP. In an open canopy environment, such as upland and slope land vegetation communities in GNP, application of optical remote sensing to quantify NPV biomass is highly affected by litter decay (Nagler et al., 2000; Daughtry, 2001; Nagler et al., 2003) and availability of BSC and bare soil (Li and Guo, 2016). Moreover, acquisition of high-quality optical images is sometimes difficult because of clouds, haze, and smoke (Avitabile et al., 2012).

Unlike optical images, SAR images can be acquired under all weather conditions, although factors such as clouds, precipitation, and wind may exert an influence on the interpretation of SAR data focusing on the land and sea surface (Danklmayer et al., 2009, Alpers et al., 2016). Potential of SAR data for quantifying NPV has been demonstrated in croplands using field measurements (McNairn et al., 2001) and TerraSAR-X images (Pacheco et al., 2010), and the forests of West Africa using ALOS-1 PALSAR data (Carreiras et al., 2012). The application of C-band dual-pol Radarsat-2 imagery for NPV biomass estimation in Canadian mixed prairies yielded an r^2 of 0.30 (Finnigan, 2013). However, the advantage of quad-pol Radarsat-2 images was not investigated. The effects of incidence angle and polarization of Radarsat-2 images on NPV biomass estimation were also not explored. As Radarsat Constellation Mission (RCM) will be fulfilled in 2018, high temporal and spatial resolution of Radarsat-2 images will be a valuable asset for ecosystem monitoring (http://www.asc-csa.gc.ca/eng/satellites/radarsat/).

Fully polarimetric SAR data have demonstrated potential in differentiating crops, croplands and grasslands, and macrophyte species. For example, the Polarimetric L-band ALOS-1 PALSAR

data identified diverse macrophyte species in the Amazon floodplain wetlands (Sartori et al., 2011). TerraSAR-X images have demonstrated advantages over C-band Radsarsat-2 images for identifying crops (McNairn et al., 2009). The research of Li et al. (2012) showed the superiority of polarimetric decomposition over the linear polarization for rice mapping using C-band Radarsat-2 images. The study of McNairn et al. (2009) also concluded that polarimetric decomposition is superior to linear polarization for identifying crop types. The Freeman-Durden classification of Radarsat-2 images could identify native grasslands from croplands, but had difficulty in separating native grasslands from improved grasslands (Smith and Buckley, 2011). These studies contributed greatly to agriculture management and environment conservation. Nevertheless, limited research was conducted to investigate the potential of fully polarimetric C-band SAR images to quantify NPV biomass in grasslands.

The purpose of this chapter is to investigate the potential of Quad-pol Radarsat-2 images for quantifying NPV biomass in semiarid mixed grasslands characterized by large amounts of NPV, PV, BSC, and bare soil. Specifically, this research was to 1) determine suitable fine Quad-pol Radarsat-2 images for quantifying NPV biomass; and 2) explore the optimum SAR parameter(s) for NPV biomass estimation. The potential of Radarsat-2 images for quantifying total aboveground biomass was also investigated. This study was conducted based on the hypothesis that SAR parameters (e.g., volume scattering) that are sensitive to change in canopy vegetation are useful for estimating standing dead vegetation biomass, while SAR parameters sensitive to change in ground surface are useful for quantifying plant litter on the surface. SAR parameters sensitive to canopy vegetation were retrieved and applied to NPV and total biomass estimation, as were the parameters sensitive to ground surface.

4.4 Data

4.4.1 Biomass data

Dry aboveground NPV biomass used in this study was collected during June 20 to July 2, 2014. Fourteen sites were surveyed using a stratified random sampling design with four upland, three valley, five sloped, and two disturbed communities (Figure 1-5 (a)) for field data sampling. Data sampling and processing procedures were presented in Section 1.6.2.

Dry green grass biomass, green forb biomass, shrub biomass, NPV biomass, and total dry biomass (aboveground biomass) at upland, slope, valley, and disturbed sites are summarized in Table 4-1. Table 4-1 shows high variation in biomass among sample sites, which indicates a good representation of sites sampled in the study area. The percentage of NPV biomass ranges from 59% of total dry biomass in valley sites to 81% of total dry biomass in disturbed communities. The average NPV biomass in upland is 386.5 g/m^2, accounting for 70% of total aboveground biomass.

Table 4-1 Descriptive analysis of aboveground biomass data sampled in the summer of 2014 (NPV includes standing dead vegetation, plant litter on the surface, and moss and lichens).

		PV				
Sites	Statistical description	Grass (g/m^2)	Forb (g/m^2)	Shrub (g/m^2)	NPV (g/m^2)	Total aboveground biomass(g/m^2)
	Average	122.7	22.2	16.9	386.5	548.3
	Max	222.1	115.0	311.5	791.0	1196.5
	Min	38.2	0.0	0.0	65.7	172.1
Upland	StdDev	51.6	24.8	64.0	236.9	265.8
	Average	95.6	28.8	7.3	258.6	390.3
	Max	295.1	246.0	123.7	909.0	983.2
	Min	12.8	0.0	0.0	12.7	46.6
Slope	StdDev	61.9	42.5	23.5	216.8	244.4
	Average	124.6	31.7	12.1	247.8	416.3
	Max	273.0	136.1	110.4	972.2	1084.0
	Min	16.1	0.0	0.0	20.9	76.2
Valley	StdDev	62.7	39.2	27.4	211.9	226.5
	Average	136.5	0.0	9.5	624.3	770.2
	Max	228.9	0.0	75.9	950.0	1175.3
	Min	19.0	0.0	0.0	480.4	603.2
Disturbed	StdDev	77.5	0.0	26.8	147.0	185.2

4.4.2 SAR data and preprocessing

In total, this study analyzed 12 Radarsat-2 fine quad-pol single look complex (SLC) images acquired from June 2 through August 30, 2014 (Table 4-2). The incident angles of the images ranged from 18.54° to 46.5°, and the spatial resolution was 5 m. Temperature, dewpoint

temperature, wind speed, and precipitation around the acquisition time, as well as precipitation within three days before acquisition at Val Marie, Saskatchewan (Table 4-2) were downloaded from the Environment Canada website to check the effects of wind, dew, and rain on the data quality. Based on the environmental data (Table 4-2), the quality of those images was not directly compromised by dew or rainfall. However, the wetness of the canopy, surface litter, and soil moisture caused by heavy precipitation may exert influence on the June 15 FQ23, the June 18 FQ12 image, the June 19 FQ5 image, the June 28 FQ3 image, and the August 30 image.

Table 4-2 Radarsat-2 data description and environmental conditions (T denotes temperature at acquisition, Dew-T is dewpoint temperature, and P is total precipitation in the acquisition day)

Date	Beam mode	Incident angle (°)	Spatial Resolution X × Y (m)	Wind (km/h)	T (°C)	Dew-T (°C)	P (mm)	3-day P (mm)	12-hour P (mm/h)
Jun 02	FQ1	18.5-20.3	4.73 × 4.83	6	7.8	6.9	0	5.3	0
Jun 08	FQ27	45.2-46.5	4.73 × 4.85	5	2.5	1.1	0	0	0
Jun 12	FQ10	29.2-30.9	4.73 × 5.18	4	1.3	-0.5	0	0.6	0
Jun 15	FQ23	41.9-43.3	4.73 × 4.94	15	10.1	8.8	0.2	9.6	0.1
Jun 18	FQ12	31.5-32.9	4.73 × 4.96	11	14.5	10.3	24.9	89	0
Jun 19	FQ5	23.4-25.3	4.73 × 4.97	15	9.7	7.1	0.4	113.7	0
Jun 28	FQ3*	20.9-22.9	4.73 × 5.33	25	15.2	8	0.7	20	20
Jul 02	FQ27	45.2-46.5	4.73 × 4.85	6	11.9	10.9	0	2.7	0
Jul 05	FQ7*	25.8-27.6	4.73 × 4.74	30	27.9	6.9	0	0	0
Jul 06	FQ10	29.2-30.9	4.73 × 5.18	6	13.7	11.6	0	0	0
Jul 09	FQ23	41.9-43.3	4.73 × 4.94	8	12.6	11	0	4.5	0
Aug 30	FQ5	23.4-25.3	4.73 × 4.97	22	15.2	10.1	2.8	0.3	0

* All the images were collected at the right look direction.

The Radarsat-2 images were orthorectified based on the Radar Specific Model in Radar Ortho Suite, an add-on in PCI Geomatica 2015. The Digital Elevation Model (DEM) used for orthorectification was ASTER Global Digital Elevation Model Version 2 (GDEM V2). The digital number (DN) of Radarsat-2 images was converted to backscatter coefficient through sigma-nought (σ°) calibration. A 5 × 5 boxcar filter was applied to reduce speckle noise of the orthorectified Radarsat-2 SLC images. The boxcar filter can be applied to both detected and SLC data to reduce speckles through averaging the covariance (or coherency) metrics of neighboring pixels (Lee et al. 2015). In this study, boxcar filtering was applied to the orthorectified Radarsat-2 SLC data using PSBOXCAR algorithm with 5 * 5 pixel size in PCI Geomatica. This step increased the estimated number of looks from a single look to multiple looks, meeting the requirements of algorithms for performing the Cloude and Pottier decomposition (Cloude and Pottier, 1997) and Freeman-Durden decomposition (Freeman and Durden, 1998). The boxcar filter is the most commonly used algorithm when there are no distinct features on the image and when there is no concern on preservation of spatial resolution (Lee et al., 2015). It is effective in reducing speckles for forest and cropland biomass estimation (Wiseman et al., 2014, Lee et al., 2015). The boxcar filter was used in this study because a comparison using our data indicated that the images filtered with the boxcar approach had a better estimation on biomass than those filtered by the Lee adaptive filter approach. A flow chart (Figure 4-1) was created to demonstrate the procedures for image pre-processing, data retrieval, and data analysis.

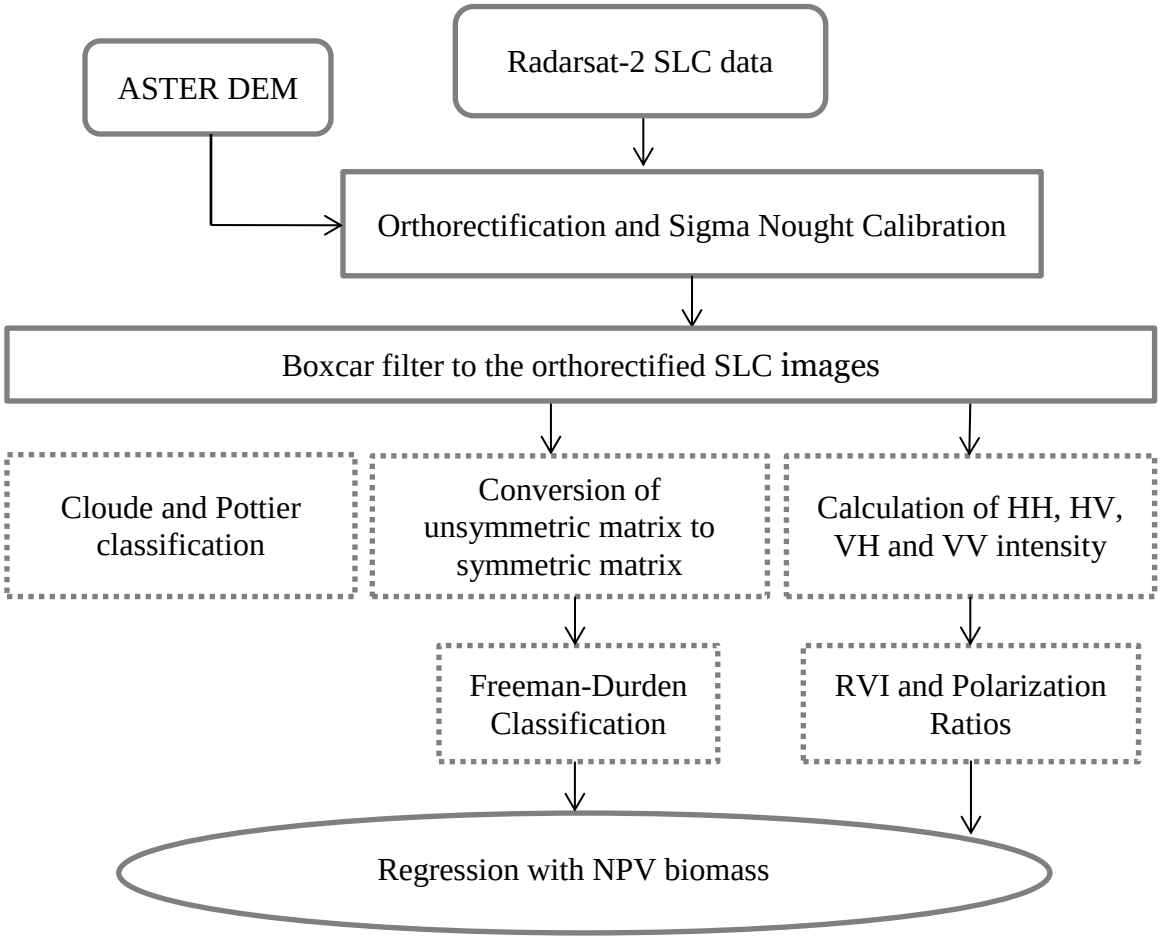

Figure 4-1 The procedure of Radarsat-2 image processing and data retrieval and analysis

4.5 Methods

It is hypothesized that SAR parameters (e.g., volume scattering) that are sensitive to change in canopy vegetation are useful for estimating standing dead vegetation biomass, while SAR parameters sensitive to change in ground surface are useful for quantifying plant litter on the surface. SAR parameters sensitive to canopy vegetation were retrieved and applied to NPV and total biomass estimation, as were the parameters sensitive to ground surface. Prior to the calculation of SAR parameters, differences in backscattering mechanisms resulting from images with different incidence angles were analyzed.

4.5.1 Scattering mechanism

The Cloude and Pottier decomposition (Cloude and Pottier, 1997) was applied to the Boxcar filtered Radarsat-2 SLC images to explore the scattering mechanism of the sampling sites at different imaging incidence angles. The Cloude and Pottier decomposition calculated the eigenvalues of the covariance or coherence matrix of the image to obtain the entropy (H, between 0 and 1) and the anisotropy (A, between 0 and 1), and parameterized each eigenvector in terms of four angles, including the alpha angle (0° - 90°) (Cloude and Pottier, 1997). The entropy (H) indicates the degree of mixing between surface, volume, and double bounce scattering and the anisotropy (A) is dependent on the ratio between probabilities based on second and third eigenvalues (Cloude and Pottier, 1997). The alpha angle depicts the scattering mechanism of the eigenvector. The alpha angle (0°, 45°, and 90°) indicates a trihedral scatter (a smooth surface), a dipole scatter, and a dihedral scatter respectively. An entropy-alpha plane was used to demonstrate the scattering mechanism of the sampling sites.

4.5.2 NPV biomass estimation from SAR polarimetric data

The asymmetric matrix of each filtered Radarsat-2 SLC image was converted to a symmetric matrix prior to the Freeman-Durden decomposition. The Freeman-Durden classification decomposes the total backscatter into the contribution of volume scattering (dipole scattering), double bounce (dihedral scattering), and surface scattering (Bragg scattering) (Freeman and Durden, 1998). Co-polarization ratios (HH/VV) and cross-polarization ratios (VH/HH and VH/VV) were generated. HV/HH, HV/VV were not analyzed as HV and VH backscatter are similar (Moran et al., 2012a). The depolarization ratio ($\boldsymbol{x_v}$)**,** which is sensitive to soil surface roughness (Ulaby et al., 1986, Gherboudj et al., 2011), was calculated using eq. (4.1):

$$x_v = \sigma_{vh}(dB) - \sigma_{vv}(dB) \quad (4.1)$$

Where σ_{vh} and σ_{vv} are the VH cross-polarization and VV co-polarization backscatter coefficients in decibels (dB) respectively. Radar vegetation index (RVI) (Kim and van Zyl, 2009) was characterized by the ratio of cross-polarization backscatter to the total scattering (eq. (4.2)),

$$RVI = \frac{8\sigma_{HV}}{\sigma_{HH}+\sigma_{vv}+2\sigma_{HV}} \quad (4.2)$$

where σ_{HV} is the cross-polarization backscattering and σ_{HH} and σ_{vv} are the co-polarization backscattering in power units. The RVI is sensitive to biomass variation, but less affected by environmental conditions, including soil moisture (Kim and van Zyl, 2009). The value of RVI is not only determined by vegetation condition, but also controlled by incident angle of the radar images. This is because an increase in incidence angle will increase the path length of the radar pulse through the vegetation canopy (Kim et al., 2012).

SAR parameters, including RVI, co-polarization ratio, cross-polarization ratios, depolarization ratio, the Freeman-Durden decomposition components, and Entropy and Alpha angle of the Cloude and Pottier decomposition, were retrieved within a 19 × 19 pixel window size to match the 100 × 100 m sampling site. The retrieved SAR parameters were individually averaged within each plot to correlate with the biomass data within the plot. Before the analysis, outliers of the biomass data were checked at the quadrat level using SPSS using the method introduced in Chapter 3 (Hoaglin and Lglewicz, 1987). Values identified as outliers based on the criteria were doubled checked with the photos taken at the quadrats. After checking, one disturbed plot with over 90% alfalfa and one upland plot with apparently low biomass measurement were excluded from analysis. The sample number for analysis of most images is 12, except for the July 5 image that covers 10 sampling sites. Since plant surface litter and moss and lichen are a significant contributor to NPV biomass, all the derived radar parameters, including surface scattering, were investigated. Accuracy of NPV biomass and total aboveground biomass estimations was quantitatively measured using leave-one-out cross-validation. Relative Root Mean Square Error (rRMSE) was used to measure the accuracy. The determined best SAR image and SAR parameter was also used to create an NPV biomass map to investigate the potential of quantifying spatial variations of NPV biomass.

4.6 Results

4.6.1 Scattering Mechanism

The entropy-alpha planes of the June 2 FQ1 and the June 8 FQ27 Radarsat-2 images are presented in Figure 4-2 to demonstrate the scattering mechanism of images with different incidence angles. Environmental effects on the quality of these three images are negligible

(Table 4-2). Therefore, variations in the scattering mechanism can be considered a result of different incidence angles. Shown by the scattering mechanism plot, the FQ1 image on June 2 is dominated by smooth surface backscattering, while the FQ27 image on June 8 is characterized by rough surface scattering and volume scattering, as a result of low penetration capability through the canopy. Although vegetation growth from June 2 to June 8 may contribute to the volume scattering of the FQ27 image, the dramatic decrease in the surface scattering of the FQ27 images on June 8 was more likely a result of a larger incidence angle. The scattering mechanism explored the capability of the images with small incidence angles to quantify the surface plant litter portion of biomass, and the ability of the images with large incidence angles to quantify standing dead vegetation biomass.

(a) June 2 FQ 1 image

(b) June 8 FQ 27 image

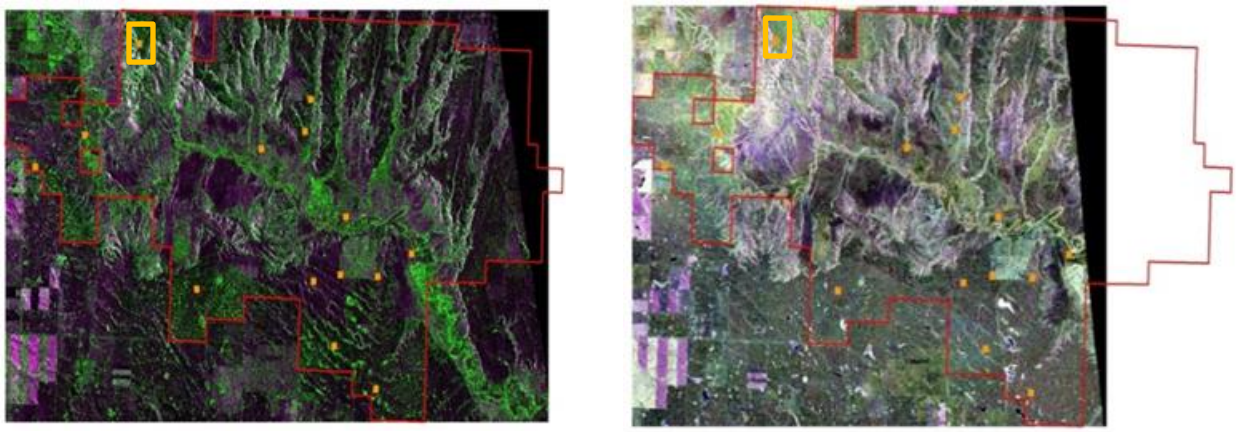

(c) June 2, FQ1

(d) June 8, FQ27

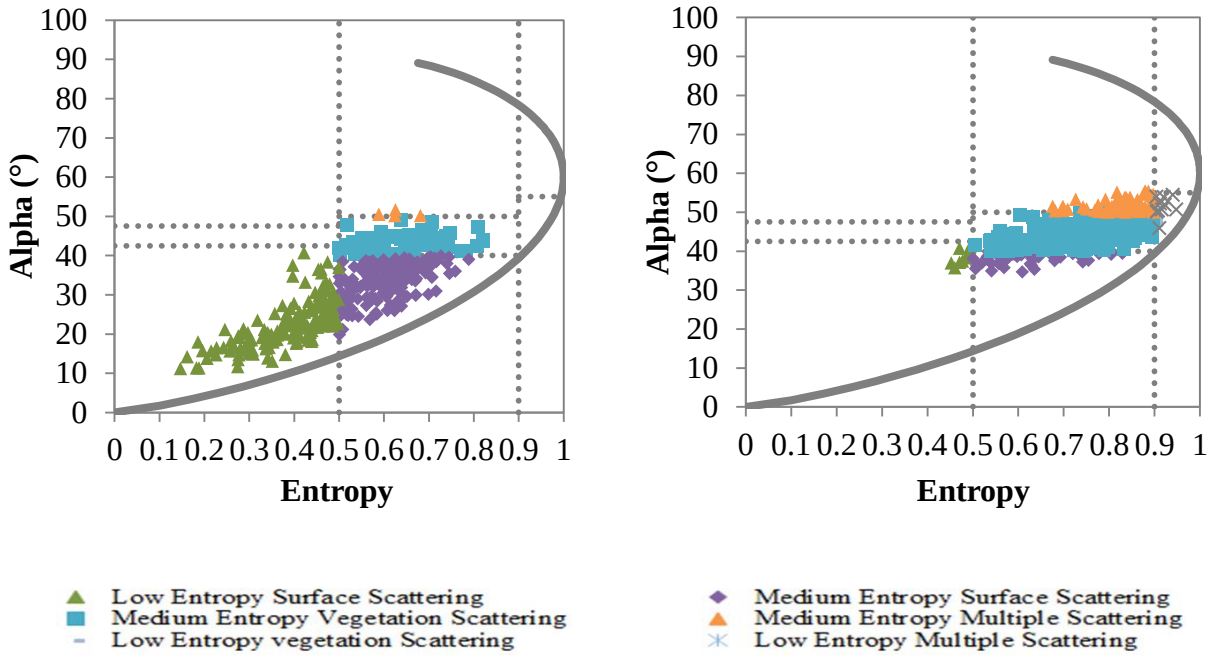

Figure 4-2 The Radarsat-2 images (Red: HH, Green: HV, and Blue: VV) with the field sampling sites (yellow dots) on (a) the June 2 FQ 1 image and (b) the June 8 FQ 27 image; and the scattering mechanism of Radarsat-2 images on: (c) the June 2 2014 FQ1image and (d) the June 8 2014 FQ27 image are demonstrated using backscattering at one upland sampling site encompassed by the orange square in (a) and (b).

4.6.2 Radarsat-2 response and biomass

The relationships between NPV biomass and various Radarsat-2 parameters are presented in Table 4-3. The largest r^2 value for quantifying NPV biomass is 0.70, achieved by using the cross-polarization ratio (VH/VV) calculated from the June 15 FQ23 image. The volume scattering of

the June 08 FQ27 image and the depolarization ratio of the June 15 FQ23 image have an r^2 value of 0.69 for NPV biomass estimation.

The cross-polarization ratio (VH/VV) and the de-polarization ratio calculated from the VH and VV bands of all the images, except for the FQ10 images on June 12 and July 06 and the July 09 FQ23 image, yield better NPV biomass estimations than RVI, co-polarization ratio (HH/VV) and cross-polarization ratio (VH/HH). However, performance of VH/VV and de-polarization ratio changes as incidence angles of the images and vegetation phenology change. From middle growing season (mid-May to mid-June) to peak growing season (late June to mid-July), NPV biomass remains unchanged. From Table 4-3, in the middle growing season, the VH/VV ratio and de-polarization ratios derived from the large incidence angle FQ23 image outperform those calculated from the smallest incidence angle FQ1 image and the largest incidence angle FQ27 image. The medium incidence angle FQ10 and FQ12 images have the worst performances for NPV biomass estimation. In the peak growing season, the VH/VV and de-polarization ratio of the June 28 FQ3 image are superior for quantifying NPV biomass, compared to those calculated from larger incidence angle images, including the July 02 FQ27, July 05 FQ7, July 06 FQ10 and July 09 FQ23 images.

The decomposition components of the Cloude and Pottier decomposition are more promising than the Freeman-Durden classification for quantifying NPV biomass (Table 4-3), although the largest r^2 value achieved is not beyond those obtained by the VH/VV and de-polarization ratio. Incidence angle of the images and vegetation phenology also have an influence on performance of the decomposition components. In the middle growing season, when incidence angle is smaller than that of the FQ10 image, both entropy (H) and Alpha angle have a significant relationship with NPV biomass with an r^2 larger than 0.60, but smaller than 0.69. When incidence angle is larger than that of FQ10, there is no significant relationship between H/Alpha angle and NPV biomass. Nevertheless, volume scattering of the Freeman-Durden decomposition extracted from the largest incidence angle FQ27 image yields an r^2 value of 0.69 for quantifying NPV biomass, followed by the smallest incidence angle FQ1 image. In the peak growing season, the H and Alpha angle of the FQ3 images on June 28 have similar performance with the VH/VV and de-polarization ratios. Volume scattering extracted from the July 9 FQ23 images has a

significant r^2 value (0.38) for NPV biomass estimation. Surface scattering is not a significant contributor for quantifying NPV biomass.

Table 4-3 The Relationship (r^2 values) between various Radrsat-2 parameters and non-photosynthetic vegetation (NPV) biomass (D-ratio is depolarization ratio; Entropy (H) and Alpha angle were derived from the Cloude and Pottier decomposition; V and S represent volume scattering and surface scattering, respectively, which were derived from the Freeman-Durden decomposition)

Date	Beam mode	RVI	HH/ VV	VH/ HH	VH/ VV	D-ratio	H	Alpha	V	S
02-Jun	FQ1		0.45	0.46	0.53	0.51	0.51	**0.57**	0.52	
08-Jun	FQ27	0.34			0.48	0.43			**0.69**	
12-Jun	FQ10	0.46	0.43	0.35	0.44	0.4		0.41		
15-Jun	FQ23	0.57	0.58	0.36	**0.70**	**0.69**				
18-Jun	FQ12	0.38								
19-Jun	FQ5	0.45		0.34	0.47	0.58	**0.65**	0.60		
28-Jun	FQ3	0.55		0.44	0.63	**0.65**	0.59	**0.63**		0.44
02-Jul	FQ27									
05-Jul	FQ7					0.34	0.35			
06-Jul	FQ10	0.36								
09-Jul	FQ23	0.48		0.35					0.38	

Note: only r^2 values significant at the 0.05 level are demonstrated.

The performance of Radarsat-2 on total aboveground biomass estimation is summarized in Table 4-4. To account for the increase in green vegetation during the growing season until it reaches the peak in late June or early July, only the images acquired near the field days were used for aboveground biomass estimation. The June 28 FQ3 images demonstrated the greatest ability with the r^2 value of 0.70 achieved by the de-polarization ratio, followed by the VH/VV and RVI with an r^2 of 0.65 and 0.57, respectively.

Entropy and Alpha angle extracted from the June 28 FQ3 image have an r^2 value similar to that of VH/VV and de-polarization ratio for quantifying total aboveground biomass. The entropy extracted from the FQ5 image acquired on June 19 has an r^2 value of 0.62, which is comparable to that of the June 28 FQ3 image. Entropy and Alpha angle derived from images with an incidence angle larger than that of the FQ7 image have no significant relationship with total aboveground biomass. Volume scattering of the FQ23 image acquired on July 09, 2014 has a

significant relationship with total aboveground biomass, while surface scattering of the June 28 FQ3 image can significantly account for the variations in total aboveground biomass.

Table 4-4 The relationship (r^2 values) between various Radrsat-2 parameters and total aboveground biomass (D-ratio is depolarization ratio; Entropy (H) and Alpha angle were derived from the Cloude and Pottier decomposition; V and S present volume scattering and surface scattering, respectively, which were derived from the Freeman-Durden decomposition)

Date	Beam mode	RVI	HH/ VV	VH/ HH	VH/ VV	D-ratio	H	Alpha	V	S
15-Jun	FQ23	0.39	0.51		0.51	0.5				
18-Jun	FQ12	0.38								
19-Jun	FQ5	0.37			0.38	0.52	0.62	0.55		
28-Jun	FQ3	0.57		0.42	**0.65**	**0.70**	0.60	**0.65**		0.45
02-Jul	FQ27									
05-Jul	FQ7	0.36		0.48	0.52	0.52				
06-Jul	FQ10									
09-Jul	FQ23								0.41	

* Note: only r^2 values significant at the 0.05 level are demonstrated.

The best relationships between Radarsat-2 response and NPV and total aboveground biomass identified in Table 4-3 and Table 4-4 are plotted in Figure 4-3. The main purpose of Figure 4-3 is to address whether NPV biomass is measured directly or indirectly as a component of total aboveground biomass. From the middle to peak growing season, NPV biomass is unchanged without cure of green vegetation and removal of NPV by ground overflow and wind etc., while total aboveground biomass increases as green vegetation increases. So NPV biomass sampled in the field season (June 20 to July 2) generally equal to that in middle growing season; however total aboveground biomass sampled in the field season is larger than that in middle growing season. Therefore, SAR parameters from June 15 and June 19 yield better estimation of NPV biomass than total aboveground biomass. In the peak growing season, using the June 28 image, total aboveground biomass estimate is slightly better than the NPV biomass estimate. The very similar r^2 values for measuring total aboveground and NPV biomass in the peak growing season suggest that NPV, as a merely part of the total vegetation, may be indirectly measured as a part of the total aboveground biomass.

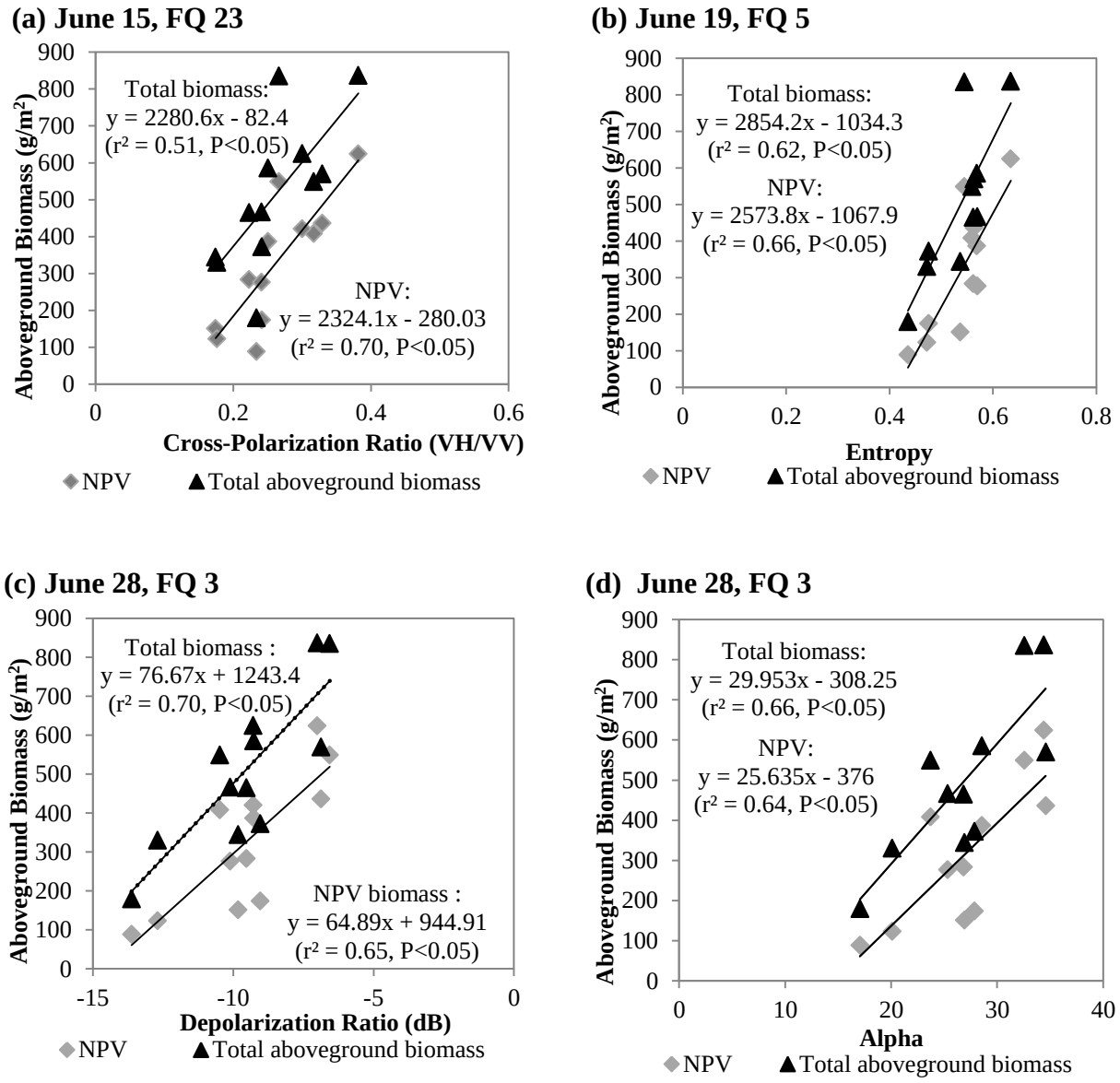

Figure 4-3 The Radarsat-2 response and non-photosynthetic vegetation (NPV) and total aboveground biomass: (a) the cross-polarization VH/VV ratio of the June 15 FQ 23 image, (b) the Entropy of the June 19 FQ5 image, (c) the cross-polarization ratio of the June 28 FQ 3 image, and (d) the Alpha angle of the June 28 FQ3 image.

4.6.3 Accuracy Assessment

Accuracy of NPV biomass and total aboveground biomass estimation using the VH/VV ratio extracted from the June 15 FQ23 image and the depolarization ratio of the June 28 FQ3 image was assessed using a leave-one-out cross-validation approach (Figure 4-4). Relative RMSE (rRMSE) for NPV biomass and total aboveground biomass estimation using the VH/VV ratio of

the FQ23 image acquired on June 15, 2014 are 9% and 8.4%, respectively. The rRMSE (12.6%) for NPV biomass estimation is higher, while it (6.9%) is lower for total aboveground biomass estimation using the depolarization ratio of the June 28 FQ3 image.

Figure 4-4 shows that using the June 15 FQ23 image, both NPV biomass and total aboveground biomass in valley and disturbed vegetation communities are well estimated (stay close to the 1:1 line). Comparatively, accuracy of biomass estimation in slope and upland vegetation communities is lower. Using the small incidence angle FQ3 image, NPV biomass is generally underestimated, except for one upland site and one slope site. Using the FQ3 image, total aboveground biomass in valley and slope land is better estimated than that in upland and disturbed communities. This indicates that vegetation biomass can be better estimated in valley and disturbed communities where vegetation biomass is larger than other sampling sites in the study area, as long as the saturation threshold of SAR images is not reached in dense vegetation communities.

(a) VH/HH for NPV biomass, June 15 FQ23 image

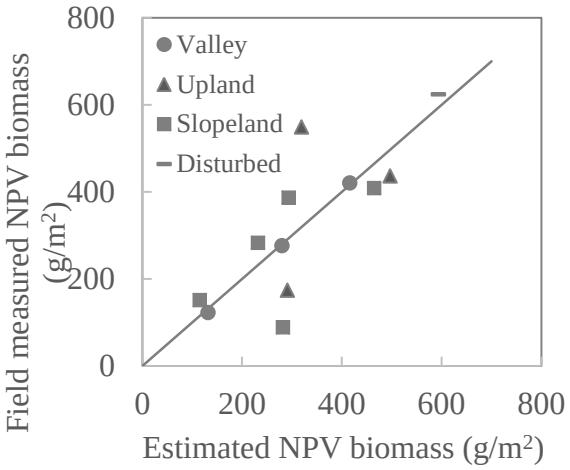

(b) VH/HH for total aboveground biomass, June 15 FQ23 image

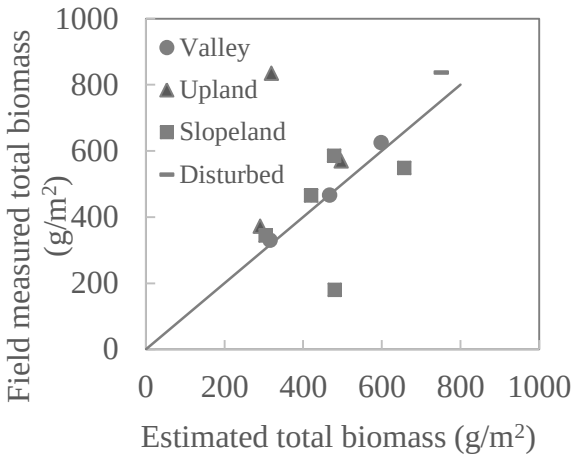

(c) De-polarization ratio for NPV biomass, June 28 FQ3 image

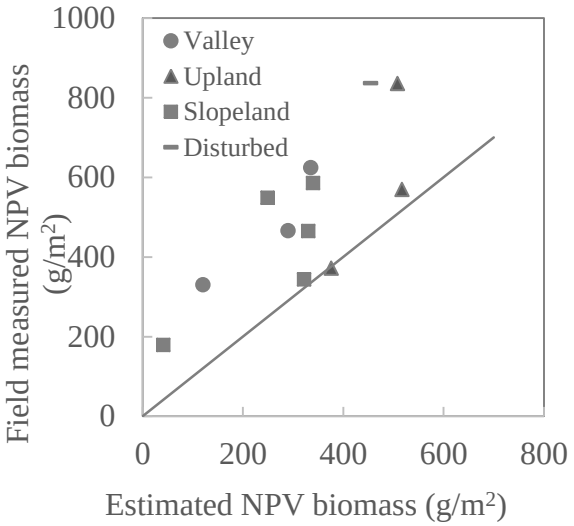

(d) De-polarization ratio for total aboveground biomass, June 28 FQ3 image

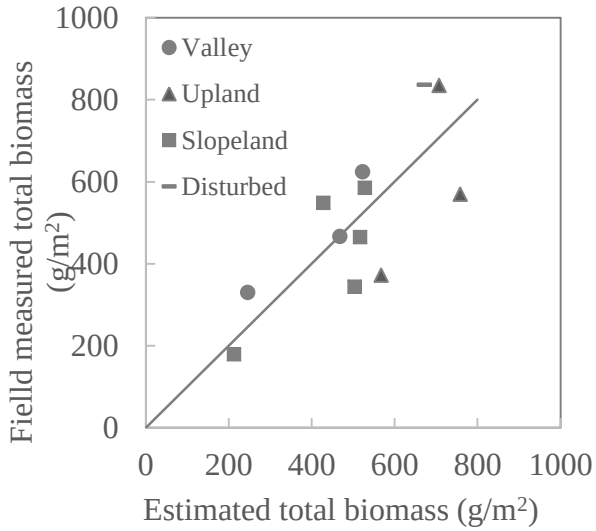

Figure 4-4 Comparison of estimated and field measured non-photosynthetic vegetation (NPV) and total aboveground biomass: (a) the cross-polarization VH/VV ratio of the June 15 FQ 23 image for NPV biomass estimation (rRMSE = 9%), (b) the cross-polarization VH/VV ratio of the June 15 FQ 23 image for quantifying total aboveground biomass (rRMSE = 8.4%), (c) the de-polarization ratio of the June 28 FQ 3 image for NPV biomass estimation (rRMSE=12.6%), and (d) the de-polarization ratio of the June 28 FQ3 image for quantifying total aboveground biomass (rRMSE= 6.9%).

4.6.4 NPV biomass map

The NPV biomass map was created using the cross-polarization ratio (VH/VV) calculated from the FQ23 SAR image acquired on June 15, 2014 (Figure 4-5). The NPV map shows high NPV

biomass along the Frenchman River, and the prairie dog town marked by the red square shows very low NPV biomass. The rRMSE is 9% based on the cross-validation. However, the RMSE is as large as 155 g/m^2. Notably, the majority of the study area shows low NPV biomass close to zero, which means the spatial variations of NPV biomass estimated using the FQ23 image is not quite meaningful.

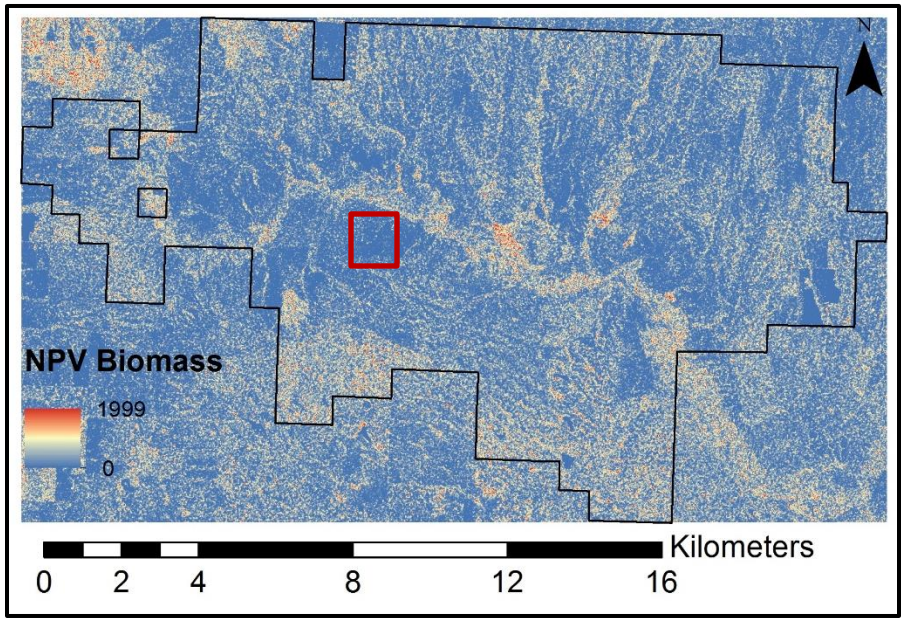

Figure 4-5 The NPV biomass map derived from the cross-polarization VH/VV ratio of the June 15 FQ 23 image (rRMSE = 9%, RMSE=155 g/m^2).

4.7 Discussion

The largest r^2 values for NPV and total aboveground biomass estimation were achieved by the VH/VV ratio of the FQ23 image acquired on June 15, 2014. It indicated the potential of Radarsat-2 data for quantifying NPV biomass in middle growing season when capability of optical images, including Landsat 8 OLI and Sentinel-2A, is limited (Chapter 3). In the peak growing season, depolarization ratio of the June 28 FQ3 image has the best performance for NPV and total aboveground biomass estimation. However, the performance of June 28 image for biomass estimation was affected by increased SAR backscattering as a result of increased moisture from the 0.7 mm daily precipitation on June 28th, and 20 mm total precipitation within 3 days (June 26 to June 28). The performance of Radarsat-2 images for NPV and total above

ground biomass estimation in the early growing season was not evaluated due to the lack of images.

4.7.1 Incidence angle effects

The performance of the Radarsat-2 images on quantifying NPV biomass was affected by incidence angle, ground cover that was highly related to vegetation phenology, and environment condition (e.g., wetness of canopy and soil surface, etc.). NPV biomass was nearly unchanged from the early growing season until the peak growing season in GNP. The volume scattering of the June 2 FQ1 image is not as good as that of the June 8 FQ27 image for estimating NPV biomass, because the FQ1 image, with a small incidence angle, has more ability to penetrate the canopy (Figure 4-2(c)), and therefore cannot quantify standing dead vegetation biomass very well. The good performance of volume scattering of the June 8 FQ27 images on NPV biomass estimation is attributed to its large incidence angle which enables them to capture the standing dead biomass, a substantial component of NPV biomass. Besides the precipitation influence on the FQ12 image, the moderate canopy penetration capability to plant surface litter and ability to capture canopy volume scattering of the FQ10 and FQ12 images accounted for the lower r^2 values for quantifying NPV biomass.

The superiority of the June 15 FQ23 and the June 8 FQ27 images for NPV biomass estimation is consistent with the finding that radar images with a large incidence angle and reduced penetration to soil surface are more sensitive to crop residue in harvested cropland (McNairn et al., 1996). Also, SAR images with large incidence angles are more sensitive to surface roughness (Baghdadi et al., 2002; 2008).

4.7.2 Environmental Effects

Besides incidence angle effects, wind and precipitation play a role in NPV and total aboveground biomass estimation using SAR data. Strong wind blows down standing dead vegetation and green vegetation, alters surface roughness and changes exposure of plant litter on the surface, and thus affects backscattering. Such change in backscattering affects NPV biomass estimation. The poor performance of the July 02 FQ27 image for NPV biomass estimation can be attributed to wind effects and precipitation may account for the reduced r^2 value for quantifying NPV

biomass using the July 09 FQ23 image (Table 4-2). The difference in performance of the July 05 FQ7 and July 06 FQ10 images for biomass estimation is possibly partially attributed to the strong wind on July 5, besides the small incidence angle difference. Also, the July 5 image covers only 10 sites, which also possibly makes a difference.

Precipitation increases background and canopy moisture, which increases dielectricity and further enhances backscattering. This enhanced backscattering from increased moisture reduced the ability of SAR data to detect NPV that usually has very low water content. The reduced r^2 value for quantifying NPV and total aboveground biomass using the July 09 FQ23 image may be accounted for by precipitation. Although incidence angle of the June 19 FQ5 and June 18 FQ12 makes a lot difference in biomass estimation, the large amount of precipitation (Table 4-2) is also a possible reason of the bad performance of the June 18 image.

4.7.3 Suitable SAR parameters

Selecting a suitable SAR parameter is vital for quantifying NPV biomass and total aboveground biomass. The cross-polarization ratio (VH/VV) and depolarization ratio outperformed the co-polarization ratio (HH/VV) for NPV and total aboveground biomass estimation. This finding agrees with the finding of Ferrazzoli et al. (1997) that the availability of cross-polarization was important for biomass estimation in croplands and forests. It also explained the much smaller r^2 (0.30) on NPV biomass estimation achieved by the co-polarization Radarsat-2 image in the study area (Finnigan, 2013). The good performance of VH/VV is attributed to the sensitivity of cross-polarization backscatter coefficients (VH) to standing vegetation biomass and the sensitivity of VV backscatter coefficient to the vertical structure of vegetation (Bartsch et al., 2016). The inferiority of the co-polarization ratio is because co-polarization backscattering is primarily from surface scattering (Wiseman et al., 2014).

The VH/VV and depolarization ratio are also superior to other SAR parameters analyzed in this study for NPV and total biomass estimation, including RVI and decomposition components of the Freeman-Durden decomposition with an exception of volume scattering of the June 8 FQ27 image. Superiority of the VH/VV and depolarization is also demonstrated, in contrast with entropy and Alpha angle. Entropy and Alpha angle of steep incidence angles (in this study, the

FQ1-FQ3 mode) have similar performance with the VH/VV and depolarization ratio for quantifying NPV and total aboveground biomass. However, when using shallow incidence angle images, such as the June 15 FQ23 and June 8 FQ27 images, entropy and Alpha angle are inferior to the VH/VV and depolarization ratio.

4.8 Conclusions

This study investigated the application of C-band, fine quad-pol, and Radarsat-2 data for quantifying NPV biomass and total aboveground in a conserved semiarid mixed grassland, characterized by a large amount of dead vegetation material and high percentage of biological soil crust. The FQ3 Radarsat-2 image is most suitable for quantifying NPV and total aboveground biomass in the peak growing season. However, Radarsat-2 images with a large incidence angle, such as FQ23, are recommended for NPV and total aboveground biomass estimation in middle growing seasons. Creating an NPV biomass map using a SAR image is still challenging.

The depolarization ratio and the cross-polarization ratios (VH/VV) are the best SAR parameters for quantifying NPV and total aboveground biomass. Entropy and alpha angle decomposed using Radarsat-2 images with small incidence angles also have potential.

This was the first study, to our knowledge, done to investigate the potential effectiveness of multi-angular, multi-temporal fine Quad-pol Radarsat-2 images for quantifying NPV biomass in grasslands. This has the potential to significantly contribute to grassland management that uses NPV biomass and (or) total aboveground biomass as an indicator of ecosystem health, fire risk assessment, and herbivore carrying capacity estimation, among other things. It also contributes to our understanding of grassland ecology, hydrology, and climatology that use biomass as a model input.

CHAPTER 5:NON-PHOTOSYNTHETIC VEGETATION AND REMOTE SENSING OF ECOSYSTEM HEALTH

5.1 Preface

This chapter reviews the potential, the challenges, and the opportunity of remote sensing including optical, SAR, and LiDAR to assess and monitor ecosystem health. It discusses the contribution of my research to quantify NPV biomass for grassland ecosystem health assessment. Section 5.2 to 5.7 was published as a review paper in *Sensors*.

Li Z, Xu D and Guo X. (2014) Remote sensing of ecosystem health: opportunities, challenges, and future perspectives. Sensors 14: 21117-21139. *DOI*: 10.3390/s141121117.

Zhaoqin Li came up with the idea, reviewed the literature, and wrote this manuscript. Dr. Dandan Xu reviewed the concept of ecosystem health assessment. This manuscript was finished under the direction of Dr. Xulin Guo. The authors hold the copyright, as it was published through Open Access Publishing (MDPI).

5.2 Abstract

Maintaining a healthy ecosystem is essential for maximizing sustainable, good quality ecological services to human beings. Ecological and conservation research has provided a strong scientific background to identify ecological health indicators and correspondingly, plan effective conservation. At the same time, ecologists assert a strong need for spatially explicit and temporally effective ecosystem health assessment (EHA) based on remote sensing data. Currently, remote sensing of ecosystem health is only based on one of a few ecosystem attributes: vigor, organization, or resilience. However, an effective ecosystem health assessment should be a comprehensive and dynamic measure of all three ecosystem attributes. This chapter reviews opportunities for remote sensing including optical, Radar, and LiDAR, to directly estimate indicators of the three ecosystem attributes. It discusses the main challenges to developing a remote sensing-based spatially-explicit comprehensive ecosystem health protocol and the contribution of my NPV research to EHA. Finally, it provides a future perspective. The

main challenges to developing a remote sensing-based spatially-explicit EHA system are: 1) scale, 2) transportability, 3) data availability; and 4) uncertainties in health indicators estimated from remote sensing data. My research on NPV benefits EHA by providing NPV biomass estimates and an approach for measuring spatially explicit NPV biomass that is applicable in grassland ecosystems. My NPV research also contributes to EHA by providing a solution to reducing the uncertainties in quantifying ecosystem vigor and organization.

5.3 Introduction

Ecosystems worldwide are threatened by anthropological activities and natural disturbances (Tolba and El-Kholy, 1992). Under such pressure, maintaining a healthy ecosystem is essential for supplying stable and sustainable goods and services for human societies (Burkhard et al., 2009). Assessing and monitoring ecosystem health not only provides early warning of environmental degradation but also identifies the cause of an existing problem (Rapport et al., 2009). It is therefore an important early step for ecological conservation and ecological service assessment.

Ecosystem health assessment (EHA) as a part of environmental management began in the late 1980's. Ecosystem health merged the concept of ecosystem monitoring with health science (Rapport et al., 1998) and integrated social and physical science (Patil et al., 2001). The early definition of ecosystem health was simply animal health or plant health (Wicklum and Davies, 1995). However, this definition should consider the complexity of the ecosystem to emphasize the connections between community processes and the physical environment (Begon et al., 2009). Early ecosystem health research evaluated it using keystone species (Costanza et al., 1992). However, keystone species evaluation cannot fully represent the energy flux, nutrient cycle, productivity, diversity, or response capacity to disturbance, although it may indirectly reflect interactions among keystone species, other species, or the physical environment in the ecosystem. In 1999, Costanza and Mageau defined ecosystem health as "a comprehensive, multiscale, dynamic, hierarchical measure of system resilience, organization, and vigor" (Costanza and Mageau, 1999). According to this definition, the condition of one specific ecosystem can be assessed by measuring its integrated ecosystem attributes: vigor, organization,

and resilience (Costanza and Mageau, 1999). Nevertheless, it is impossible to set up multiple specific health indicators for all ecosystems to assess their status (Jorgensen et al., 2005).

There is an urgent need to understand and monitor spatial heterogeneity of ecosystem health (Nelson et al., 2009) to optimize conservation efforts (Polasky et al., 2008). However, the original EHA was conducted based on field ecological data and/or models driven by such field data. These cannot be widely applied at a large spatial scale (Chen and Wang, 2005) and have difficulty in providing spatially and temporally explicit assessment (Kerr and Ostrovsky, 2003).

Remote sensing data have the potential to assess and monitor ecosystem health at various temporal and spatial scales across a broad spatial extent (Kerr and Ostrovsky, 2003; Ludwig et al., 2007). They can be used to directly detail ecological health indicators, such as productivity, species richness, and resilience, after natural and human-induced disturbance (Kerr and Ostrovsky, 2003). They can indirectly provide inputs for spatially explicit ecological process modeling (Hilker et al., 2008). To date, the application of remote sensing on EHA or monitoring has been focused on single ecosystem attributes, such as productivity (Nayak et al., 2010; Brinkmann et al., 2011; Wang and Yang, 2012), species invasion (Naito and Cairns, 2011; Mohamed et al., 2011), or response to stress (Dubinin et al., 2010), or climate change (Bao et al., 2010; Gao et al., 2010). The methods and conclusions of these studies are beneficial to more current ecological studies using remote sensing. However, it is challenging if not impossible to understand a complex ecosystem through one ecosystem attribute (Costanza and Mageau, 1999). A comprehensive and dynamic EHA with the integration of ecosystem vigor, organization, and resilience is urgently needed. Establishing such a spatially explicit EHA and monitoring system faces lots of challenges (Li et al., 2014) and with them, opportunities. This challenge would benefit from the close collaboration of remote sensing specialists and ecologists (Barrios, 2007).

This chapter proposes a framework for developing a remote sensing based EHA system, documents opportunities and challenges to develop a comprehensive EHA system, and discusses the contribution of my research on quantifying NPV biomass using remote sensing approaches to EHA.

5.4 A Framework of a Remote Sensing-Based Ecosystem Health Assessment

The spatially explicit nature of remote sensing data with frequent revisits provides an opportunity to assess and monitor the spatial heterogeneity of ecosystem health. Nonetheless, concerns have been raised that remote sensing specialists may pay more attention to technology than ecological problems (Aplin, 2005; Newton et al., 2009), while ecologists may not have sufficient remote sensing background to address ecological problems at relevant scales (Barrios, 2007). Thus, efforts need to be made to bridge the research gap of the two communities.

To develop a comprehensive remote sensing based EHA system, one might follow the procedures proposed in Figure 5-1 with the participation of remote sensing experts and ecologists. The cooperation of the experts in both fields allows effective health indicators to be identified and ensures that those indicators can be measured using remote sensing data.

Although Figure 5-1 includes indirect estimation of health indicators through modeling using remote sensing data as an input, this chapter focuses on the questions Q7a: Are there any routine remote sensing products for health indicators? and Q7b: What kind of imagery and approach can be used to estimate health indicators? Additionally, I will address challenges and future opportunities to develop a remote sensing based spatially explicit EHA and monitoring system.

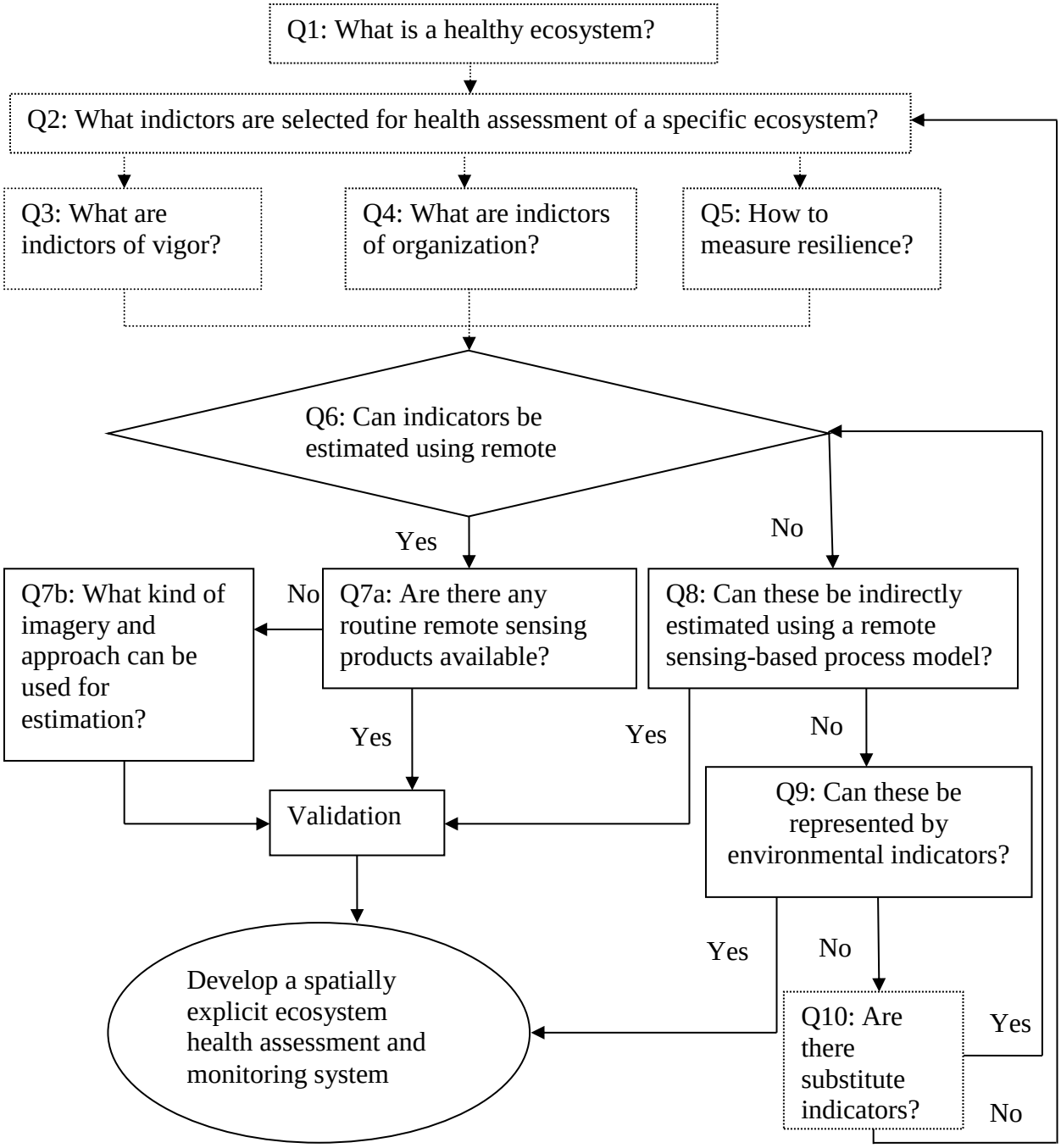

Figure 5-1 Procedures to integrate the expertise of remote sensing experts and ecologists to develop a remote sensing based Ecosystem Health Assessment and Monitoring System. The questions outlined in dotted lines shows the contribution of ecologists.

5.5 Remote Sensing of Ecosystem Health

Dynamic and integrated measures of ecosystem attributes (vigor, organization, and resilience) allow an effective EHA and monitoring. For each ecosystem attribute, there are a number of indicators, although those indicators may be different for different ecosystems. This section summarizes the potential of remote sensing to estimate indicators of the three ecosystem attributes: vigor, organization, and resilience.

5.5.1 Remote sensing of vigor

Vigor can be measured through metabolism, yield, and soil fertility (Rapport et al., 1999). The most commonly used vigor indicator is the NPP or Gross Primary Production (GPP) of an ecosystem (Costanza and Mageau, 1999; Boesch, 2000). Other indicators that are directly or indirectly associated with NPP are green vegetation cover, green vegetation biomass, NPV cover or biomass, green ratio (green/dead vegetation cover or biomass), bare soil cover and BSC cover in semiarid and arid regions, and vegetation biochemical properties (chlorophyll, nitrogen, phosphorous, and moisture content, among others). In addition, an increase in NPP sometimes does not mean an improved ecosystem if that increase is attributed to the expansion of invasive plant species (Boesch, 2000). Therefore, distribution of invasive plant species is another potential indicator of ecosystem vigor.

5.5.1.1 NPP or GPP

Changes in NPP are often used to evaluate environmental degradation in the context of desertification, pollution impacts, climate change, and deforestation (Running et al., 2004). NPP has been estimated and monitored using optical remote sensing images since the 1970's (Feng et al., 2010), yet remote sensing derived daily global NPP products were not operationally produced until the mid-2000's (Turner et al., 2006). The modeling approach for predicting NPP is based on the light use efficiency (LUE) concept proposed by Monteith (Monteith, 1972) and modified by Prince (Prince, 1991). Based on their concept, the GPP of one ecosystem can be a function of the absorbed Photosynthetically Active Radiation (PAR) or absorbed solar radiation at 400 to 700 nm wavelengths and the photosynthetic efficiency that is specific for an individual

plant type. NPP is the product of GPP by subtracting respiration. This LUE-based modeling approach has been applied to produce MODIS global 8-day GPP and annual NPP at 1 km spatial resolution products (MOD17; Turner et al., 2006) that have been available for monitoring ecological conditions and environmental changes (Zhao et al., 2005) since the mid-2000's.

For studies at regional or smaller scales, a statistical empirical model of GPP or NPP and a vegetation index, such as Normalized Difference Vegetation Index (NDVI), is more practical, considering the large number of parameters of LUE model which greatly affect the accuracy of GPP (or NPP) (Feng et al., 2010). A good NDVI-GPP (or NPP) relationship has been observed in low biomass vegetated areas, such as the Arctic tundra (Boelman et al., 2003) and the steppe (Wylie et al., 2003). However, NDVI becomes saturated at high vegetation biomass (Myneni et al., 1995) including areas of dense grass, forest, and cropland, and thus results in a significant difference in spatial distribution of NDVI and NPP (Xu et al., 2012). The enhanced vegetation index (EVI) was thus developed for MODIS and has shown an ability to overcome the saturation limitation of NDVI (Olofsson et al., 2008). In addition, the accuracy of GPP estimation from the empirical relationship with vegetation indices is influenced by the spectral resolution of remote sensing data. For example, NDVI derived from EO-1 Hyperion and MODIS with higher spectral resolution yielded more accurate GPP estimation than Landsat ETM+ with lower spectral resolution in a mountainous meadow ecosystem (Gianelle et al., 2009).

5.5.1.2 Green vegetation, NPV, BSC, and bare soil cover

The fractional cover of green vegetation, NPV, and bare soil can be estimated simultaneously using an SMA approach (e.g., Roberts et al., 1993; Gill and Phinn, 2009; Guerschman et al., 2009), or using the empirical relationships between cover and spectral indices (e.g. Nagler et al., 2003; Carlson and Ripley, 1997). Green vegetation cover and bare soil estimation will not be discussed in depth here, as the former has been routinely produced as remotely sensed products from MODIS, AVHRR, and SPOT-VGT, etc., and the latter can be estimated together with NPV and PV. NPV is a significant component of vegetation productivity in grasslands, savannas, shrublands, dry woodlands (Asner, 1998), as well as wetlands (Schile et al., 2013). BSC is present in semiarid and arid areas worldwide (West, 1990). Both NPV and BSC are ecologically important, yet estimating their abundance using remote sensing methods is still very challenging.

The theory, approaches, opportunities, and challenges of remote sensing of NPV were discussed in Chapter 1.

The spectral characteristics of BSC have been investigated by many researchers (e.g., Graetz and Gentle, 1982; O'NEILL, 1994; Karnieli et al., 1996; Zhang et al., 2007) using field measurements. Although an absorption feature at approximately 680 nm has always been observed in BSC samples, there is a noticeable difference in the spectra as dominant BSC species change (Karnieli, 1997; Zhang et al., 2007). A recent study found that water absorption features at approximately 1450 nm can be used to differentiate BSC from green vegetation and the spectra of the most developed BSCs is characterized by a steeper slope between about 680 and 750 nm (Chamizo et al., 2012). Based on spectral characteristics, many efforts have been made to detect and map BSC using Landsat MSS, TM, or ETM+ images (Tsoar and Karnieli, 1996; Karnieli, 1997; Lewis et al., 2001; Chen et al., 2005; Zhang et al., 2007). These studies have demonstrated that remote sensing has great potential to detect and map the spatial distribution of BSC at a large spatial extent in a timely and efficient manner (Karnieli et al., 2001; Chen et al., 2005). However, spectral variation of different BSC communities makes the derived spectral indices less universally applicable for mapping BSC cover. The crust index developed for mapping cyanobacteria-dominated BSC (Karnieli, 1997) is not suitable for lichen-dominated BSC covering large areas of cool and cold deserts (Belnap, 2003). Another BSC index (BSCI) was proposed to discriminate lichen-dominated BSC from land surfaces of bare sand and dry plant material in a desert (Chen et al., 2005). However, its use was highly influenced by the predetermined lower and upper thresholds of BSCI. Besides the crust indices, continuum removal (Weber et al., 2008), SMA approaches (Ustin et al., 2009), and partial least squares regression-linear discriminant analysis (Chamizo et al., 2012) have also been used for BSC investigation. The conclusions of these studies are not always consistent among study areas. For instance, hyperspectral images were thought to not be able to effectively differentiate BSCs when there was a mixed pixel with plants (Hill et al., 1998). Nevertheless, Weber et al. (2008) concluded that hyperspectral images could work reliably for BSC identification in the presence of both plants and plant litter using the continuum removal crust identification algorithm (CRCIA). Also, Ustin et al. (2009) asserted the application of hyperspectral images for monitoring local or even regional changes of BSC in the southwestern deserts of the United

States. The inconsistency in findings indicated that further research is needed in more arid and semiarid ecosystems, such as mixed grasslands using ground hyperspectral data.

5.5.1.3 Vegetation biochemical properties

Vegetation biochemical properties, such as chlorophyll, nitrogen, and phosphorous are strongly related to ecosystem functioning, and thus are important indicators of ecosystem health assessment (Homolová et al., 2013). Chlorophyll controls photosynthesis and is thus an indicator of plant health and GPP (Leith, 1975). Phosphorous, as an indicator of the nutrient quality of plant and plant growth rate (Homolová et al., 2013), can also be an indicator of plant health. Nitrogen, being an important component of chlorophyll, is also strongly associated with plant health and GPP. Remote sensing of vegetation biochemical properties has been successfully conducted at a leaf level for several decades using narrow band spectral indices derived from ground and space hyperspectral data. Efforts have been made to scale up biochemical content to canopy level using remote sensing data in crops, forests (He and Mui, 2010) and semiarid mixed grassland (Wong and He, 2013). Methods used for scaling up biochemical contents from leaf to canopy level were summarized by He and Mui (2010). Biochemical content estimation at a landscape level remains challenging despite recent and promising advances (He and Mui, 2010; Mitchell et al., 2012).

Due to its importance, chlorophyll has drawn the particular attention of both ecologists and remote sensing scientists. Chlorophyll has been estimated using red edge position (REP) based on the finding that an increase in chlorophyll content will be reflected on the spectra as the wavelength edge of red absorption features move to even longer wavelengths (Curran, 1989). However, REP cannot accurately measure high chlorophyll content (Curran, 1989; Munden et al., 1994). In addition, spectral indices developed for chlorophyll estimation were summarized and compared by Haboudane et al. (2002) and Wu et al. (2008), and a red-edge based vegetation index has demonstrated more potential for chlorophyll content estimation in a semiarid mixed grassland ecosystem of Canada (Wong and He, 2013). The estimation of chlorophyll mainly uses continuous wavelength ranges or narrow band spectral indices. However, space sensed data with fine spectral resolution, including the Medium Resolution Imaging Spectrometer (MERIS) and the upcoming new satellite Sentinel-2A, have also demonstrated great potential for chlorophyll

estimation (Dash and Curran, 2004; Delegido et al., 2011). The terrestrial chlorophyll index (MICI) was developed based on bands 8, 9, and 10 of the MERIS, and global composites of MICI at a 300 m spatial resolution, as a unique terrestrial chlorophyll product that has been produced under the support of the ESA since 2006 (Curran et al., 2007).

There are some remote sensing studies of vegetation nitrogen at leaf and canopy levels that have high accuracy (Homolová et al., 2013). There has only been limited research on phosphorous estimation and this has proven less successful than nitrogen estimation (Ramoelo et al., 2011). The commonly used approach for estimating these vegetation biochemical properties are empirical methods based on *in situ* measures of biochemical content using remotely sensed data. The most widely used wavelengths for measuring nitrogen and phosphorous are the NIR and SWIR regions (Ramoelo et al., 2011). This suggests that estimates of these biochemical properties are highly influenced by canopy water content. To minimize water absorption effects and other influences from atmospheric, soil, redundancy of hyperspectral data, spectral indices, first derivative, continuum removal, and log-transformed spectra have been used to boost the absorption features of vegetation biochemical properties. Water-removed spectra constructed, based on a nonlinear combination of dry-matter and leaf water spectra (Gao and Goetzt, 1995) increased the accuracy of nitrogen and phosphorous estimation of savanna grass compared to first derivative and continuum removal spectra (Ramoelo et al., 2011). The commonly used empirical models for predicting biochemical properties based on biochemical spectra features are simple linear regression, partial least-squares regression (PLSR), and stepwise multiple linear regression (SMLR). The spectral indices used for nitrogen estimation can be found in Tian et al. (2011) but are used mainly for crops, while no vegetation index has yet been specifically designed for phosphorous estimation (Homolová et al., 2013).

5.5.1.4 Invasive plant species

Invasive plant species in diverse ecosystems can be shrubs, trees, and herbs that alter the biodiversity, structure, and function of ecosystems (He et al., 2011). Identification of invasive tree and shrub species using remote sensing was successfully demonstrated (Fuller, 2005; Asner et al., 2008; Lawes and Wallace, 2008; Walsh et al., 2008) using multispectral medium spatial resolution Landsat images, high spatial resolution IKONOS, or hyperspectral images. Remote

sensing of herb species is much more difficult and highly dependent on their separation from surrounding species and the background (Mullerova et al., 2013). Due to its difficulty, identification of herb species was largely conducted using hyperspectral images (reviews by Huang and Asner, 2009; He et al., 2011). However, high spatial resolution IKONOS (4 m) with texture information (Laba et al., 2010) and very high spatial resolution aerial photography (Jones et al., 2011; Mullerova et al., 2013) also mapped herb invaders with high accuracy. Therefore, one should be cautious to select remote sensing data with suitable spatial and spectral resolution for specific species recognition (for review see Huang and Asner, 2009). Methods used for invasive species identification mainly include visual interpretation and pixel-based and object-oriented image classification (Huang and Asner, 2009). The spatial resolution issue may be overcome through methods that include SMA of one pixel (Walsh et al., 2008) and combinations of other ancillary data. Spectra resolution limitations may be overcome by selecting appropriate periods or by using time series data to maximize differences in spectra between invasive species, native species, and backgrounds.

5.5.2 Remote sensing of organization

Ecosystem organization represents both species diversity and the interactions among species within that ecosystem (Costanza, 1992). Indicators of organization can be species richness, landscape diversity, and structural traits including canopy height, LAI, canopy morphology, and horizontal structure represented by the spatial arrangement of green vegetation, NPV, and bare soil. Since remote sensing of green vegetation, NPV, and bare soil has been reviewed in the last section, species richness and biodiversity, and structural traits are the focus in this section.

5.5.2.1 Species richness and biodiversity

Species richness is a primary measure of regional or community biodiversity (Gotelli and Colwell, 2001). Due to the ecological importance of biodiversity, considerable research and a few reviews (Gould, 2000; Nagendra, 2001; Turner et al., 2003; Gillespie et al., 2008; Olofsson et al., 2008) have been completed on the topic of remote sensing of species richness. To date, species richness studies have largely used imagery of one sensor at a specific time (Gillespie, 2005). Only more recently have researchers used images of multiple passive sensors over

multiple time periods (Levin et al., 2007). Remote sensing of species richness can be classified as direct mapping and indirect modeling approaches (Nagendra, 2001; Gillespie et al., 2008). Direct mapping of species distribution using remote sensing is similar to mapping invasive plant species in terms of approaches, potential and limitations. Indirect modeling approaches have been widely used to predict species richness based on the empirical relationships between field species distribution and information derived from remote sensing, such as land cover, landscape metrics, NPP, and spectral variation (Nagendra, 2001; Gillespie et al., 2008).

The rationale on why land cover and landscape metrics can be correlated with species richness or biodiversity is that land cover and landscape metrics, including fragmentation (Kerr and Ostrovsky, 2003), have certain associations with species distributions. Such land cover information has been used for predicting species richness (Luoto et al., 2002; Kerr and Ostrovsky, 2003). This method may be suitable for species richness investigation at large spatial scales. However, prediction accuracy of species richness using such methods has been questioned on three levels: 1) environmental factors including temperature, precipitation, disturbance, and others were neglected (Griffiths and Lee, 2000), 2) the method is highly affected by spatial resolution of remote sensing imagery (Saura, 2004), and 3) the derived landscape-metrics do not contain internal information of the metrics (Gillespie, 2005).

The relationship between NPP and species richness was established based on the species-energy theory which hypothesizes that species richness is correlated with NPP (Currie, 1991). Thus, NDVI in close relationship with NPP (Prince, 1991) has been widely used to predict species richness (Nagendra, 2001; Kerr and Ostrovsky, 2003). The utilization of NDVI is primarily based on NDVI variation, and a positive relationship between NDVI and species richness was found in Fairbanks and McGwire (2004) and Levin et al. (2007). However, there are inconsistent conclusions that attribute little correlation between NDVI variation and species richness. Research indicated that NDVI variation has a negative relationship with species richness (Gillespie, 2005), and the hypothesis of the research is that low NDVI variation and higher homogeneity consequently result in higher species richness (Mackey and Currie, 2001). Although there are inconsistent conclusions, using NDVI for species richness prediction is still an effective method at large spatial scales (Mackey and Currie, 2001).

The application of spectral variation to predict species richness is based on the spectral variation hypothesis (SVH) proposed by Palmer et al. (2002) which assumes that higher variation in spectra, the higher heterogeneity of habitats allowing coexistence of more species, and consequently higher species richness (Rocchini et al., 2007). In this domain, spectral indices, land-cover heterogeneity, and spectral variability derived from optical remote sensing data have been used to predict species richness (Rocchini, 2007). SVH approaches will be an important direction for optical remote sensing of species richness (Gillespie et al., 2008).

Overall, landscape metrics and NDVI approaches are more suitable for species richness estimation at large spatial scales, while SVH can be used at a fine scale. However, prediction of species richness is affected by both spatial and spectral resolutions of satellite imagery (Rocchini, 2007). For the SVH approach, multispectral imagery has difficulty to provide sufficient information for species richness prediction as is hard use for retrieving biochemical and canopy structure information (Cohen et al., 1990). Hyperspectral images have an advantage as they can provide information on canopy biochemical elements including chlorophyll, nitrogen, and cellulose content (Jacquemoud et al., 1996). In addition, ancillary data, such as temperature, precipitation, and topography, can significantly contribute to species richness estimation (Camathias et al., 2013).

5.5.2.2 Structural traits

Structural traits including canopy height, LAI and canopy morphology can be derived from optical remote sensing data through empirical relationships with vegetation indices or image texture metrics (Wulder et al., 2004; Falkowski et al., 2009). Global LAI products have been produced using MODIS and Cyclopes remote sensing data (Fang et al., 2012). Nevertheless, more accurate estimation of these structural parameters can be achieved through LiDAR (e.g., Van Leeuwen and Nieuwenhuis, 2010; Asner et al., 2012) and Radar data (e.g., Kasischke et al., 1997; Andrew et al., 2014). For example, global tree height has been mapped using point samples from the spaceborne LiDAR GLAS data, and spatial continuity of tree height has been measured via MODIS reflectance data (Lefsky, 2010).

5.5.3 Remote sensing of resilience

Ecosystem resilience refers to an ecosystem's ability to remain in its current state and return to that state following disturbance (Costanza, 1992). Disturbances principally consist of natural climate change, wildfire, and anthropological activities, such as grazing and prescribed fire. Resilience at a given time may be assessed based on the ratio of a given ecosystem health indicator, such as aboveground biomass, measured before and after a disturbance (Tilman and Downing, 1996). Remote sensing with a capacity for ecosystem health indicator retrieval also provides an opportunity to estimate ecosystem resilience to disturbances. However, such remote sensing data should be frequently acquired in a long time series to cover the regeneration time.

NDVI data have been widely used to evaluate ecosystem resilience to climate change (e.g., Li and Guo, 2012; Pravalie et al., 2014), fire (e.g., Díaz-Delgado et al., 2002; Van Leeuwen, 2008; van Leeuwen et al., 2010), and grazing (e.g., Numata et al., 2007; Paudel and Andersen, 2010; Yang et al., 2012). Other vegetation indices (e.g. Adjusted Transformed Soil-Adjusted Vegetation Index, ATSAVI) have been frequently used. Considering the requirement for time-series data, Landsat MSS, TM, ETM+, and OLI, MODIS, AVHRR, and SPOT-VEG NDVI data are normally options for resilience estimation. Nevertheless, precautions should be taken to minimize the effects of seasonal and inter-annual variation of phenology and climate when using these NDVI data for evaluating resilience (Díaz-Delgado et al., 2002). To minimize such effects, the quotient NDVI (average NDVI measured in the disturbed area divided by the average NDVI measured in the surrounding undisturbed area) was calculated for resilience evaluation (Díaz-Delgado et al., 2002). However, the surrounding undisturbed area should have similar vegetation, topography, and geology to the disturbed area (Díaz-Delgado et al., 2002). In many instances, although the surrounding undisturbed area can be a good reference, it is difficult to find suitable benchmarks (Bastin et al., 2012). Thus, a dynamic reference-cover method was proposed to separate grazing and rainfall effects in rangelands using remote sensing imagery (Bastin et al., 2012).

5.6 Challenges to Developing a Remote Sensing-based EHA System

Remotely sensed data can be used to retrieve a variety of ecosystem health indicators as surveyed above. However, different indicators may require different remote sensing data for higher estimation accuracy. Hence, there are multiple challenges to combining indicators of vigor, organization, and resilience for establishing a comprehensive, temporally and spatially explicit EHA system. In addition to the lack of a good solution to estimate NPV and BSC cover using remote sensing data as reviewed, there are other challenges such as 1) scale, 2) Transportability difficulty, 3) data availability, and 4) uncertainties in retrieved ecosystem health indicators from remotely sensed data.

5.6.1 Scale issue

Species distribution and ecological processes are dependent on scale and the growing conditions of the species (Vannier et al., 2011) that is partially controlled by soil and topography. Spatial scale issues have been identified as a major challenge in ecological assessment of remote sensing (Vannier et al., 2011). In part, the accuracy of the retrieval of vegetation properties using remote sensing depends on sensor spatial resolution (Numata et al., 2008). Using remote sensing data, especially low spatial resolution data such as the 1 km spatial resolution AVHRR for ecosystem health assessment may introduce uncertainties resulting from land surface heterogeneity and mixed pixels containing more land cover types (Li et al., 2012). GPP calculated using the Region Production Efficiency Model (REG-PEM; Li et al., 2008) with all model inputs obtained from AVHRR 1 km remote sensing data, is significantly different from the GPP calculated using Landsat TM 30 m data (Li et al., 2012). However, finer spatial resolution remote sensing data cannot guarantee the higher accuracy of ecosystem assessment (Feng et al., 2010). For example, MODIS EVI at 250 m resolution cannot be used for estimating GPP of coniferous forests, while MODIS 1 km EVI can (Olofsson et al., 2008). It was also found that when the spatial resolution of remote sensing data is higher than 60-80 m, the accuracy of forest classification decreases (Woodcock and Strahler, 1987). At the same time, a suitable spatial scale or satellite image at optimal spatial resolution can improve vertical vegetation structure estimation (e.g. LAI) in grasslands because the land surface heterogeneity is minimized (Rahman et al., 2003; He et al.,

2006; Li and Guo, 2013). An optimum resolution for a specific research goal can be determined using wavelet or semivariogram analysis.

In addition, some retrieval algorithms and models for ecosystem health indicators, such as biochemical properties, are derived at small scales for homogeneous land surface (Wu and Li, 2009). Applying these algorithms and models to large scales (typically implying a heterogeneous land surface), may incur scale effects. Besides heterogeneity, the linearity or nonlinearity of retrieval models is the other influence on scale effects, and the former may result in smaller scale effects than the latter for mixed pixels with an unknown mixture of different land covers (Chen, 1999). Therefore, precautions should be taken to select up-scaling approaches for the purpose of minimizing scale effects. Some scaling methods have been summarized, although no universal scaling method has been found (Wu and Li, 2009). More recently, a conceptual framework was proposed to scale up biochemical content in semi-arid mixed grassland from leaf to canopy level (He and Mui, 2010), and the estimation of grassland chlorophyll content at leaf, canopy, and landscape scales is reasonably accurate (Wong and He, 2013).

Besides spatial resolution and scaling methods, the accuracy of ecological assessment using optical remote sensing also relies on spectral and temporal resolutions of sensors (Numata et al., 2008; Vannier et al., 2011). Some ecological health indicators may be retrieved from remote sensing using high spatial resolution imagery, while others may need higher spectral resolution or temporal resolution data. Thus, to develop a comprehensive EHA and monitoring system, data fusion can be a solution. The fused imagery can provide the maximum amount of useful information (Welch and Ehlers, 1987), and thus have significant advantages over independent source data (Hall and Llinas, 1997).

5.6.2 Transportability issue

The approaches used to retrieve health indicators from remotely sensed data are commonly empirical relationships between the predicted variables and reflectance (or spectral indices) of optical sensors, backscatter (or variables derived from backscatter, such as canopy water content and cross-polarized ratio) of Radar, or LiDAR intensity. Indicators retrieved from empirical relationships can be difficult to transfer to different sensors and study areas (Andrew et al.,

2014). Nevertheless, efforts have been made to develop general models with promise in estimating foliar nitrogen (Martin et al., 2008) and biomass (Asner et al., 2012).

The other approaches used for retrieving health indicators from optical sensors are inversion of radiative transfer models and SMA approaches. Radiative transfer models provide better transportability for estimating health indicators. However, inversions of radiative transfer models are difficult to implement due to having many input parameters, and are difficult to invert even with approaches such as neural networks (Trombetti et al., 2008). SMA approaches are also more general to operate, while the temporal and spatial variability of end members may reduce their generality (Somers et al., 2011).

5.6.3 Data availability

Ecosystem health indicators, such as biochemical properties and invasive species identification, require hyperspectral images. Others, including canopy height and canopy morphology, may need LiDAR data. Hyperspectral and LiDAR sensors usually are not activated until requested. In addition, the imagery acquired has a very small footprint and consequently does not provide global coverage, and are usually costly (Ayanu et al., 2012).

5.6.4 Uncertainties in ecosystem health indicators

Uncertainties in the estimated ecosystem health indicators are one of the most important factors to be accounted for while developing an EHA system. There are still potential uncertainties in indicator estimation even if the most appropriate remotely sensed data and approaches are used.

5.6.4.1 Optical data for estimating health indicators

Selecting appropriate optical images with suitable spatial, temporal, and spectral resolution is expected to yield better estimation of health indicators (Andrew et al., 2014). However, the accuracy of quantifying or mapping ecosystem health indicators is still hindered by the existence of NPV, BSC, and bare soil in sparsely vegetated areas due to their contribution to the spectra (Huete, 1988; Karnieli et al., 1996; Van Leeuwen and Huete, 1996) (Figures 1-2,1-3). Also,

optical data are only sensitive to top-of-canopy in densely vegetated environments (Blanchard et al., 2011).

The presence of NPV, BSC, and bare soil affect spectral indices derived from optical remote sensing data and designed for the estimation of biophysical variables (Van Leeuwen and Huete, 1996), such as LAI, green vegetation biomass, and fAPAR, all of which are important attributes of EHA. LAI, fAPAR could be overestimated for ecosystems with randomly distributed sparse PV and NPV mixtures, while underestimated for dense mixtures, due to the effects of NPV (Van Leeuwen and Huete, 1996). NPV accounts for the similar variation in spectral indices that include NDVI and Modified Soil-adjusted Vegetation Index (MSAVI) (Li and Guo, 2010) as green vegetation in semiarid mixed grassland.

The presence of live BSC can increase NDVI values by as much as 0.30 units in semiarid environments, which may result in overestimation of ecosystem productivity and misinterpretation of vegetation dynamics (Karnieli et al., 1996; Belnap, 2003).

Effects of bare soil on spectra have been extensively investigated since the early 1970's (Colwell, 1974; Huete et al., 1985). The exerted influence on the spectra significantly affects NDVI and further affects LAI estimation (Huete, 1988) and green vegetation cover with the largest errors in grassland and shrub areas (Montandon and Small, 2008). Thus, many efforts have been made to develop vegetation indices (e.g. a soil-adjusted vegetation index (SAVI; Huete, 1988) and a modified soil adjusted vegetation index (MSAVI; Qi et al., 1994) to minimize soil brightness effects. Minimizing bare ground effects improved r^2 values by 0.23 in estimating N in semiarid shrubland using HyMap hyperspectral data (Mitchell et al., 2012).

However, little research has been conducted to study the total effects of NPV, BSC and bare soil on vegetation indices, evaluate their effects on the determination of a single EHA attribute (e.g. LAI and productivity, etc.), and further identify their effects on a comprehensive EHA.

5.6.4.2 SAR data

SAR data have been widely used for structure and moisture content related ecosystem health indicators. However, estimation accuracy is dependent on many factors, such as instrument characteristics, including frequency or wavelength, polarization, incident angle, look direction, and spatial resolution (Ghasemi et al., 2010). The properties of the land surface, including surface roughness and moisture content also have an influence on estimation accuracy (Zheng et al., 2014).

5.6.4.3 LiDAR data

LiDAR data have also been used for retrieving ecosystem health indicators. The application of LiDAR data is based on the structure information LiDAR data can detect. The way LiDAR data are received (discrete return and full waveform LiDAR) and the footprint (Jensen, 2009) may cause uncertainties in estimating health indicators. Full waveform LiDAR can provide more structural details than discrete LiDAR data. Small footprint LiDAR has an advantage over detailed local mapping, and large footprint LiDAR is more suitable for investigating interactions with multiple vertical structures and taking more ground samples (http://web.pdx.edu/~jduh/courses/geog493f11/Week04.pdf).

5.7 My NPV Research Contribution to EHA

NPV is an indicator of ecosystem vigor and a component of ecosystem organization measures in diverse ecosystems, including savannah and grasslands. NPV quantification using remote sensing methods has demonstrated certain success in savannah and croplands. However, quantifying NPV biomass in semiarid grasslands remains challenging (Chapter 1). My research provided a solution to quantify NPV biomass using optical Landsat 8 OLI and Sentinel-2A images, or fully polarimetric Radarsat-2 images in semiarid grasslands. This approach is also applicable in other grassland ecosystems.

NPV, together with BSC and bare soil, reduces the accuracy of estimating biophysical and biochemical variables using optical remote sensing data because of their contribution to the canopy spectra (Figures 1-2 and 1-4). My NPV research explored the best timing for NPV

estimation, which can indirectly contribute to improving the accuracy of biophysical and biochemical estimates with optical remote sensing tools. This contribution is made by providing the quantity of NPV biomass that can be used to estimate NPV effects on spectra and information on when the influence of BSC and bare soil on the spectra is the least. In this regard, my NPV research indirectly contributes to grassland EHA and management.

My research to quantify NPV biomass using quad-pol Radarsat-2 images showed the great potential of C-band SAR data for grassland EHA and management. Radarsat-2 data not only provided better NPV biomass estimates even in the middle growing season when the application of optical remote sensing such as Landsat 8 OLI and Sentinel-2A was constrained, but also yielded improved estimates of LAI and canopy height (Li and Guo, 2017). In this regard, my NPV research contributes grassland EHA through investigating the potential of C-band SAR data for retrieving ecosystem vigor and organization.

My research to estimate vegetation phenology and climate effects on vegetation growth in Chapter 2 not only provides phenology information used for quantifying NPV biomass with remote sensing approaches, but also supported grassland ecosystem resilience studies as an important component of EHA.

5.8 Discussion and Conclusion

A healthy ecosystem can provide the best quality ecological services to human beings, yet ecosystems worldwide have been impacted by climate change and anthropogenic activities. A comprehensive and dynamic ecosystem health assessment with the involvement of both ecologists and remote sensing specialists is needed.

The intrinsic temporal and spatial properties of remote sensing data provide an opportunity to developing a spatially explicit health ecosystem assessment and monitoring system. Currently, the issue of utilizing remote sensing to assess ecosystem health is that the assessment is only based on a single indicator of one ecosystem attribute. However, a comprehensive assessment should be a dynamic measure of three key ecosystem attributes: vigor, organization, and resilience. The retrieval of different ecosystem health indicators may need diverse remote

sensing data sources including optical, Radar, and LiDAR data, or optical data with different temporal, spectral, and spatial resolutions. To develop a comprehensive health ecosystem process with indicators of ecosystem vigor, organization, and resilience retrieved from different remote sensing imagery. Currently one must face the challenges of scale, transportability, data availability, and uncertainties in the estimation of indicators. Moreover, retrieval of some indicators, such as Non-Photosynthetic Vegetation (NPV) biomass and Biological Soil Crust (BSC) cover, is still challenging.

As the technology in developing LiDAR, Radar, and multi-angle optical sensors and methodologies for information retrieval improve; the uncertainties of estimation of health indicators should decrease (Koch, 2010). The integration of multi-sensor data provides an opportunity to relieve the effects of scale. As the methods to develop integrated models increase, the advantages of multiple sensors can be used while minimizing disadvantages of each data source (Koch, 2010). The multi-sensor data may provide an opportunity to minimize scale issues and reduce uncertainties surrounding health indicators. In addition, newly operational sensors and upcoming sensors will provide more opportunities for remote sensing of ecosystem health. Newly operational 10-day syntheses PROBA-V 333 m NDVI products since November 2013 are free for use and fill the gap of data discontinuity of SPOT 4 and SPOT vegetation-1 and vegetation-2 sensors (http://proba-v.vgt.vito.be/). The newly operational WorldView-3 satellite, Sentinel-2A, the proposed Radarsat-2 constellation, and NovaSAR-S at low cost will provide more opportunities for developing a spatially explicit ecosystem health assessment. For example, my research on quantifying NPV biomass using Landsat 8 OLI and Sentinel-2A, and Radarsat-2 has shown the advantages of the newly operational remote sensors for EHA. As technological innovations in acquiring Radar, LiDAR, hyperspectral and multi-angle optical remote sensing data improved, and algorithms and methods for retrieving information and integrating multi-sensor data advance, developing a comprehensive, dynamic, and spatially explicit ecosystem health assessment and monitoring system will face even fewer challenges.

New sensors and upgraded technology for data processing will increase the availability of remote sensing data and provide ecologists with remote sensing products (e.g., biophysical parameter estimation, canopy structure, NPV biomass and BSC cover estimation, etc.) with fewer

uncertainties. This is expected to contribute to ecological knowledge by providing more accurate temporal and spatial details of ecological indicators, and thus aid ecologists in selecting more representative ecosystem health indicators. In turn, the progress of ecological studies to understand ecosystem health will provide feedback on the application of remote sensing data that may facilitate the design of remote sensors and the processing of remote sensing data. Through close collaboration, ecologists can obtain useful information on remote sensing data with regard to data attributes, application, limitation, and cost, while remote sensing specialists can acquire the most effective ecosystem health indicators in an efficient way. This will gradually bridge the research gap between ecologists and remote sensing specialists.

Policy makers and environmental scientists, as well as economists, play an important role in maintaining a sustainable environment while maximizing ecological services, according to the conceptual frame-work used by the Millennium Ecosystem Assessment (MEA) (MEA, 2005 a-e). The conceptual frame-work of MEA focuses on the ecological services an ecosystem can provide, the benefits the ecological services have for human, and how human activities affect ecosystems and ecological services (Carpenter et al., 2009). Thus, understanding the dynamics of coupled social–ecological systems and investigating the relationships between ecosystem services and humans are critical for comprehensive ecosystem assessment.

5.9 Addendum

I removed a review of NPV remote sensing to avoid repitition and added a statement on the contribution of my NPV research to ecosystem health assessment. I also deleted statements on future opportunities for data acquisition in the original paper because the scheduled platforms have now been launched.

CHAPTER 6: CONCLUSIONS, LIMITATIONS, AND FUTURE RESEARCH

6.1 Summary

The hypothesis that remote sensing can provide a solution for quantifying NPV biomass in semi-arid mixed grassland where NPV estimation is not only affected by the presence of PV and bare soil, but also by BSC, is accepted based on the results of this dissertation. Below is a summary of chapters 2, 3, 4, and 5:

- Chapter 2 fulfilled Objective 1 - estimating vegetation phenology as well as climate impacts on vegetation phenology and productivity. Both temperature and precipitation have a significant effect on intra-annual vegetation growth. Estimating vegetation phenology was the initial step towards investigating the potential for NPV prediction using multispectral and Radarsat-2 images in Chapter 3 and Chapter 4.
- Newly operational multispectral imaging sensors, including Landsat 8 OLI and Sentinel-2A MSI can provide reasonable NPV biomass estimation at different growing stages, except for green-up. Quantifying spatial variations of NPV biomass using Landsat 8 OLI images is possible (Chapter 3).
- Fully polarimetric C-band SAR (i.e. Radarsat-2 in this study) images can quantify NPV biomass at different vegetation stages (Chapter 4). Nevertheless, careful consideration should be given to imaging incidence angle and SAR parameters.
- Remote sensing, including optical, SAR, and LiDAR has provided substantial opportunities for quantifying or mapping ecosystem attributes in the context of EHA and monitoring (Chapter 5). However, challenges remain that can be alleviated with improved imaging acquisition technology and data processing algorithms. My research contributes to grassland EHA and management in three respects. First, my research found a solution for quantifying NPV biomass as an indicator of ecosystem vigor and component of ecosystem organization. Second, my research findings can be used to reduce uncertainties for estimating other indicators of ecosystem vigor and organization. Third, my research explored the potential of C-band SAR data for quantifying grassland ecosystem vigor and organization.

6.2 Contribution

6.2.1 Scientific contribution

Scientifically, a critical gap was addressed in quantitatively estimating NPV biomass in mixed grassland using both optical and radar remote sensing approaches. The results of this research identified the most suitable spectral bands and spectral indices of optical remote sensing for quantifying NPV biomass in grasslands. This research also explored the most useful Radarsat-2 SAR parameter(s) for estimating NPV. In addition, the results of this research will provide inputs to the modeling of terrestrial ecosystems, hydrology, and climate with the expectation of improving model predictability.

6.2.2 Practical contribution

Practically, this research contributes to grassland Ecosystem Health Assessment (EHA), monitoring and grassland management by providing temporally and spatially explicit NPV biomass data. It provides an opportunity to improve the accuracy of remote sensing (C-band SAR data) for measuring ecosystem vigor and organization using NPV as additional information in the application of optical remote sensing data in semiarid grasslands. In addition, this research attempts to investigate grassland ecosystem resilience to climate change using a low spatial resolution (1km) AVHRR NDVI product.

Broadly, this research is important for natural resource management and environmental management by quantifying NPV biomass as well as developing approaches for estimating NPV biomass. The presence of NPV contributes to soil nutrition which is indispensable for maintaining ecosystem vigor and essential for maintaining soil stability (Arsenault and Bonn, 2005). Soil stability not only affects air and water quality, but also exerts influence on habitat conservation of wildlife. In Saskatchewan, species at risk, including Hairy Prairie-clover, Western Spiderwort, and Small-flowered Sand-verbena, benefit from NPV biomass. In addition, NPV as a carbon source has impacts on global climate that, in turn, affect the environment (air, water, and soil).

6.2.3 Value added to previous GNP research

In Grasslands National Park, optical remote sensing data have been used to measure grassland growth and productivity (Yang et al., 2012, 2013; Xu and Guo, 2015), evaluate grassland condition in response to climate change (Piwowar, 2011; Li and Guo, 2012, He et al. 2012, a & b), grazing, and fire (Yang et al., 2011, 2013; Xu and Guo, 2015), map wildlife habitat (Shen et al., 2013, a & b), and estimate forage quality (Guo et al., 2010) and leaf CO_2 exchange rate (Guo et al., 2011). While these studies have advanced our understanding of how to monitor specific elements of the grassland community, the accuracy of retrieved biophysical variables (e.g., leaf area index and productivity) using optical remote sensing was limited by the presence of non-photosynthetic vegetation (NPV), biological soil crust (BSC), and bare soil. This is because of their unique spectral properties (Van Leeuwen and Huete, 1996). Research has been conducted in GNP to study the influence of NPV on vegetation indices (Yang and Guo, 2014; Xu et al., 2014). Nevertheless, these studies have all focused on green vegetation. NPV, as an essential grassland ecosystem health indicator and a vital input for wild fire prediction, has been rarely studied because of the difficulty in separating NPV from green vegetation, biological soil crust, and bare soil.

My fundamental research to determine the most suitable wavelength and spectral index for quantifying NPV biomass using optical remote sensing data paves the way to comprehensive grassland ecosystem health and wild fire prediction and simulation modeling. In addition, most remote sensing research has been conducted using optical remote sensing data with limited research being conducted on exploring the potential of polarimetric SAR for grassland management. The documented literature includes Zhang et al. (2006)'s study on the application of Radarsat-1 to assess grassland biophysical heterogeneity and the MSc thesis of Finnigan (2013) on evaluating grassland biomass using dual-pol Radarsat-2 images. However, Finnigan's research did not provide a solution for quantifying NPV biomass using dual-pol Radarsat-2 images. My exploration on the potential of fully polarimetric Radarsat-2 data indicates that the best SAR parameters for measuring NPV biomass are cross-polarization ratios, which explained why Finnigan's research with co-polarization Radarsat-2 did not show promise. Overall, my investigation of the ability of fully polarimetric Radarsat-2 at different incidence angles to retrieve biophysical variables, including NPV biomass, pioneers the application of SAR in GNP.

The planned Radarsat constellation (scheduled launch in 2018) will fly over Canadian terrestrial ecosystems daily taking high spatial resolution images. This will provide a great opportunity for terrestrial ecosystem monitoring.

6.3 Transferability

Transferability of the methods and findings of this research should be considered. The methods used to quantify NPV biomass with optical and Radarsat-2 images can be applied to any terrestrial ecosystem. However, the findings of this research are only applicable in GNP-like grassland ecosystems that are characterized by large amounts of dead vegetation including standing dead plants and surface plant litter, BSC, and bare soil. During the study period, GNP has undergone light-intensity grazing and a large wildfire. This may constrain the transferability of the findings.

6.4 Limitations

Although Landsat 8 OLI and Sentinel-2A MSI with improved spectral resolution (narrower wavelength ranges) over Landsat TM/ETM+ images have demonstrated potential for NPV biomass estimation in this research, their application, particularly in the red-edge bands of Sentinel-2A, is limited compared to the red-edge of ground hyperspectral data. Therefore, hyperspectral images to fully explore the potential of red-edge wavelength ranges and to better identify effects of PV, bare soil, and BSC on NPV biomass would have improved my results.

Additionally, Radarsat-2 images with full beam modes (FQ1-FQ27) would have been interesting to include. This is so that the influence of incidence angles on estimating NPV biomass could have been comprehensively evaluated. In addition, the lack of high spatial resolution and high vertical accuracy digital elevation model (DEM, e.g. LiDAR DEM or SAR DEM) may influence the retrieval of radar backscatter coefficients at the scale of a pixel. However, this research used the average of backscatter coefficient within a 19 × 19 pixel window for NPV biomass estimation that greatly reduced uncertainty of backscatter coefficient retrieval caused by DEM.

6.5 Future research

This research on NPV biomass estimation with remote sensing approaches can be furthered in three important ways. First, to further improve NPV estimation using optical remote sensing data, quantifying the contribution to the spectra of PV, NPV, bare soil, and BSC using a radiative transfer model and/or hyperspectral images using the SMA method is necessary. In addition, current studies using optical data on NPV estimation have focused more on spectral resolution of sensors, while spatial resolution effects are also worth investigation. The effect of spatial resolution can be investigated by comparing the results of this research with the findings using high spatial resolution (e.g., the WV-3 satellite with spatial resolution 0.31 m) to quantify NPV biomass. The WV-3 satellite sensor has two bands of ASTER for calculating SINDRI that have demonstrated better performance for NPV estimation than multispectral indices (Serbin et al., 2013). In addition, using geostatistical approaches such as semivariogram and wavelet analysis to investigate the spatial variation of NPV biomass, and further, to identify the most suitable spatial resolution for quantifying NPV biomass is also an important direction.

Second, to advance the quantification of NPV biomass using SAR data, further research is needed on improving the accuracy of NPV biomass estimation through investigating and minimizing the effects of wavelength, incidence angle, and spatial resolution of SAR data using both theoretical scattering models and SAR images. In addition, the effects of PV, BSC, and bare soil on NPV biomass estimation with SAR data should be explored using a theoretical scattering modeling. Comparing ASTER DEM 30 m with LiDAR DEM 50 cm (or <50 cm) for SAR backscatter coefficient retrieval, and evaluating the propagated influence on NPV estimation, is a worthy study direction.

Third, it would be interesting to explore the potential of integrated SAR and optical data for NPV estimation. Each of these data sources has its own merits and drawbacks and integrated multi-sensor data can combine advantages of multiple sensors, while minimizing the disadvantages of the other (Koch, 2010). With technological innovations in data acquisition, improved algorithms for data retrieval and analysis, and a better understanding of the interactions and contributions of PV, NPV, and backgrounds to reflectance, backscatter, or laser pulse one sensor, we should expect NPV estimation to be quickly operational.

REFERENCES

Aase J and Tanaka D. (1991) Reflectances from four wheat residue cover densities as influenced by three soil backgrounds. Agronomy Journal 83: 753-757.

Adair M, Cihlar J, Park B, et al. (2002) GeoComp-n, an advanced system for generating products from coarse and medium resolution optical satellite data. Part 1: System characterization. Canadian Journal of Remote Sensing 28: 1-20.

Aguilar J, Evans R and Daughtry CST. (2012) Performance assessment of the cellulose absorption index method for estimating crop residue cover. Journal of Soil and Water Conservation 67: 202-210.

Akinremi O, McGinn S and Cutforth H. (1999) Precipitation Trends on the Canadian Prairies*. Journal of Climate 12: 2996-3003.

Al-Bakri J and Taylor J. (2003) Application of NOAA AVHRR for monitoring vegetation conditions and biomass in Jordan. Journal of Arid Environments 54: 579-593.

Alpers W, Zhang B, Mouche A, et al. (2016) Rain footprints on C-band synthetic aperture radar images of the ocean-Revisited. Remote Sensing of Environment 187: 169-185.

Amri R, Zribi M, Lili-Chabaane Z, et al. (2011) Analysis of vegetation behavior in a North African semi-arid region, using SPOT-VEGETATION NDVI data. Remote Sensing 3: 2568-2590.

Andrew ME, Wulder MA and Nelson TA. (2014) Potential contributions of remote sensing to ecosystem service assessments. Progress in Physical Geography: 0309133314528942.

Angel J, Easterling W and Kirtsch S. (1993) Towards defining appropriate averaging periods for climate normals. Climate Bulletin 27: 29-44.

Anyamba A and Eastman J. (1996) Interannual variability of NDVI over Africa and its relation to El Niño/Southern Oscillation. Remote Sensing 17: 2533-2548.

Anyamba, A.; Tucker C and Eastman, J. (2001) NDVI anomaly patterns over Africa during the 1997/98 ENSO warm event. International Journal of remote sensing 22 (10):1847-1859.

Anyamba A, Tucker CJ and Mahoney R. (2002) From El Niño to La Niña: vegetation response patterns over East and Southern Africa during the 1997-2000 period. Journal of Climate 15: 3096-3103.

Aplin P. (2005) Remote sensing: ecology. Progress in Physical Geography 29: 104-113.

Arsenault É and Bonn F. (2005) Evaluation of soil erosion protective cover by crop residues using vegetation indices and spectral mixture analysis of multispectral and hyperspectral data. Catena 62: 157-172.

Asner GP. (1998) Biophysical and Biochemical Sources of Variability in Canopy Reflectance. Remote Sensing of Environment 64: 234-253.

Asner GP, Townsend AR and Bustamante MMC. (1999) Spectrometry of pasture condition and biogeochemistry in the Central Amazon. Geophysical Research Letters 26: 2769-2772.

Asner GP and Lobell DB. (2000) A biogeophysical approach for automated SWIR unmixing of soils and vegetation. Remote Sensing of Environment 74: 99-112.

Asner GP and Heidebrecht KB. (2002) Spectral unmixing of vegetation, soil and dry carbon cover in arid regions: comparing multispectral and hyperspectral observations. International Journal of Remote Sensing 23: 3939-3958.

Asner GP and Heidebrecht KB. (2003) Imaging spectroscopy for desertification studies: Comparing AVIRIS and EO-1 Hyperion in Argentina drylands. IEEE Transactions on Geoscience and Remote Sensing 41: 1283-1296.

Asner GP, Borghi CE and Ojeda RA. (2003) Desertification in Central Argentina: Changes in ecosystem carbon and nitrogen from imaging spectroscopy. Ecological Applications 13: 629-648.

Asner GP, Elmore AJ, Hughes RF, et al. (2005) Ecosystem structure along bioclimatic gradients in Hawai'i from imaging spectroscopy. Remote Sensing of Environment 96: 497-508.

Asner GP, Jones MO, Martin RE, et al. (2008) Remote sensing of native and invasive species in Hawaiian forests. Remote Sensing of Environment 112: 1912-1926.

Asner GP, Mascaro J, Muller-Landau HC, et al. (2012) A universal airborne LiDAR approach for tropical forest carbon mapping. Oecologia 168: 1147-1160.

Asrar G, Myneni R and Choudhury B. (1992) Spatial heterogeneity in vegetation canopies and remote sensing of absorbed photosynthetically active radiation: a modeling study. Remote Sensing of Environment 41: 85-103.

Avitabile V, Baccini A, Friedl MA, et al. (2012) Capabilities and limitations of Landsat and land cover data for aboveground woody biomass estimation of Uganda. Remote Sensing of Environment 117: 366-380.

Ayanu YZ, Conrad C, Nauss T, et al. (2012) Quantifying and mapping ecosystem services supplies and demands: a review of remote sensing applications. Environmental Science and Technology 46: 8529-8541.

Baghdadi N, King C, Bourguignon A, et al. (2002) Potential of ERS and RADARSAT data for surface roughness monitoring over bare agricultural fields: application to catchments in Northern France. International Journal of Remote Sensing 23: 3427-3442.

Baghdadi N, Zribi M, Loumagne C, et al. (2008) Analysis of TerraSAR-X data and their sensitivity to soil surface parameters over bare agricultural fields. Remote Sensing of Environment 112: 4370-4379.

Balzarolo M, Vicca S, et al. (2016) Matching the phenology of Net Ecosystem Exchange and vegetation indices estimated with MODIS and FLUXNET in-situ observations. Remote Sensing of Environment 174: 290-300.

Bannari A, Haboudane D, McNairn H, et al. (2000) Modified Soil Adjusted Crop Residue Index (MSACRI): A new index for mapping crop residue. Proceedings of the Geoscience and Remote Sensing Symposium, 2000 (IGARSS 2000) 2936-2938.

Bannari A, Pacheco A, Staenz K, et al. (2006) Estimating and mapping crop residues cover on agricultural lands using hyperspectral and IKONOS data. Remote Sensing of Environment 104: 447-459.

Bannari A, Morin D, Bonn F, et al. (1995) A review of vegetation indices. Remote sensing reviews 13: 95-120.

Bao YH, Wu L, Eerdemutu, et al. (2010) Research on Grassland Snow Disaster Risk Management Information System in Pastoral Area. Chinese Perspective on Risk Analysis and Crisis Response 13: 451-456.

Barrios E. (2007) Soil biota, ecosystem services and land productivity. Ecological economics 64: 269-285.

Bartsch A, Widhalm B, Kuhry P, et al. (2016) Can C-Band SAR be used to estimate soil organic carbon storage in tundra. Biogeosciences 13:pp.5453-5470.

Bastin G, Scarth P, Chewings V, et al. (2012) Separating grazing and rainfall effects at regional scale using remote sensing imagery: A dynamic reference-cover method. Remote Sensing of Environment 121: 443-457.

Bater CW, Coops NC, Gergel SE, et al. (2009) Estimation of standing dead tree class distributions in northwest coastal forests using LiDAR remote sensing. Canadian Journal of Forest Research 39: 1080-1091.

Beaudoin A, Le Toan T and Gwyn Q. (1990) SAR observations and modeling of the C-band backscatter variability due to multiscale geometry and soil moisture. IEEE Transactions on Geoscience and Remote Sensing 28: 886-895.

Begon M, Townsend CR and Harper JL. (2009) Ecology: from individuals to ecosystems: Wiley. com.

Belnap J. (2003) The world at your feet: desert biological soil crusts. Frontiers in Ecology and the Environment 1: 181-189.

Biard F, Bannari A and Bonn F. (1995) SACRI (Soil Adjusted Corn Residue Index): un indice utilisant le proche etle moyen infrarouge pour la de´tection des re´sidus de cultures de maı¨s. 17th Canadian Symposium on Remote Sensing. Canadian Remote Sensing Society, Ottawa, Canada, pp. 417–423.

Biard F and Baret F. (1997) Crop residue estimation using multiband reflectance. Remote Sensing of Environment 59: 530-536.

Bindlish R, Jackson T, Gasiewski A, et al. (2008) Aircraft based soil moisture retrievals under mixed vegetation and topographic conditions. Remote Sensing of Environment 112: 375-390.

Blanchard SD, Jakubowski MK and Kelly M. (2011) Object-based image analysis of downed logs in disturbed forested landscapes using LiDAR. Remote Sensing 3: 2420-2439.

Black S and Guo X. (2008) Estimation of grassland CO2 exchange rates using hyperspectral remote sensing techniques. International Journal of Remote Sensing 29: 145-155.

Boelman NT, Stieglitz M, Rueth HM, et al. (2003) Response of NDVI, biomass, and ecosystem gas exchange to long-term warming and fertilization in wet sedge tundra. Oecologia 135: 414-421.

Boesch DF. (2000) Measuring the health of the Chesapeake Bay: toward integration and prediction. Environmental research 82: 134-142.

Bonanomi G, Caporaso S and Allegrezza M. (2009) Effects of nitrogen enrichment, plant litter removal and cutting on a species-rich Mediterranean calcareous grassland. Plant Biosystems 143: 443-455.

Brinkmann K, Dickhoefer U, Schlecht E, et al. (2011) Quantification of aboveground rangeland productivity and anthropogenic degradation on the Arabian Peninsula using Landsat imagery and field inventory data. Remote Sensing of Environment 115: 465-474.

Buddenbaum H, Seeling S and Hill J. (2013) Fusion of full-waveform lidar and imaging spectroscopy remote sensing data for the characterization of forest stands. International Journal of Remote Sensing 34: 4511-4524.

Burke IC, Yonker C, Parton W, et al. (1989) Texture, climate, and cultivation effects on soil organic matter content in US grassland soils. Soil science society of America journal 53: 800-805.

Burkhard B, Kroll F, Müller F, et al. (2009) Landscapes' capacities to provide ecosystem services–a concept for land-cover based assessments. Landscape online 15: 22.

Byrne KM, Lauenroth WK, Adler PB, et al. (2011) Estimating Aboveground Net Primary Production in Grasslands: A Comparison of Nondestructive Methods. Rangeland Ecology & Management 64: 498-505.

Camathias L, Bergamini A, Kuchler M, et al. (2013) High-resolution remote sensing data improves models of species richness. Applied Vegetation Science 16: 539-551.

Cao X, Chen J, Matsushita B, et al. (2010) Developing a MODIS-based index to discriminate dead fuel from photosynthetic vegetation and soil background in the Asian steppe area. International Journal of Remote Sensing 31: 1589-1604.

Carlson TN and Ripley DA. (1997) On the relation between NDVI, fractional vegetation cover, and leaf area index. Remote Sensing of Environment 62: 241-252.

Carpenter SR, Mooney HA, Agard J, et al. (2009) Science for managing ecosystem services: Beyond the Millennium Ecosystem Assessment. Proceedings of the National Academy of Sciences 106 (5):1305-1312.

Carreiras JM, Vasconcelos MJ and Lucas RM. (2012) Understanding the relationship between aboveground biomass and ALOS PALSAR data in the forests of Guinea-Bissau (West Africa). Remote Sensing of Environment 121: 426-442.

Chamizo S, Stevens A, Canton Y, et al. (2012) Discriminating soil crust type, development stage and degree of disturbance in semiarid environments from their spectral characteristics. European Journal of Soil Science 63: 42-53.

Chavez RO, Clevers J, Herold M, et al. (2013) Assessing water stress of desert tamarugo trees using in situ data and very high spatial resolution remote sensing. Remote Sensing 5: 5064-5088.

Chen J, Yuan Zhang M, Wang L, et al. (2005) A new index for mapping lichen-dominated biological soil crusts in desert areas. Remote Sensing of Environment 96: 165-175.

Chen JM. (1999) Spatial scaling of a remotely sensed surface parameter by contexture. Remote Sensing of Environment 69: 30-42.

Chen ZH and Wang J. (2005) Establishing a ecosystem health model in arid and semi-arid area by using remote sensing data. IGARSS 2005: IEEE International Geoscience and Remote Sensing Symposium, Vols 1-8, Proceedings: 2953–2956.

Chen J, Zhang MY, Wang L, et al. (2005) A new index for mapping lichen-dominated biological soil crusts in desert areas. Remote Sensing of Environment 96: 165-175.

Chen JM. (1999) Spatial scaling of a remotely sensed surface parameter by contexture. Remote Sensing of Environment 69: 30-42.

Chen Z and Wang J. (2005) Establishing a ecosystem health model in arid and semi-arid area by using remote sensing data. Sensing Technology and Application 20(6): 558–562.

Chimner R, Welker J, Morgan J, et al. (2010) Experimental manipulations of winter snow and summer rain influence ecosystem carbon cycling in a mixed-grass prairie, Wyoming, USA. Ecohydrology 3: 284-293.

Cho MA, Mathieu R, Asner GP, et al. (2012) Mapping tree species composition in South African savannas using an integrated airborne spectral and LiDAR system. Remote Sensing of Environment 125: 214-226.

Cihlar J. (2012) Pilot study on quantification of non-photosynthetic vegetation biomass in Canadian prairie grasslands. Technical report no: K1A50-11-0036.

Cihlar J, Chen J, Li Z, et al. (2002) GeoComp-n, an advanced system for the processing of coarse and medium resolution satellite data. Part 2: Biophysical products for northern ecosystems. Canadian Journal of Remote Sensing 28: 21-44.

Clevers J, De Jong S, Epema G, et al. (2002) Derivation of the red edge index using the MERIS standard band setting. International Journal of Remote Sensing 23: 3169-3184.

Cloude SR and Pottier E. (1997) An entropy based classification scheme for land applications of polarimetric SAR. IEEE Transactions on Geoscience and Remote Sensing 35: 68-78.

Cohen WB, Spies TA and Bradshaw GA. (1990) Semivariograms of digital imagery for analysis of conifer canopy structure. Remote Sensing of Environment 34: 167-178.

Cohen WB and Goward SN. (2004) Landsat's role in ecological applications of remote sensing. Bioscience 54: 535-545.

Colwell JE. (1974) Vegetation canopy reflectance. Remote Sensing of Environment 3: 175-183.

Costanza R and Mageau M. (1999) What is a healthy ecosystem? Aquatic ecology 33: 105-115.

Costanza R, Norton BG and Haskell BD. (1992) Ecosystem health: new goals for environmental management: Island Pr.

Costanza R. (1992) Toward an operational definition of ecosystem health. Ecosystem health: New goals for environmental management: 239-256.

Costanza R and Mageau M. (1999) What is a healthy ecosystem? Aquatic ecology 33: 105-115.

Coughenour MB. (1985) Graminoid responses to grazing by large herbivores: adaptations, exaptations, and interacting processes. Annals of the Missouri Botanical Garden: 852-863.

Coupland RT. (1992) Natural grasslands: introduction and western hemisphere: Elsevier Science Publishers BV, the Netherlands 8A:151-179.

Curran P, Dash J, Lankester T, et al. (2007) Global composites of the MERIS terrestrial chlorophyll index. International Journal of Remote Sensing 28: 3757-3758.

Curran PJ. (1989) Remote sensing of foliar chemistry. Remote Sensing of Environment 30: 271-278.

Currie DJ. (1991) Energy and large-scale patterns of animal-and plant-species richness. American Naturalist: 27-49.

Danklmayer A, Doring BJ, Schwerdt M, et al. (2009) Assessment of atmospheric propagation effects in SAR images. IEEE Transactions on Geoscience and Remote Sensing 47: 3507-3518.

Dash J and Curran P. (2004) The MERIS terrestrial chlorophyll index. International Journal of Remote Sensing 25(23):5403-5413.

Datt B. (1999) A new reflectance index for remote sensing of chlorophyll content in higher plants: tests using Eucalyptus leaves. Journal of Plant Physiology 154: 30-36.

Daughtry C, McMurtrey J, Chappelle E, et al. (1995) Potential for discriminating crop residues from soil by reflectance and fluorescence. Agronomy Journal 87: 165-171.

Daughtry CST, McMurtrey JE, Chappelle EW, et al. (1996) Measuring crop residue cover using remote sensing techniques. Theoretical and Applied Climatology 54: 17-26.

Daughtry CST. (2001) Discriminating crop residues from soil by shortwave infrared reflectance. Agronomy Journal 93: 125-131.

Daughtry CST, Hunt ER and McMurtrey JE. (2004) Assessing crop residue cover using shortwave infrared reflectance. Remote Sensing of Environment 90: 126-134.

Daughtry CST, Hunt ER, Doraiswamy PC, et al. (2005) Remote sensing the spatial distribution of crop residues. Agronomy Journal 97: 864-871.

Daughtry CST, Doraiswamy PC, Hunt ER, et al. (2006) Remote sensing of crop residue cover and soil tillage intensity. Soil & Tillage Research 91: 101-108.

Daughtry CST and Hunt ER. (2008) Mitigating the effects of soil and residue water contents on remotely sensed estimates of crop residue cover. Remote Sensing of Environment 112: 1647-1657.

Daughtry CST, Serbin G, Reeves JB, et al. (2010) Spectral Reflectance of Wheat Residue during Decomposition and Remotely Sensed Estimates of Residue Cover. Remote Sensing 2: 416-431.

Davis SK. (2005) Nest-site selection patterns and the influence of vegetation on nest survival of mixed-grass prairie passerines. The Condor 107: 605-616.

Davidson A and Csillag F. (2003) A comparison of three approaches for predicting C4 species cover of northern mixed grass prairie. Remote Sensing of Environment 86: 70-82.

Delegido J, Fernandez G, Gandia S, et al. (2008) Retrieval of chlorophyll content and LAI of crops using hyperspectral techniques: application to PROBA/CHRIS data. International Journal of Remote Sensing 29: 7107-7127.

Delegido J, Verrelst J, Alonso L, et al. (2011) Evaluation of Sentinel-2A red-edge bands for empirical estimation of green LAI and chlorophyll content. Sensors 11: 7063-7081.

Deutsch ES, Bork EW and Willms WD. (2010) Separation of grassland litter and ecosite influences on seasonal soil moisture and plant growth dynamics. Plant Ecology 209: 135-145.

Díaz-Delgado R, Lloret F, Pons X, et al. (2002) Satellite evidence of decreasing resilience in Mediterranean plant communities after recurrent wildfires. Ecology 83: 2293-2303.

Donath TW and Eckstein RL. (2010) Effects of bryophytes and grass litter on seedling emergence vary by vertical seed position and seed size. Plant Ecology 207: 257-268.

Dubinin M, Potapov P, Lushchekina A, et al. (2010) Reconstructing long time series of burned areas in arid grasslands of southern Russia by satellite remote sensing. Remote Sensing of Environment 114: 1638-1648.

Easterling DR, Evans J, Groisman PY, et al. (2000) Observed variability and trends in extreme climate events: a brief review. Bulletin of the American Meteorological Society 81: 417-425.

Eckstein RL and Donath TW. (2005) Interactions between litter and water availability affect seedling emergence in four familial pairs of floodplain species. Journal of Ecology 93: 807-816.

Eklundh L and Olsson L. (2003) Vegetation index trends for the African Sahel 1982–1999. Geophysical Research Letters 30:1430-1433.

Elmore AJ, Asner GP and Hughes RF. (2005) Satellite monitoring of vegetation phenology and fire fuel conditions in Hawaiian drylands. Earth Interactions 9: 1-21.

Elvidge CD. (1990) Visible and near infrared reflectance characteristics of dry plant materials. Remote Sensing 11: 1775-1795.

Erdody TL and Moskal LM. (2010) Fusion of LiDAR and imagery for estimating forest canopy fuels. Remote Sensing of Environment 114: 725-737.

Facelli JM and Pickett STA. (1991) plant litter - its dynamics and effects on plant community structure. Botanical Review 57: 1-32.

Fairbanks DH and McGwire KC. (2004) Patterns of floristic richness in vegetation communities of California: regional scale analysis with multi-temporal NDVI. Global Ecology and Biogeography 13: 221-235.

Falkowski MJ, Wulder MA, White JC, et al. (2009) Supporting large-area, sample-based forest inventories with very high spatial resolution satellite imagery. Progress in Physical Geography 33: 403-423.

Fang H, Wei S and Liang S. (2012) Validation of MODIS and CYCLOPES LAI products using global field measurement data. Remote Sensing of Environment 119: 43-54.

Fargey KS, Larson SD, Grant SJ, et al. (2000) Grasslands National Park Field Guide. Val Marie, SK: Prairie Wind & Silver Sage-Friends of Grasslands Inc.

Farrar T, Nicholson S and Lare A. (1994) The influence of soil type on the relationships between NDVI, rainfall, and soil moisture in semiarid Botswana. II. NDVI response to soil oisture. Remote Sensing of Environment 50: 121-133.

Feng X, Fu B, Yang X, et al. (2010) Remote sensing of ecosystem services: An opportunity for spatially explicit assessment. Chinese Geographical Science 20: 522-535.

Ferrazzoli P, Paloscia S, Pampaloni P, et al. (1997) The potential of multifrequency polarimetric SAR in assessing agricultural and arboreous biomass. IEEE Transactions on Geoscience and Remote Sensing 35: 5-17.

Filella I and Penuelas J. (1994) The red edge position and shape as indicators of plant chlorophyll content, biomass and hydric status. International Journal of Remote Sensing 15: 1459-1470.

Finnigan C. (2013) Developing a grassland biomass monitoring tool using a time series of dual polarimetric SAR and optical data. MSc thesis. University of Saskatchewan.

Fisher RJ and Davis SK. (2010) From Wiens to Robel: A review of grassland-bird habitat selection. The Journal of Wildlife Management 74: 265-273.

Frank A. (2003) Evapotranspiration from northern semiarid grasslands. Agronomy Journal 95: 1504-1509.

Freeman A and Durden SL. (1998) A three-component scattering model for polarimetric SAR data. IEEE Transactions on Geoscience and Remote Sensing 36: 963-973.

Fuller D. (2005) Remote detection of invasive Melaleuca trees (Melaleuca quinquenervia) in South Florida with multispectral IKONOS imagery. International Journal of Remote Sensing 26: 1057-1063.

Galvanek D and Leps J. (2012) The effect of management on productivity, litter accumulation and seedling recruitment in a Carpathian mountain grassland. Plant Ecology 213: 523-533.

Gao BC and Goetz AF. (1994) Extraction of dry leaf spectral features from reflectance spectra of green vegetation. Remote Sensing of Environment 47: 369-374.

Gao BC and Goetzt AF. (1995) Retrieval of equivalent water thickness and information related to biochemical components of vegetation canopies from AVIRIS data. Remote Sensing of Environment 52: 155-162.

Gao BC. (1996) NDWI—A normalized difference water index for remote sensing of vegetation liquid water from space. Remote Sensing of Environment 58: 257-266.

Gao Q, Wan Y, Xu H, et al. (2010) Alpine grassland degradation index and its response to recent climate variability in Northern Tibet, China. Quaternary International 226: 143-150.

García M, Riaño D, Chuvieco E, et al. (2011) Multispectral and LiDAR data fusion for fuel type mapping using Support Vector Machine and decision rules. Remote Sensing of Environment 115: 1369-1379.

Ghasemi N, Sahebi MR and Mohammadzadeh A. (2010) A review on biomass estimation methods using synthetic aperture radar data. International Journal of Geomatics and Geosciences 1: 776-788.

Gherboudj I, Magagi R, Berg AA, et al. (2011) Soil moisture retrieval over agricultural fields from multi-polarized and multi-angular RADARSAT-2 SAR data. Remote Sensing of Environment 115: 33-43.

Gianelle D, Vescovo L, Marcolla B, et al. (2009) Ecosystem carbon fluxes and canopy spectral reflectance of a mountain meadow. International Journal of Remote Sensing 30: 435-449.

Gill T and Phinn S. (2008) Estimates of bare ground and vegetation cover from Advanced Spaceborne Thermal Emission and Reflection Radiometer (ASTER) short-wave-infrared reflectance imagery. Journal of Applied Remote Sensing 2: 023511-023519.

Gill TK and Phinn SR. (2009) Improvements to ASTER-derived fractional estimates of bare ground in a savanna rangeland. IEEE Transactions on Geoscience and Remote Sensing 47: 662-670.

Gillespie TW, Foody GM, Rocchini D, et al. (2008) Measuring and modelling biodiversity from space. Progress in Physical Geography 32: 203-221.

Gillespie TW. (2005) Predicting woody-plant species richness in tropical dry forests: a case study from South Florida, USA. Ecological Applications 15: 27-37.

Gitelson AA and Merzlyak MN. (1996) Signature analysis of leaf reflectance spectra: algorithm development for remote sensing of chlorophyll. Journal of Plant Physiology 148: 494-500.

Gliner JA, Morgan GA and Leech NL. (2010) Research methods in applied settings: An integrated approach to design and analysis (2nd edition): Routledge. Taylor & Francis Group, NY USA.

Gotelli NJ and Colwell RK. (2001) Quantifying biodiversity: procedures and pitfalls in the measurement and comparison of species richness. Ecology Letters 4: 379-391.

Gould W. (2000) Remote sensing of vegetation, plant species richness, and regional biodiversity hotspots. Ecological Applications 10: 1861-1870.

Goward SN, Huemmrich KF and Waring RH. (1994) Visible-near infrared spectral reflectance of landscape components in western Oregon. Remote Sensing of Environment 47: 190-203.

Graetz R and Gentle M. (1982) The relationships between reflectance in the Landsat wavebands and the composition of an Australian semi-arid shrub rangeland. Photogrammetric Engineering and Remote Sensing 48: 1721-1730.

Griffiths G and Lee J. (2000) Landscape pattern and species richness; regional scale analysis from remote sensing. International Journal of Remote Sensing 21: 2685-2704.

Guerschman JP, Hill MJ, Renzullo LJ, et al. (2009) Estimating fractional cover of photosynthetic vegetation, non-photosynthetic vegetation and bare soil in the Australian tropical savanna region upscaling the EO-1 Hyperion and MODIS sensors. Remote Sensing of Environment 113: 928-945.

Guo X, Wilmshurst J, McCanny S, et al. (2004) Measuring spatial and vertical heterogeneity of grasslands using remote sensing techniques. Journal of Environmental Informatics 3: 24-32.

Guo Q, Li W, Yu H, et al. (2010) Effects of topographic variability and lidar sampling density on several DEM interpolation methods. Photogrammetric Engineering and Remote Sensing 76: 701-712.

Guo X, Black S, and He Y. (2011) Estimation of leaf CO2 exchange rates using a SPOT image. International Journal of Remote Sensing 32(2):353-366.

Haboudane D, Miller JR, Tremblay N, et al. (2002) Integrated narrow-band vegetation indices for prediction of crop chlorophyll content for application to precision agriculture. Remote Sensing of Environment 81: 416-426.

Hall DL and Llinas J. (1997) An introduction to multisensor data fusion. Proceedings of the IEEE 85: 6-23.

Hardisky M, Klemas V and Smart RM. (1983) The influence of soil salinity, growth form, and leaf moisture on the spectral radiance of Spartina alterniflora canopies. Photogrammetric Engineering and Remote Sensing 49: 77-83.

He KS, Rocchini D, Neteler M, et al. (2011) Benefits of hyperspectral remote sensing for tracking plant invasions. Diversity and Distributions 17: 381-392.

He Y, Guo X and Wilmshurst J. (2006) Studying mixed grassland ecosystems I: suitable hyperspectral vegetation indices. Canadian Journal of Remote Sensing 32: 98-107.

He Y, Guo X and Wilmshurst J. (2009) Reflectance measures of grassland biophysical structure. International Journal of Remote Sensing 30: 2509-2521.

He Y and Mui A. (2010) Scaling up semi-arid grassland biochemical content from the leaf to the canopy level: Challenges and opportunities. Sensors 10: 11072-11087.

He Y, Dixon P, Wilmshurst J, et al. (2012) AVHRR NDVI baseline for natural vegetation ecosystems in northern Canadian National Parks. Journal of Geophysics and Remote Sensing 1(1): 1000103.

Henry HAL, Brizgys K and Field CB. (2008) Litter decomposition in a California annual grassland: Interactions between photo degradation and litter layer thickness. Ecosystems 11: 545-554.

Hewins DB, Archer SR, Okin GS, et al. (2013) Soil-Litter Mixing Accelerates Decomposition in a Chihuahuan Desert Grassland. Ecosystems 16: 183-195.

Hilker T, Coops NC, Wulder MA, et al. (2008) The use of remote sensing in light use efficiency based models of gross primary production: A review of current status and future requirements. Science of the Total Environment 404: 411-423.

Hill J, Udelhoven T, Schutt B, et al. (1998) Differentiating biological soil crusts in a sandy arid ecosystem based on multi-and hyperspectral remote sensing data. First EARSeL Workshop on Imaging Spectroscopy Zurich: Remote Sensing Laboratories, University of Zurich.

Hirsch RM, Slack JR and Smith RA. (1982) Techniques of trend analysis for monthly water quality data. Water Resources Research 18: 107-121.

Hmimina G, Dufrêne E, Pontailler JY, et al. (2013) Evaluation of the potential of MODIS satellite data to predict vegetation phenology in different biomes: An investigation using ground-based NDVI measurements. Remote Sensing of Environment 132: 145-158.

Hoaglin DC and Iglewicz B. (1987) Fine-tuning some resistant rules for outlier labeling. Journal of the American Statistical Association 82: 1147-1149.

Homolová L, Malenovský Z, Clevers JGPW, et al. (2013) Review of optical-based remote sensing for plant trait mapping. Ecological Complexity 15: 1-16.

Huang CY and Asner GP. (2009) Applications of remote sensing to alien invasive plant studies. Sensors 9: 4869-4889.

Huang S, Crabtree RL, Potter C, et al. (2009) Estimating the quantity and quality of coarse woody debris in Yellowstone post-fire forest ecosystem from fusion of SAR and optical data. Remote Sensing of Environment 113: 1926-1938.

Huang S, Potter C, Crabtree RL, et al. (2010) Fusing optical and radar data to estimate sagebrush, herbaceous, and bare ground cover in Yellowstone. Remote Sensing of Environment 114: 251-264.

Huang W, Sun G, Dubayah R, et al. (2013) Mapping biomass change after forest disturbance: Applying LiDAR footprint-derived models at key map scales. Remote Sensing of Environment 134: 319-332.

Hudak AT, Bright BC, Negron J, et al. (2012) Predicting Live and Dead Tree Basal Area in Bark Beetle-Affected Forests from Discrete-Return LiDAR. SilviLaser 2012, Sept. 16-19, Vancouver, Canada.

Hudak AT, Crookston NL, Evans JS, et al. (2008) Nearest neighbor imputation of species-level, plot-scale forest structure attributes from LiDAR data. Remote Sensing of Environment 112: 2232-2245.

Huemmrich KF and Goward SN. (1997) Vegetation canopy PAR absorptance and NDVI: An assessment for ten tree species with the SAIL model. Remote Sensing of Environment 61: 254-269.

Huete A, Jackson R and Post D. (1985) Spectral response of a plant canopy with different soil backgrounds. Remote Sensing of Environment 17: 37-53.

Huete AR. (1988) A soil-adjusted vegetation index (SAVI). Remote Sensing of Environment 25: 295-309.

Huete A and Tucker C. (1991) Investigation of soil influences in AVHRR red and near-infrared vegetation index imagery. International Journal of Remote Sensing 12: 1223-1242.

Hunt ER and Rock BN. (1989) Detection of changes in leaf water content using near-and middle-infrared reflectances. Remote Sensing of Environment 30: 43-54.

Hyde P, Dubayah R, Walker W, et al. (2006) Mapping forest structure for wildlife habitat analysis using multi-sensor (LiDAR, SAR/InSAR, ETM+, Quickbird) synergy. Remote Sensing of Environment 102: 63-73.

Jackson RD, Allen-Diaz B, Oates LG, et al. (2006) Spring-water nitrate increased with removal of livestock grazing in a california oak savanna. Ecosystems 9: 254-267.

Jackson H and Prince SD. (2016) Degradation of non-photosynthetic vegetation in a semi-arid rangeland. Remote Sensing 8: 692; doi: 10.3390/rs8080692

Jacquemoud S, Ustin S, Verdebout J, et al. (1996) Estimating leaf biochemistry using the PROSPECT leaf optical properties model. Remote Sensing of Environment 56: 194-202.

Jacques DC, Kergoat L, Hiernaux P, et al. (2014) Monitoring dry vegetation masses in semi-arid areas with MODIS SWIR bands. Remote Sensing of Environment 153: 40-49.

Jaskierniak D, Lane PN, Robinson A, et al. (2011) Extracting LiDAR indices to characterise multilayered forest structure using mixture distribution functions. Remote Sensing of Environment 115: 573-585.

Jensen JR. (2009) Remote Sensing of the Environment: An Earth Resource Perspective 2nd edition: Pearson Education India.

Jensen K and Gutekunst K. (2003) Effects of litter on establishment of grassland plant species: the role of seed size and successional status. Basic and Applied Ecology 4: 579-587.

Jones D, Pike S, Thomas M, et al. (2011) Object-based image analysis for detection of Japanese knotweed sl taxa (Polygonaceae) in Wales (UK). Remote Sensing 3: 319-342.

Jorgensen SE, Xu F-L and Costanza R. (2005) Handbook of ecological indicators for assessment of ecosystem health: CRC press, Taylor & Francis Group.

Justice CO, Eck T, Tanre D, et al. (1991) The effect of water vapour on the normalized difference vegetation index derived for the Sahelian region from NOAA AVHRR data. International Journal of Remote Sensing 12: 1165-1187.

Karnieli A, Shachak M, Tsoar H, et al. (1996) The effect of microphytes on the spectral reflectance of vegetation in semiarid regions. Remote Sensing of Environment 57: 88-96.

Karnieli A. (1997) Development and implementation of spectral crust index over dune sands. International Journal of Remote Sensing 18: 1207-1220.

Karnieli A, Kokaly R, West N, et al. (2001) Remote sensing of biological soil crusts. Biological soil crusts: structure, function, and management. Springer, 431-455.

Kasischke ES, Melack JM and Craig Dobson M. (1997) The use of imaging radars for ecological applications—a review. Remote Sensing of Environment 59: 141-156.

Kaufmann RK, Zhou L, Knyazikhin Y, et al. (2000) Effect of orbital drift and sensor changes on the time series of AVHRR vegetation index data. IEEE Transactions on Geoscience and Remote Sensing 38: 2584-2597.

Keeling C, Chinf J and Whorf T. (1996) Increased activity of northern vegetation inferred from atmospheric CO_2 measurements. Nature 382:146-149.

Kerr JT and Ostrovsky M. (2003) From space to species: ecological applications for remote sensing. Trends in Ecology and Evolution 18: 299-305.

Kim Y and van Zyl JJ. (2009) A time-series approach to estimate soil moisture using polarimetric radar data. IEEE Transactions on Geoscience and Remote Sensing 47: 2519-2527.

Kim Y, Yang Z, Cohen WB, et al. (2009) Distinguishing between live and dead standing tree biomass on the North Rim of Grand Canyon National Park, USA using small-footprint LiDAR data. Remote Sensing of Environment 113: 2499-2510.

Kim Y, Jackson T, Bindlish R, et al. (2012) Radar vegetation index for estimating the vegetation water content of rice and soybean. IEEE Geoscience and Remote Sensing Letters 9: 564-568.

Koch B. (2010) Status and future of laser scanning, synthetic aperture radar and hyperspectral remote sensing data for forest biomass assessment. ISPRS Journal of Photogrammetry and Remote Sensing 65: 581-590.

Kogan FN. (1997) Global drought watch from space. Bulletin of the American Meteorological Society 78: 621-636.

Kunkel K and Court A. (1990) Climatic means and normal - a statement of the American Association of State Climatologists (AASC). Bulletin of the America Meteorological Society 71 (2), 201-204.

Laba M, Blair B, Downs R, et al. (2010) Use of textural measurements to map invasive wetland plants in the Hudson River National Estuarine Research Reserve with IKONOS satellite imagery. Remote Sensing of Environment 114: 876-886.

Lamb EG. (2008) Direct and indirect control of grassland community structure by litter, resources, and biomass. Ecology 89: 216-225.

Lawes RA and Wallace JF. (2008) Monitoring an invasive perennial at the landscape scale with remote sensing. Ecological Management and Restoration 9: 53-59.

Lawton D, Leahy P, Kiely G, et al. (2006) Modeling of net ecosystem exchange and its components for a humid grassland ecosystem. Journal of Geophysical Research 111: G04013.

Lee JS, Ainsworth TL, Wang Y, et al. (2015) Polarimetric SAR speckle filtering and the extended sigma filter. IEEE Transactions on Geoscience and Remote Sensing 53: 1150-1160.

Lee K-S, Cohen WB, Kennedy RE, et al. (2004) Hyperspectral versus multispectral data for estimating leaf area index in four different biomes. Remote Sensing of Environment 91: 508-520.

Lefsky MA, Cohen WB, Parker GG, et al. (2002) Lidar Remote Sensing for Ecosystem Studies: LiDAR, an emerging remote sensing technology that directly measures the three-dimensional distribution of plant canopies, can accurately estimate vegetation structural attributes and should be of particular interest to forest, landscape, and global ecologists. BioScience 52: 19-30.

Lefsky MA, Hudak AT, Cohen WB, et al. (2005) Geographic variability in lidar predictions of forest stand structure in the Pacific Northwest. Remote Sensing of Environment 95: 532-548.

Lefsky MA. (2010) A global forest canopy height map from the Moderate Resolution Imaging Spectroradiometer and the Geoscience Laser Altimeter System. Geophysical Research Letters 37:L15401.

Lieth H. (1975) Primary production of the major vegetation units of the world. Primary productivity of the biosphere. Springer, 203-215.

Levin N, Shmida A, Levanoni O, et al. (2007) Predicting mountain plant richness and rarity from space using satellite-derived vegetation indices. Diversity and Distributions 13: 692-703.

Lewis M, Jooste V and de Gasparis AA. (2001) Discrimination of arid vegetation with airborne multispectral scanner hyperspectral imagery. IEEE Transactions on Geoscience and Remote Sensing 39: 1471-1479.

Li S, Niu Z, Yan H, et al. (2008) Modeling gross primary production in Jiangxi Province using MODIS images. International Conference on Earth Observation Data Processing and Analysis. International Society for Optics and Photonics, 72854G-72854G-72811.

Li S, Xiao J, Hu Z, et al. (2012) Spatial Scaling Analysis in Gross Primary Production Estimation. Advances in Computational Environment Science. Springer, 259-263.

Li Z and Guo X. (2010) A suitable vegetation index for quantifying temporal variation of leaf area index (LAI) in semiarid mixed grassland. Canadian Journal of Remote Sensing 36: 709-721.

Li Z and Guo X. (2012) Detecting climate effects on vegetation in northern mixed prairie using NOAA AVHRR 1-km time-series NDVI data. Remote Sensing 4: 120-134.

Li Z and Guo X. (2013) Leaf area index estimation in semiarid mixed grassland by considering both temporal and spatial variations. Journal of Applied Remote Sensing 7: 073567-073567.

Li Z and Guo X. (2014) Topographic Effects on Vegetation Biomass in Semiarid Mixed Grassland under Climate Change Using AVHRR NDVI Data. British Journal of Environment and Climate Change 4: 229.

Li Z, Xu D and Guo X. (2014) Remote sensing of ecosystem health: opportunities, challenges, and future perspectives. Sensors 14: 21117-21139.

Li Z and Guo X. (2016) Remote sensing of terrestrial non-photosynthetic vegetation using hyperspectral, multispectral, SAR, and LiDAR data. Progress in Physical Geography 40 (2):276-304.

Li Z and Guo X. (2017) Grassland canopy vertical structure retrieval from multi-angular and multi-temporal fine quad-pod Radarsat-2 images. Proceeding of the Spatial Knowledge and Information – Canada, Feb 23 – Feb 25, 2017, Banff, Canada.

Li J, Lewis J, Rowland J, et al. (2004) Evaluation of land performance in Senegal using multi-temporal NDVI and rainfall series. Journal of Arid Environments 59: 463-480.

Li S, Niu Z, Yan H, et al. (2008) Modeling gross primary production in Jiangxi Province using MODIS images. International Conference on Earth Observation Data Processing and Analysis. International Society for Optics and Photonics, 72854G-72854G-72811.

Li S, Xiao J, Hu Z, et al. (2012) Spatial scaling analysis in gross primary production estimation. Advances in Computational Environment Science. Springer, 259-263.

Li X, Zheng G, Wang J, et al. (2016) Comparison of Methods for Estimating Fractional Cover of Photosynthetic and Non-Photosynthetic Vegetation in the Otindag Sandy Land Using GF-1 Wide-Field View Data. Remote Sensing 8: 800.

Lim K, Treitz P, Wulder M, et al. (2003) LiDAR remote sensing of forest structure. Progress in Physical Geography 27: 88-106.

Liu C, Shang JL, Vachon PW, et al. (2013) Multiyear Crop Monitoring Using Polarimetric RADARSAT-2 Data. IEEE Transactions on Geoscience and Remote Sensing 51: 2227-2240.

Lotsch A, Friedl MA, Anderson BT, et al. (2003) Coupled vegetation-precipitation variability observed from satellite and climate records. Geophysical Research Letters 30:125-132.

Ludwig JA, Bastin GN, Chewings VH, et al. (2007) Leakiness: a new index for monitoring the health of arid and semiarid landscapes using remotely sensed vegetation cover and elevation data. Ecological Indicators 7: 442-454.

Luoto M, Toivonen T and Heikkinen RK. (2002) Prediction of total and rare plant species richness in agricultural landscapes from satellite images and topographic data. Landscape Ecology 17: 195-217.

MacDonald RL, Burke JM, Chen HY, et al. (2012) Relationship between aboveground biomass and percent cover of ground vegetation in Canadian Boreal Plain riparian forests. Forest Science 58: 47-53.

Mackey RL and Currie DJ. (2001) The diversity-disturbance relationship: is it generally strong and peaked? Ecology 82: 3479-3492.

Magagi R and Kerr Y. (1997) Retrieval of soil moisture and vegetation characteristics by use of ERS-1 wind scatterometer over arid and semi-arid areas. Journal of Hydrology 188: 361-384.

Marsett RC, Qi J, Heilman P, et al. (2006) Remote sensing for grassland management in the arid southwest. Rangeland Ecology and Management 59: 530-540.

Martin M, Plourde L, Ollinger S, et al. (2008) A generalizable method for remote sensing of canopy nitrogen across a wide range of forest ecosystems. Remote Sensing of Environment 112: 3511-3519.

McCombs JW, Roberts SD and Evans DL. (2003) Influence of fusing LiDAR and multispectral imagery on remotely sensed estimates of stand density and mean tree height in a managed loblolly pine plantation. Forest Science 49: 457-466.

McNairn H and Protz R. (1993) Mapping corn residue cover on agricultural fields in Oxford County, Ontario, using Thematic Mapper. Canadian Journal of Remote Sensing 19: 152-159.

McNairn H, Boisvert J, Major D, et al. (1996) Identification of agricultural tillage practices from C-Band radar backscatter. Canadian Journal of Remote Sensing 22: 154-162.

McNairn H, Shang J, Champagne C, et al. (2009) TerraSAR-X and RADARSAT-2 for crop classification and acreage estimation. Geoscience and Remote Sensing Symposium, 2009 IEEE International, IGARSS 2009. IEEE, II-898-II-901.

McNairn H, Duguay C, Boisvert J, et al. (2001) Defining the sensitivity of multi-frequency and multi-polarized radar backscatter to post-harvest crop residue. Canadian Journal of Remote Sensing 27: 247-263.

McNairn H, Duguay C, Brisco B, et al. (2002) The effect of soil and crop residue characteristics on polarimetric radar response. Remote Sensing of Environment 80: 308-320.

McNairn H and Brisco B. (2004) The application of C-band polarimetric SAR for agriculture: a review. Canadian Journal of Remote Sensing 30: 525-542.

McPhaden MJ. (1999) Genesis and evolution of the 1997-98 El Niño. Science 283: 950-954.

Merzlyak MN, Gitelson AA, Chivkunova OB, et al. (1999) Non-destructive optical detection of pigment changes during leaf senescence and fruit ripening. Physiologia Plantarum 106: 135-141.

Millennium Ecosystem Assessment (2005a) Ecosystems and Human Well-Being:Synthesis (Island Press, Washington, DC).

Millennium Ecosystem Assessment (2005b) Ecosystems and Human Well-Being: Current State and Trends (Island Press, Washington, DC).

Millennium Ecosystem Assessment (2005c) Ecosystems and Human Well-Being: Scenarios (Island Press, Washington, DC).

Millennium Ecosystem Assessment (2005d) Ecosystems and Human Well-Being: Policy responses (Island Press, Washington, DC).

Millennium Ecosystem Assessment (2005e) Ecosystems and Human Well-Being: Multiscale Assessments (Island Press, Washington, DC).

Meyer T and Okin GS. (2015). Evaluation of spectral unmixing techniques using MODIS in a structurally complex savanna environment for retrieval of green vegetation, non-photosynthetic vegetation, and soil fractional cover. Remote Sensing of Environment 161: 122-130.

Mitchell JJ, Glenn NF, Sankey TT, et al. (2012) Remote sensing of sagebrush canopy nitrogen. Remote Sensing of Environment 124: 217-223.

Mitchell SW and Csillag F. (2001) Assessing the stability and uncertainty of predicted vegetation growth under climatic variability: northern mixed grass prairie. Ecological Modelling 139: 101-121.

Mohamed AH, Holechek JL, Bailey DW, et al. (2011) Mesquite encroachment impact on southern New Mexico rangelands: remote sensing and geographic information systems approach. Journal of Applied Remote Sensing 5:053514.

Montandon L and Small E. (2008) The impact of soil reflectance on the quantification of the green vegetation fraction from NDVI. Remote Sensing of Environment 112: 1835-1845.

Monteith J. (1972) Solar radiation and productivity in tropical ecosystems. Journal of Applied Ecology 9: 747-766.

Moran MS, Alonso L, Moreno JF, et al. (2012) A RADARSAT-2 quad-polarized time series for monitoring crop and soil conditions in Barrax, Spain. IEEE Transactions on Geoscience and Remote Sensing 50: 1057-1070.

Motohka T, Nasahara KN, Oguma H, et al. (2010) Applicability of green-red vegetation index for remote sensing of vegetation phenology. Remote Sensing 2: 2369-2387.

Mücke W, Deák B, Schroiff A, et al. (2013) Detection of fallen trees in forested areas using small footprint airborne laser scanning data. Canadian Journal of Remote Sensing 39: S32-S40.

Mullerova J, Pergl J and Pysek P. (2013) Remote sensing as a tool for monitoring plant invasions: Testing the effects of data resolution and image classification approach on the detection of a model plant species Heracleum mantegazzianum (giant hogweed). International Journal of Applied Earth Observation and Geoinformation 25: 55-65.

Munden R, Curran P and Catt J. (1994) The relationship between red edge and chlorophyll concentration in the Broadbalk winter wheat experiment at Rothamsted. Remote Sensing 15: 705-709.

Mutlu M, Popescu SC, Stripling C, et al. (2008a) Mapping surface fuel models using lidar and multispectral data fusion for fire behavior. Remote Sensing of Environment 112: 274-285.

Mutlu M, Popescu SC and Zhao K. (2008b) Sensitivity analysis of fire behavior modeling with LIDAR-derived surface fuel maps. Forest Ecology and Management 256: 289-294.

Myneni RB, Hall FG, Sellers PJ, et al. (1995) The interpretation of spectral vegetation indexes. IEEE Transactions on Geoscience and Remote Sensing 33: 481-486.

Nagendra H. (2001) Using remote sensing to assess biodiversity. International Journal of Remote Sensing 22: 2377–2400.

Nagler PL, Daughtry CST and Goward SN. (2000) Plant Litter and Soil Reflectance. Remote Sensing of Environment 71: 207-215.

Nagler PL, Inoue Y, Glenn EP, et al. (2003) Cellulose absorption index (CAI) to quantify mixed soil-plant litter scenes. Remote Sensing of Environment 87: 310-325.

Naito AT and Cairns DM. (2011) Patterns and processes of global shrub expansion. Progress in Physical Geography 35: 423-442.

Nayak RK, Patel NR and Dadhwal VK. (2010) Estimation and analysis of terrestrial net primary productivity over India by remote-sensing-driven terrestrial biosphere model. Environmental Monitoring and Assessment 170: 195-213.

Negrón-Juárez RI, Chambers JQ, Guimaraes G, et al. (2010) Widespread Amazon forest tree mortality from a single cross-basin squall line event. Geophysical Research Letters 37: L16701.

Nelson E, Mendoza G, Regetz J, et al. (2009) Modeling multiple ecosystem services, biodiversity conservation, commodity production, and tradeoffs at landscape scales. Frontiers in Ecology and the Environment 7: 4-11.

Nemani RR, Keeling CD, Hashimoto H, et al. (2003) Climate-driven increases in global terrestrial net primary production from 1982 to 1999. Science 300: 1560-1563.

Newnham GJ, Verbesselt J, Grant IF, et al. (2011) Relative Greenness Index for assessing curing of grassland fuel. Remote Sensing of Environment 115: 1456-1463.

Newton AC, Hill RA, Echeverría C, et al. (2009) Remote sensing and the future of landscape ecology. Progress in Physical Geography 33: 528-546.

Nicholson S and Farrar T. (1994) The influence of soil type on the relationships between NDVI, rainfall, and soil moisture in semiarid Botswana. I. NDVI response to rainfall. Remote Sensing of Environment 50: 107-120.

Nordkvist K, Granholm AH, Holmgren J, et al. (2012) Combining optical satellite data and airborne laser scanner data for vegetation classification. Remote Sensing Letters 3: 393-401.

Numata I, Roberts DA, Chadwick OA, et al. (2007) Characterization of pasture biophysical properties and the impact of grazing intensity using remotely sensed data. Remote Sensing of Environment 109: 314-327.

Numata I, Roberts DA, Chadwick OA, et al. (2008) Evaluation of hyperspectral data for pasture estimate in the Brazilian Amazon using field and imaging spectrometers. Remote Sensing of Environment 112: 1569-1583.

Olofsson P, Lagergren F, Lindroth A, et al. (2008) Towards operational remote sensing of forest carbon balance across Northern Europe. Biogeosciences 5: 817-832.

O'Neill A. (1994) Reflectance spectra of microphytic soil crusts in semi-arid Australia. Remote Sensing 15: 675-681.

Pacheco A and McNairn H. (2010) Evaluating multispectral remote sensing and spectral unmixing analysis for crop residue mapping. Remote Sensing of Environment 114: 2219-2228.

Pacheco AM, McNairn H and Merzouki A. (2010) Evaluating TerraSAR-X for the identification of tillage occurrence over an agricultural area in Canada. In Remote Sensing (pp.78240P-78247P). International Society for Optics and Photonics.

Palmer MW, Earls PG, Hoagland BW, et al. (2002) Quantitative tools for perfecting species lists. Environmetrics 13: 121-137.

Patil GP, Brooks RP, Myers WL, et al. (2001) Ecosystem health and its measurement at landscape scale: Toward the next generation of quantitative assessments. Ecosystem Health 7: 307–316.

Patrick LB, Fraser LH and Kershner MW. (2008) Large-scale manipulation of plant litter and fertilizer in a managed successional temperate grassland. Plant Ecology 197: 183-195.

Paudel KP and Andersen P. (2010) Assessing rangeland degradation using multi temporal satellite images and grazing pressure surface model in Upper Mustang, Trans Himalaya, Nepal. Remote Sensing of Environment 114: 1845-1855.

Pennock D, Bedard-Haughn A and Viaud V. (2011) Chernozemic soils of Canada: Genesis, distribution, and classification. Canadian Journal of Soil Science 91: 719-747.

Peñuelas J, Pinol J, Ogaya R, et al. (1997) Estimation of plant water concentration by the reflectance water index WI (R900/R970). International Journal of Remote Sensing 18: 2869-2875.

Pereira LO, Freitas CC, Sant´ Anna SJS, et al. (2013) Optical and radar data integration for land use and land cover mapping in the Brazilian Amazon. GIScience & Remote Sensing: 1-21.

Pesonen A, Kangas A, Maltamo M, et al. (2010) Effects of auxiliary data source and inventory unit size on the efficiency of sample-based coarse woody debris inventory. Forest Ecology and Management 259: 1890-1899.

Pesonen A, Leino O, Maltamo M, et al. (2009) Comparison of field sampling methods for assessing coarse woody debris and use of airborne laser scanning as auxiliary information. Forest Ecology and Management 257: 1532-1541.

Pesonen A, Maltamo M, Eerikäinen K, et al. (2008) Airborne laser scanning-based prediction of coarse woody debris volumes in a conservation area. Forest Ecology and Management 255: 3288-3296.

Peters J, Van Coillie F, Westra T, et al. (2011) Synergy of very high resolution optical and radar data for object-based olive grove mapping. International Journal of Geographical Information Science 25: 971-989.

Piwowar JM. (2011) An environmental normal of vegetation vigor for the Northern Great Plains. IEEE Journal of Selected Topics in Applied Earth Observations and Remote Sensing 4: 292-302.

Polasky S, Nelson E, Camm J, et al. (2008) Where to put things? Spatial land management to sustain biodiversity and economic returns. Biological Conservation 141: 1505-1524.

Polewski P, Yao W, Heurich M, et al. (2015) Active learning approach to detecting standing dead trees from ALS point clouds combined with aerial infrared imagery. In Proceedings of the IEEE Conference on Computer Vision and Pattern Recognition Workshops (pp. 10-18).

Popescu SC and Wynne RH. (2004) Seeing the trees in the forest: using lidar and multispectral data fusion with local filtering and variable window size for estimating tree height. Photogrammetric Engineering and Remote Sensing 70: 589-604.

Pravalie R, Sîrodoev I and Peptenatu D. (2014) Detecting climate change effects on forest ecosystems in Southwestern Romania using Landsat TM NDVI data. Journal of Geographical Sciences 24: 815-832.

Prince S. (1991) Satellite remote sensing of primary production: comparison of results for Sahelian grasslands 1981-1988. International Journal of Remote Sensing 12: 1301–1311.

Qi J, Chehbouni A, Huete A, et al. (1994) A modified soil adjusted vegetation index. Remote Sensing of Environment 48: 119-126.

Qi J, Marsett R, Heilman P, et al. (2002) RANGES improves satellite-based information and land cover assessments in southwest United States. Eos, Transactions American Geophysical Union 83: 601-606.

Rahman AF, Gamon JA, Sims DA, et al. (2003) Optimum pixel size for hyperspectral studies of ecosystem function in southern California chaparral and grassland. Remote Sensing of Environment 84: 192-207.

Ramoelo A, Skidmore AK, Schlerf M, et al. (2011) Water-removed spectra increase the retrieval accuracy when estimating savanna grass nitrogen and phosphorus concentrations. ISPRS Journal of Photogrammetry and Remote Sensing 66: 408-417.

Randerson J, Field C, Fung I, et al. (1999) Increases in early season ecosystem uptake explain recent changes in the seasonal cycle of atmospheric CO_2 at high northern latitudes. Geophysical Research Letters 26(17):2765-2768.

Rapport D, Epstein P, Levins R, et al. (1998) Ecosystem Health: Blackwell Science. Malden and Oxford.

Rapport D, Böhm G, Buckingham D, et al. (1999) Ecosystem health: the concept, the ISEH, and the important tasks ahead. Ecosystem health 5: 82-90.

Rapport DJ, Gaudet CL, Constanza R, et al. (2009) Ecosystem health: principles and practice: John Wiley & Sons.

Rasran L, Vogt K and Jensen K. (2007) Effects of litter removal and mowing on germination and establishment of two fen-grassland species along a productivity gradient. Folia Geobotanica 42: 271-288.

Ren H and Zhou G. (2012) Estimating senesced biomass of desert steppe in Inner Mongolia using field spectrometric data. Agricultural and Forest Meteorology 161: 66-71.

Roberts DA, Dennison PE, Gardner ME, et al. (2003) Evaluation of the potential of Hyperion for fire danger assessment by comparison to the Airborne Visible/Infrared Imaging Spectrometer. IEEE Transactions on Geoscience and Remote Sensing 41: 1297-1310.

Roberts DA, Smith MO and Adams JB. (1993) Green vegetation, nonphotosynthetic vegetation, and soils in AVIRIS data. Remote Sensing of Environment 44: 255-269.

Rocchini D, Ricotta C and Chiarucci A. (2007) Using satellite imagery to assess plant species richness: the role of multispectral systems. Applied Vegetation Science 10: 325-331.

Rocchini D. (2007) Effects of spatial and spectral resolution in estimating ecosystem α-diversity by satellite imagery. Remote Sensing of Environment 111: 423-434.

Running SW, Nemani RR, Heinsch FA, et al. (2004) A continuous satellite-derived measure of global terrestrial primary production. Bioscience 54: 547-560.

Ruprecht E, Jozsa J, Olvedi TB, et al. (2010) Differential effects of several "litter" types on the germination of dry grassland species. Journal of Vegetation Science 21: 1069-1081.

Ruprecht E and Szabo A. (2012) Grass litter is a natural seed trap in long-term undisturbed grassland. Journal of Vegetation Science 23: 495-504.

Saatchi SS, van Zyl JJ and Asrar G. (1995) Estimation of canopy water content in Konza Prairie grasslands using synthetic aperture radar measurements during FIFE. Journal of Geophysical Research 100: 25481-25496.

Sartori LR, Imai NN, Mura JC, et al. (2011) Mapping macrophyte species in the Amazon floodplain wetlands using fully polarimetric ALOS/PALSAR data. IEEE Transactions on Geoscience and Remote Sensing 49: 4717-4728.

Saura S. (2004) Effects of remote sensor spatial resolution and data aggregation on selected fragmentation indices. Landscape Ecology 19: 197-209.

Schile LM, Byrd KB, Windham-Myers L, et al. (2013) Accounting for non-photosynthetic vegetation in remote-sensing-based estimates of carbon flux in wetlands. Remote Sensing Letters 4: 542-551.

Serbin G, Daughtry CST, Hunt ER, et al. (2009a) Effects of soil composition and mineralogy on remote sensing of crop residue cover. Remote Sensing of Environment 113: 224-238.

Serbin G, Daughtry CS, Hunt ER, et al. (2009b) Effect of soil spectral properties on remote sensing of crop residue cover. Soil Science Society of America Journal 73: 1545-1558.

Serbin G, Hunt ER, Daughtry CST, et al. (2009c) An Improved ASTER Index for Remote Sensing of Crop Residue. Remote Sensing 1: 971-991.

Serbin G, Hunt ER, Daughtry CST, et al. (2013) Assessment of spectral indices for cover estimation of senescent vegetation. Remote Sensing Letters 4: 552-560.

Serrano L, Penuelas J and Ustin SL. (2002) Remote sensing of nitrogen and lignin in Mediterranean vegetation from AVIRIS data: Decomposing biochemical from structural signals. Remote Sensing of Environment 81: 355-364.

Sheldon S, Xiao X and Biradar C. (2012) Mapping evergreen forests in the Brazilian Amazon using MODIS and PALSAR 500-m mosaic imagery. ISPRS Journal of Photogrammetry and Remote Sensing 74: 34-40.

Shen L, He Y, and Guo X. (2013a) Suitability of the normalized difference vegetation index and the adjusted transformed soil-adjusted vegetation index for spatially characterizing Loggerhead Shrike habitats in North American mixed prairie. Journal of Applied Remote Sensing 7 (1): 073574.

Shen L, He Y, and Guo X. (2013b) Exploration of Loggerhead Shrike habitats in Grassland National Park of Canada based on in situ measurements and satellite-derived adjusted transformed soil adjusted vegetation index (ATSAVI). Remote Sensing 5: 432-453.

Sims DA and Gamon JA. (2002) Relationships between leaf pigment content and spectral reflectance across a wide range of species, leaf structures and developmental stages. Remote Sensing of Environment 81: 337-354.

Smith AM and Buckley JR. (2011) Investigating RADARSAT-2 as a tool for monitoring grassland in western Canada. Canadian Journal of Remote Sensing 37: 93-102.

Smith AM, Hill MJ and Zhang Y. (2015) Estimating ground cover in the mixed prairie grassland of southern Alberta using vegetation indices related to physiological function. Canadian Journal of Remote Sensing 41: 51-66.

Somers B, Asner GP, Tits L, et al. (2011) Endmember variability in spectral mixture analysis: A review. Remote Sensing of Environment 115: 1603-1616.

Song C. (2013) Optical remote sensing of forest leaf area index and biomass. Progress in Physical Geography 37: 98-113.

Solomon S, Qin D, Manning M, et al. (2007) Climate Change 2007: The Physical Science Basis-Contribution of Working Group I to the Fourth Assessment Report of the Intergovernmental Panel on Climate Change. Cambridge University Press: Cambridge, UK.

Stoner ER and Baumgardner M. (1981) Characteristic variations in reflectance of surface soils. Soil Science Society of America Journal 45: 1161-1165.

Svoray T and Shoshany M. (2003) Herbaceous biomass retrieval in habitats of complex composition: a model merging SAR images with unmixed landsat TM data. IEEE Transactions on Geoscience and Remote Sensing 41: 1592-1601.

Swatantran A, Dubayah R, Roberts D, et al. (2011) Mapping biomass and stress in the Sierra Nevada using LiDAR and hyperspectral data fusion. Remote Sensing of Environment 115: 2917-2930.

Thiam A. (2003) The causes and spatial pattern of land degradation risk in southern Mauritania using multitemporal AVHRR-NDVI imagery and field data. Land Degradation and Development 14: 133-142.

Tian YC, Yao X, Yang J, et al. (2011) Assessing newly developed and published vegetation indices for estimating rice leaf nitrogen concentration with ground- and space-based hyperspectral reflectance. Field Crops Research 120: 299-310.

Tilman D and Downing JA. (1996) Biodiversity and stability in grasslands. Ecosystem Management. Springer, 3-7.

Tolba MK and El-Kholy OA. (1992) The world environment 1972-1992: two decades of challenge: Chapman & Hall.

Tonolli S, Dalponte M, Neteler M, et al. (2011) Fusion of airborne LiDAR and satellite multispectral data for the estimation of timber volume in the Southern Alps. Remote Sensing of Environment 115: 2486-2498.

Trombetti M, Riaño D, Rubio M, et al. (2008) Multi-temporal vegetation canopy water content retrieval and interpretation using artificial neural networks for the continental USA. Remote Sensing of Environment 112: 203-215.

Tsoar H and Karnieli A. (1996) What determines the spectral reflectance of the Negev-Sinai sand dunes. International Journal of Remote Sensing 17: 513-525.

Tucker CJ. (1979) Red and photographic infrared linear combinations for monitoring vegetation. Remote Sensing of Environment 8: 127-150.

Tucker C and Sellers P. (1986) Satellite remote sensing of primary production. International Journal of Remote Sensing 7: 1395-1416.

Tucker CJ, Slayback DA, Pinzon JE, et al. (2001) Higher northern latitude normalized difference vegetation index and growing season trends from 1982 to 1999. International Jjournal of Biometeorology 45: 184-190.

Turner DP, Cohen WB, Kennedy RE, et al. (1999) Relationships between leaf area index and Landsat TM spectral vegetation indices across three temperate zone sites. Remote Sensing of Environment 70: 52-68.

Turner DP, Ritts WD, Cohen WB, et al. (2006) Evaluation of MODIS NPP and GPP products across multiple biomes. Remote Sensing of Environment 102: 282-292.

Turner W, Spector S, Gardiner N, et al. (2003) Remote sensing for biodiversity science and conservation. Trends in Ecology and Evolution 18: 306-314.

Ulaby FT, Kouyate F, Brisco B, et al. (1986) Textural information in SAR images. IEEE Transactions on Geoscience and Remote Sensing: 235-245.

Ustin SL, Valko PG, Kefauver SC, et al. (2009) Remote sensing of biological soil crust under simulated climate change manipulations in the Mojave Desert. Remote Sensing of Environment 113: 317-328.

Van Deventer A, Ward A, Gowda P, et al. (1997) Using Thematic Mapper data to identify contrasting soil plains and tillage practices. Photogrammetric Engineering and Remote Sensing 63: 87-93.

Van Leeuwen W and Huete A. (1996) Effects of standing litter on the biophysical interpretation of plant canopies with spectral indices. Remote Sensing of Environment 55: 123-138.

Van Leeuwen WJ. (2008) Monitoring the effects of forest restoration treatments on post-fire vegetation recovery with MODIS multitemporal data. Sensors 8: 2017-2042.

Van Leeuwen M and Nieuwenhuis M. (2010) Retrieval of forest structural parameters using LiDAR remote sensing. European Journal of Forest Research 129: 749-770.

Van Leeuwen WJ, Casady GM, Neary DG, et al. (2010) Monitoring post-wildfire vegetation response with remotely sensed time-series data in Spain, USA and Israel. International Journal of Wildland Fire 19: 75-93.

Vannier C, Vasseur C, Hubert-Moy L, et al. (2011) Multiscale ecological assessment of remote sensing images. Landscape Ecology 26: 1053-1069.

Varga TA and Asner GP. (2008) Hyperspectral and LiDAR remote sensing of fire fuels in Hawaii Volcanoes National Park. Ecological Applications 18: 613-623.

Vermote E, Saleous NE, Kaufman Y, et al. (1997) Data pre-processing: Stratospheric aerosol perturbing effect on the remote sensing of vegetation: Correction method for the composite NDVI after the Pinatubo eruption. Remote Sensing Reviews 15: 7-21.

Vierling KT, Vierling LA, Gould WA, et al. (2008) Lidar: shedding new light on habitat characterization and modeling. Frontiers in Ecology and the Environment 6: 90-98.

Viña A, Gitelson AA, Nguy-Robertson AL, et al. (2011) Comparison of different vegetation indices for the remote assessment of green leaf area index of crops. Remote Sensing of Environment 115: 3468-3478.

Vogelmann J, Rock B and Moss D. (1993) Red edge spectral measurements from sugar maple leaves. International Journal of Remote Sensing 14: 1563-1575.

Walsh SJ, McCleary AL, Mena CF, et al. (2008) QuickBird and Hyperion data analysis of an invasive plant species in the Galapagos Islands of Ecuador: Implications for control and land use management. Remote Sensing of Environment 112: 1927-1941.

Wang J, Zhao ML, Willms WD, et al. (2011) Can plant litter affect net primary production of a typical steppe in Inner Mongolia? Journal of Vegetation Science 22: 367-376.

Wang RJ and Yang LW. (2012) Using RS technology to estimate net primary production of rangeland ecosystem in HulunBuir of China. Future Materials Engineering and Industry Application 365: 104-109.

Wang S and Davidson A. (2007) Impact of climate variations on surface albedo of a temperate grassland. Agricultural and Forest Meteorology 142: 133-142.

Wang J, Price K and Rich P. (2001) Spatial patterns of NDVI in response to precipitation and temperature in the central Great Plains. International Journal of Remote Sensing 22: 3827-3844.

Wang J, Rich P and Price K. (2003) Temporal responses of NDVI to precipitation and temperature in the central Great Plains, USA. International Journal of Remote Sensing 24: 2345-2364.

Wang RJ and Yang LW. (2012) Using RS technology to estimate net primary production of rangeland ecosystem in hulunbuir of china. Advanced Materials Research 365: 104-109.

Wang S and Davidson A. (2007) Impact of climate variations on surface albedo of a temperate grassland. Agricultural and Forest Meteorology 142: 133-142.

Wang W and Fang J. (2009) Soil respiration and human effects on global grasslands. Global and Planetary Change 67: 20-28.

Weber B, Olehowski C, Knerr T, et al. (2008) A new approach for mapping of Biological Soil Crusts in semidesert areas with hyperspectral imagery. Remote Sensing of Environment 112: 2187-2201.

Weise DR and Wright CS. (2013) Wildland fire emissions, carbon and climate: Characterizing wildland fuels. Forest Ecology and Management 317:26-40.

Weiss JL, Gutzler DS, Coonrod JEA, et al. (2004) Seasonal and inter-annual relationships between vegetation and climate in central New Mexico, USA. Journal of Arid Environments 57: 507-534.

Welch R and Ehlers M. (1987) Merging multiresolution SPOT HRV and Landsat TM data. Photogrammetric Engineering and Remote Sensing 53: 301-303.

West NE. (1990) Structure and function of microphytic soil crusts in wildland ecosystems of arid to semi-arid regions. Advances in Ecological Research 20: 179-223.

White MA, Asner GP, Nemani RR, et al. (2000) Measuring fractional cover and leaf area index in arid ecosystems: digital camera, radiation transmittance, and laser altimetry methods. Remote Sensing of Environment 74: 45-57.

Wicklum D and Davies RW. (1995) Ecosystem health and integrity? Canadian Journal of Botany 73: 997-1000.

Wiseman G, McNairn H, Homayouni S, et al. (2014) RADARSAT-2 Polarimetric SAR response to crop biomass for agricultural production monitoring. IEEE Journal of Selected Topics in Applied Earth Observations and Remote Sensing 7: 4461-4471.

Wong KK and He Y. (2013) Estimating grassland chlorophyll content using remote sensing data at leaf, canopy, and landscape scales. Canadian Journal of Remote Sensing 39: 155-166.

Woodcock CE and Strahler AH. (1987) The factor of scale in remote sensing. Remote Sensing of Environment 21: 311-332.

Wu C, Niu Z, Tang Q, et al. (2008) Estimating chlorophyll content from hyperspectral vegetation indices: Modeling and validation. Agricultural and Forest 148: 1230-1241.

Wu H and Li ZL. (2009) Scale issues in remote sensing: A review on analysis, processing and modeling. Sensors 9: 1768-1793.

Wulder MA, Hall RJ, Coops NC, et al. (2004) High spatial resolution remotely sensed data for ecosystem characterization. Bioscience 54: 511-521.

Wylie BK, Johnson DA, Laca E, et al. (2003) Calibration of remotely sensed, coarse resolution NDVI to CO2 fluxes in a sagebrush–steppe ecosystem. Remote Sensing of Environment 85: 243-255.

Wylie BK, Meyer D, Tieszen L, et al. (2002) Satellite mapping of surface biophysical parameters at the biome scale over the North American grasslands: a case study. Remote Sensing of Environment 79: 266-278.

Xu C, Li Y, Hu J, et al. (2012) Evaluating the difference between the normalized difference vegetation index and net primary productivity as the indicators of vegetation vigor assessment at landscape scale. Environmental Monitoring and Assessment 184: 1275-1286.

Xu D and Guo X. (2013) A study of soil line simulation from Landsat images in mixed grassland. Remote Sensing 5:4533-4550.

Xu D, Guo X, Li Z, et al. (2014) Measuring the dead component of mixed grassland with Landsat imagery. Remote Sensing of Environment 142: 33-43.

Xu D and Guo X. (2015) Evaluating the impacts of nearly 30 years of conservation on grassland ecosystem using Landsat TM images. Grassland Science 61(4): 227-242.

Yang X and Guo X. (2011) Investigating vegetation biophysical and spectral parameters for detecting light to moderate grazing effects: a case study in mixed grass prairie. Central European Journal of Geosciences 3(3): 336-348.

Yang X, Guo X and Fitzsimmons M. (2012) Assessing light to moderate grazing effects on grassland production using satellite imagery. International Journal of Remote Sensing 33: 5087-5104.

Yang X, Kovach E, and Guo X. (2013) Biophysical and spectral responses to various burn treatments in the northern mixed-grass prairie. Canadian Journal of Remote Sensing 739(2):175-184.

Yang X and Guo X. (2014) Quantifying responses of spectral vegetation indices to dead materials in mixed grasslands. Remote Sensing 6: 4289-4304.

Yao W, Krzystek P and Heurich M (2012) Identifying standing dead trees in forest areas based on 3D single tree detection from full waveform lidar data. ISPRS Annals of the Photogrammetry, Remote Sensing and Spatial Information Sciences, Volume 1-7, 2012. XXII ISPRS Congress, 25 August – 01 September 2012, Melbourne, Australia.

Yin CJ and Huang DH. (1996) A model of litter decomposition and accumulation in grassland ecosystems. Ecological Modelling 84: 75-80.

Yue YM, Zhang B, Wang KL, et al. (2010) Spectral indices for estimating ecological indicators of karst rocky desertification. International Journal of Remote Sensing 31: 2115-2122.

Zhang C, Guo X, Wilmshurst JF, et al. (2006) Application of Radarsat imagery on grassland biophysical heterogeneity assessment. Canadian Journal of Remote Sensing 32(4): 281-287.

Zhang C and Guo X. (2008) Monitoring northern mixed prairie health using broadband satellite imagery. International Journal of Remote Sensing 29(8):2257-2271.

Zhang C, Guo X, Wilmshurst JF, et al. (2008) Monitoring temporal heterogeneity in a protected mixed prairie ecosystem using 10-day NDVI composite. Prairie Forum 33(1):145-166.

Zhang X, Vincent LA, Hogg W, et al. (2000) Temperature and precipitation trends in Canada during the 20th century. Atmosphere-ocean 38: 395-429.

Zhang X, Friedl MA, Schaaf CB, et al. (2003) Monitoring vegetation phenology using MODIS. Remote Sensing of Environment 84: 471-475.

Zhang Y, Chen J, Wang L, et al. (2007) The spatial distribution patterns of biological soil crusts in the Gurbantunggut Desert, Northern Xinjiang, China. Journal of Arid Environments 68: 599-610.

Zhao M, Heinsch FA, Nemani RR, et al. (2005) Improvements of the MODIS terrestrial gross and net primary production global dataset. Remote Sensing of Environment 95: 164-176.

Zheng B, Campbell J, Serbin G, et al. (2013) Multitemporal remote sensing of crop residue cover and tillage practices: A validation of the minNDTI strategy in the United States. Journal of Soil and Water Conservation 68: 120-131.

Zheng B, Campbell JB, Serbin G, et al. (2014) Remote sensing of crop residue and tillage practices: Present capabilities and future prospects. Soil and Tillage Research 138: 26-34.

APPENDIX A: Copyright Clearance

Title: Remote sensing of terrestrial non-photosynthetic vegetation using hyperspectral, multispectral, SAR, and LiDAR data

Author: Zhaoqin Li, Xulin Guo

Publication: Progress in Physical Geography

Publisher: SAGE Publications

Date: 04/01/2016

Copyright © 2016, © SAGE Publications

Logged in as: Zhaoqin Li

LOGOUT

Gratis Reuse

- Without further permission, as the Author of the journal article you may:
  - post the accepted version (version 2) on your personal website, department's website or your institution's repository. You may NOT post the published version (version 3) on a website or in a repository without permission from SAGE.
  - post the accepted version (version 2) of the article in any repository other than those listed above 12 months after official publication of the article.
  - use the published version (version 3) for your own teaching needs or to supply on an individual basis to research colleagues, provided that such supply is not for commercial purposes.
  - use the accepted or published version (version 2 or 3) in a book written or edited by you. To republish the article in a book NOT written or edited by you, permissions must be cleared on the previous page under the option 'Republish in a Book/Journal' by the publisher, editor or author who is compiling the new work.
- When posting or re-using the article electronically, please link to the original article and cite the DOI.
- All other re-use of the published article should be referred to SAGE. Contact information can be found on the bottom of our 'Journal Permissions' page.

BACK CLOSE WINDOW

APPENDIX B: Radarsat-2 images

(a) June 2, 2014, FQ1

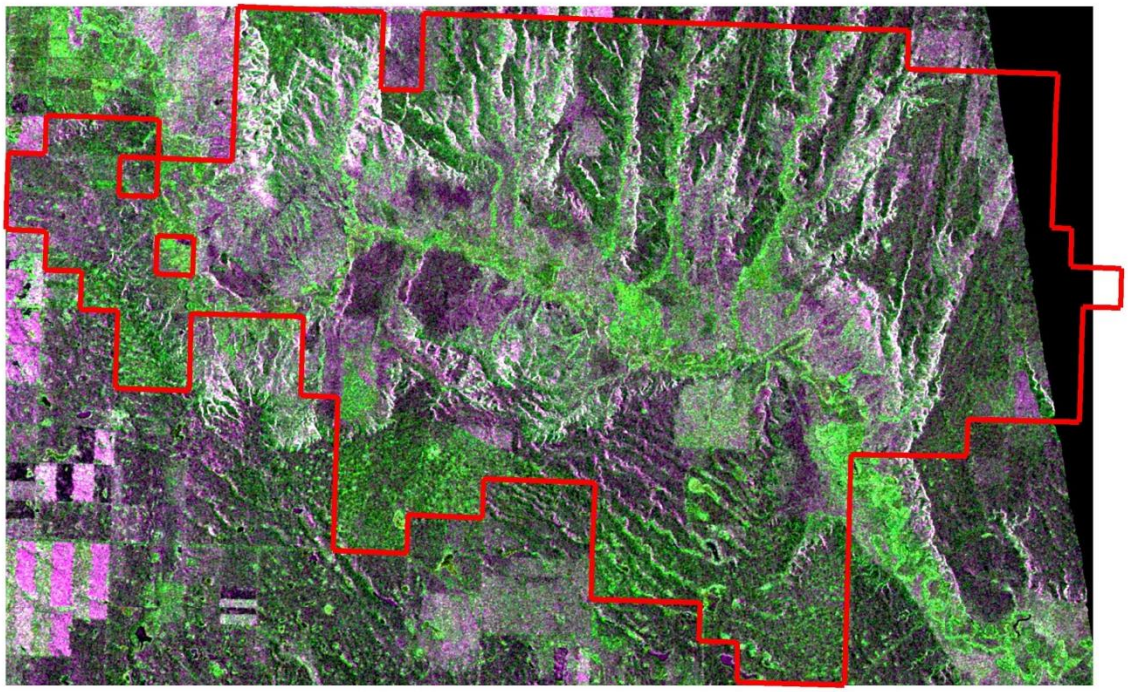

(b) June 8, 2014, FQ27

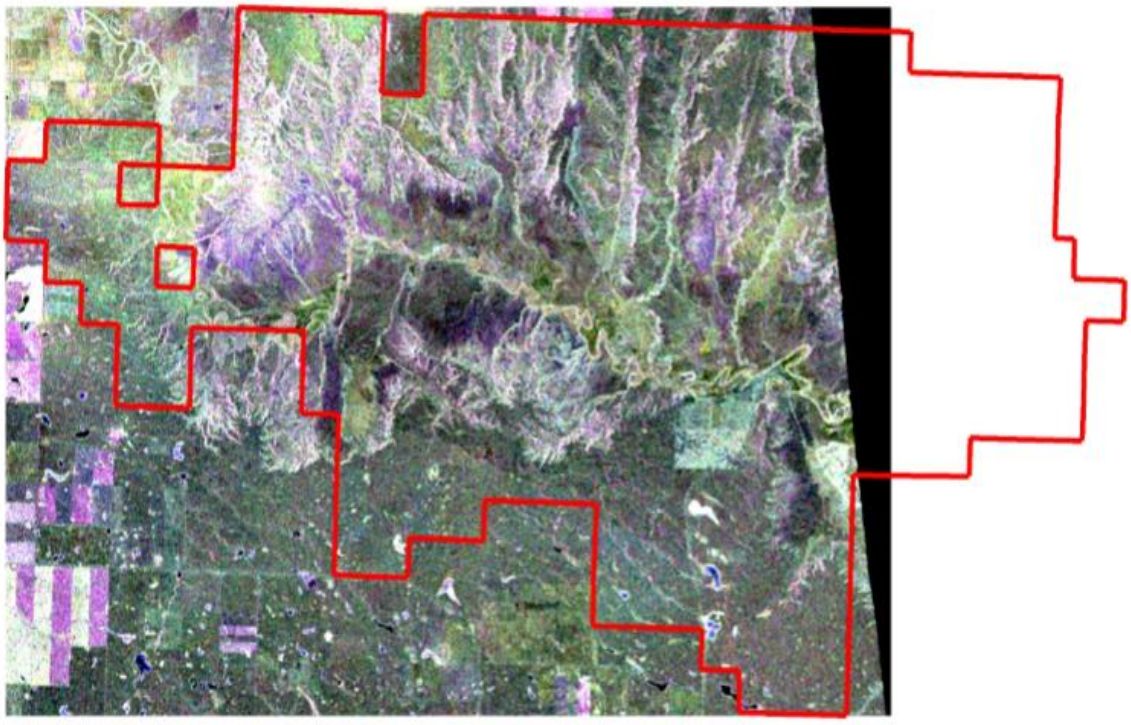

(c) June 12,2014, FQ10

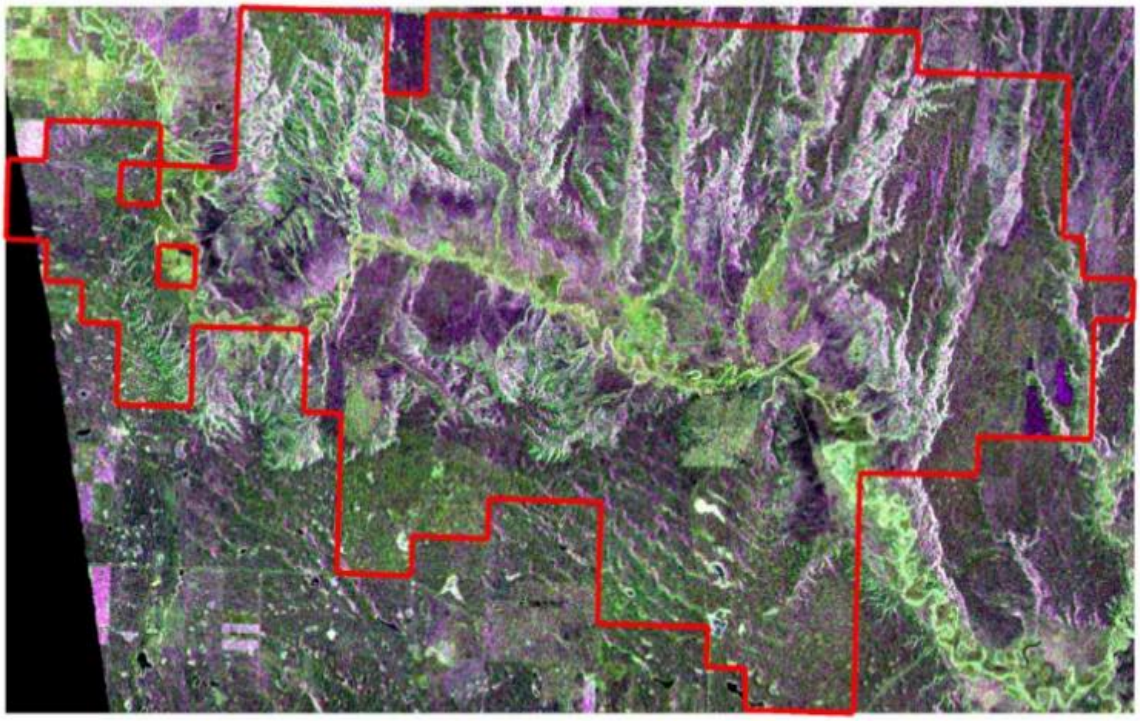

(d) June 15, 2014, FQ23

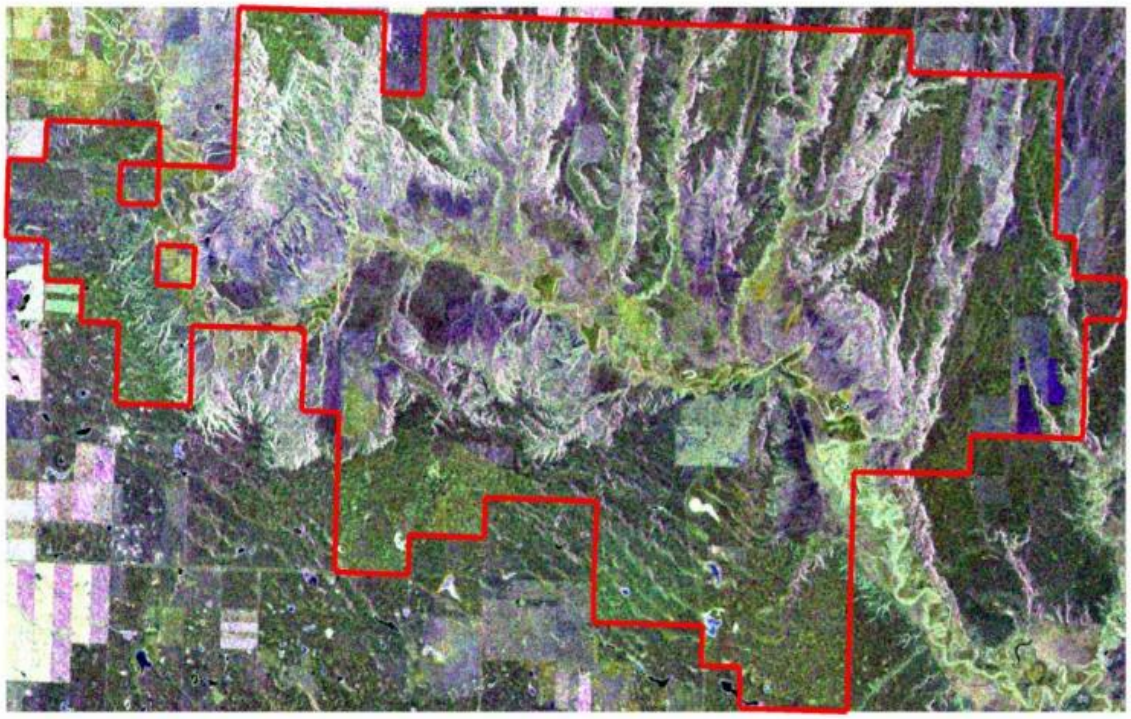

(e) June 18, 2014, FQ12

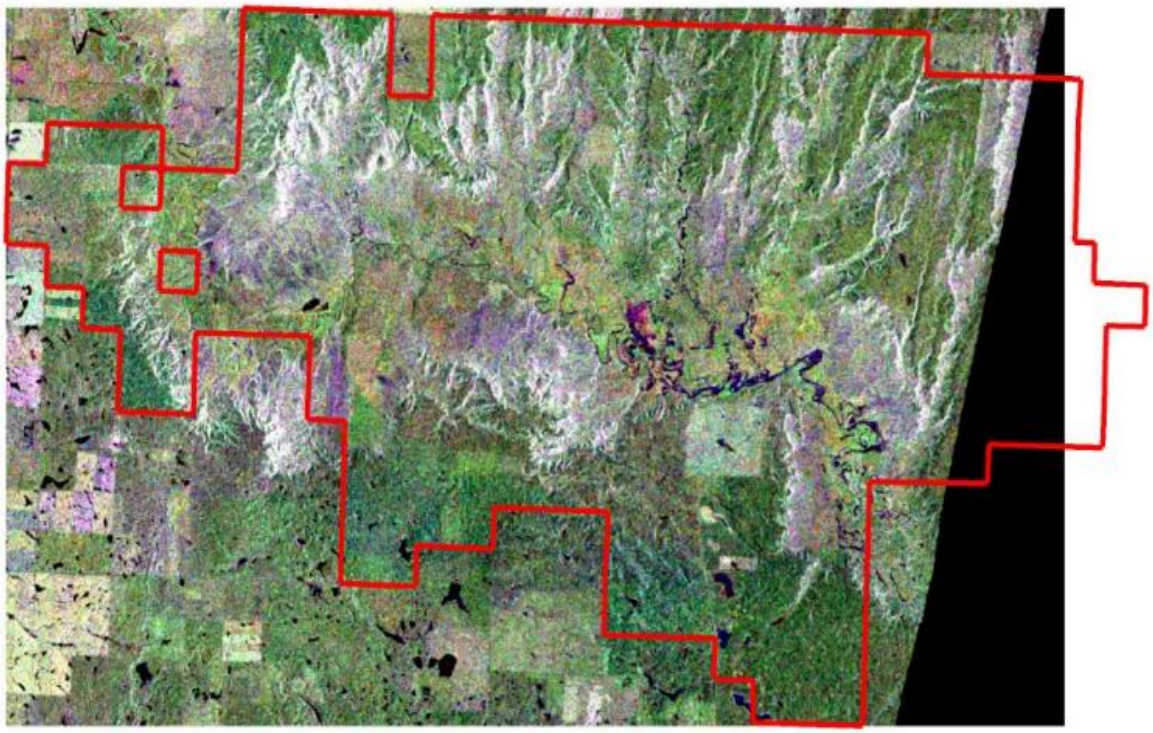

(f) June 19, 2014, FQ5

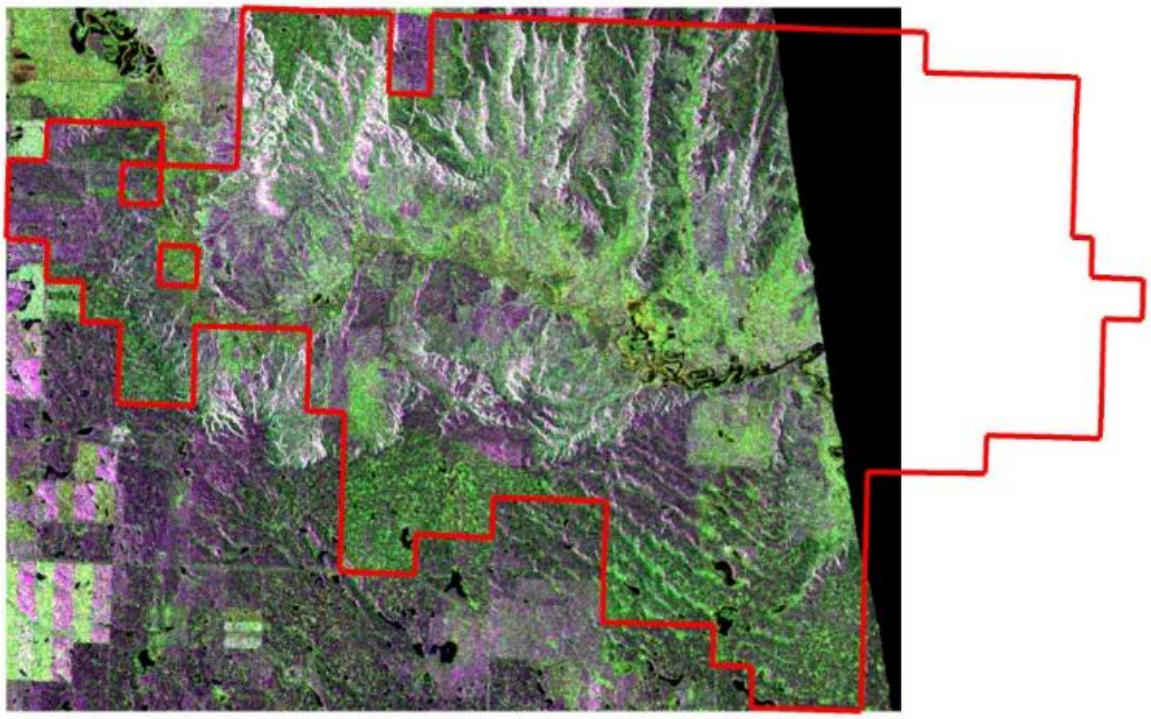

(g) June 28, 2014, FQ3

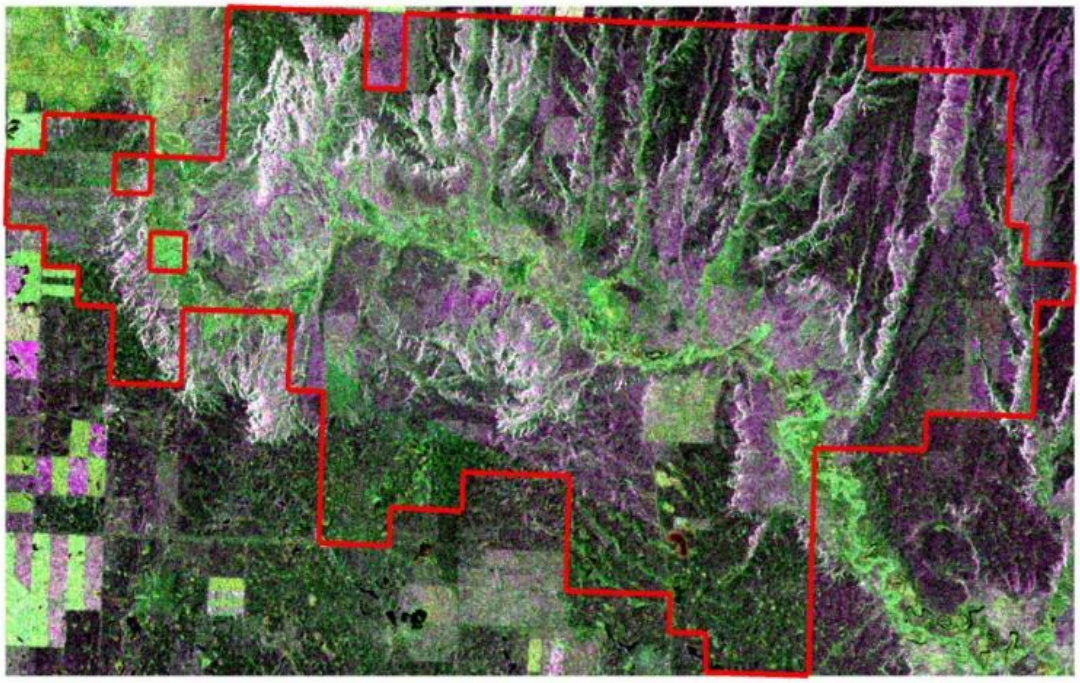

(h) July 2, 2014, FQ27

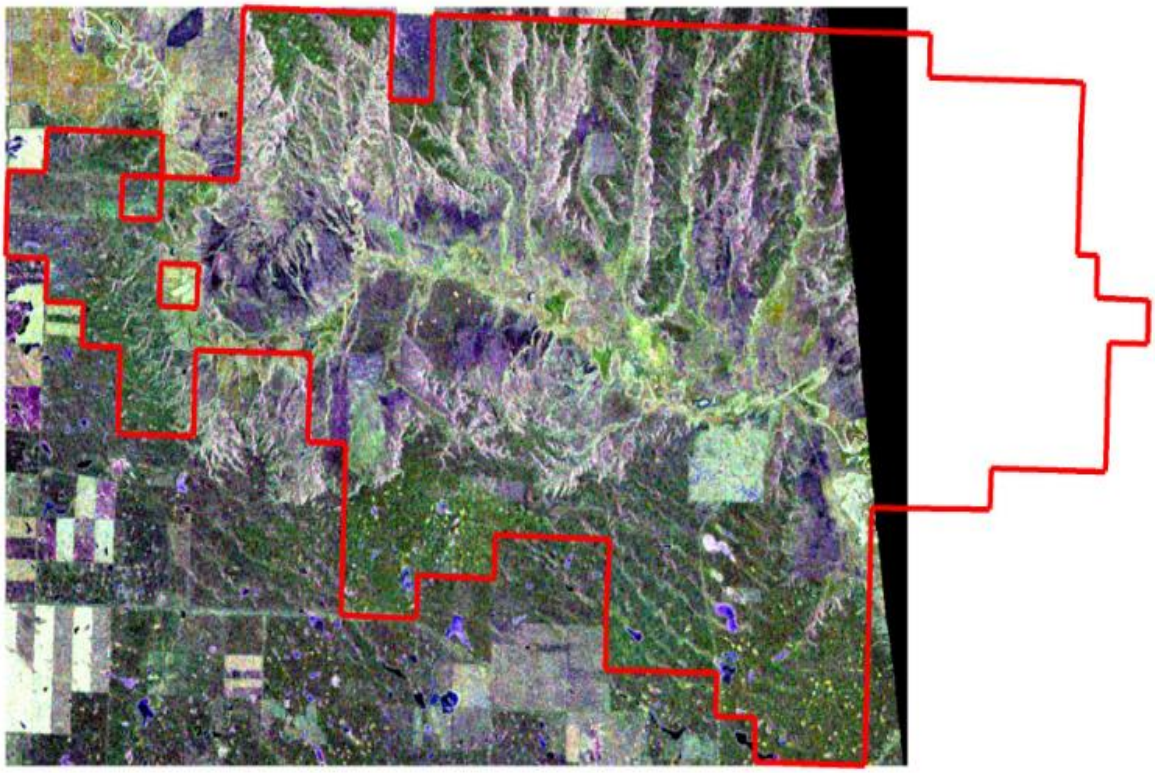

(i) July 5, 2014, FQ5

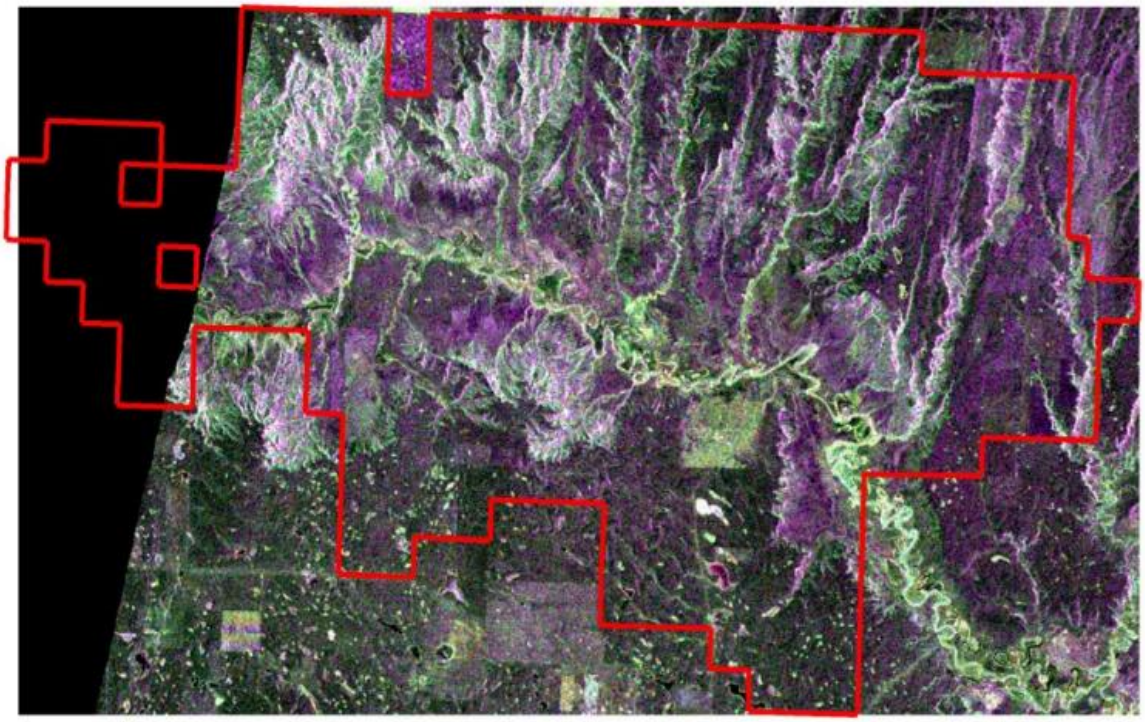

(j) July 6, 2014,FQ10

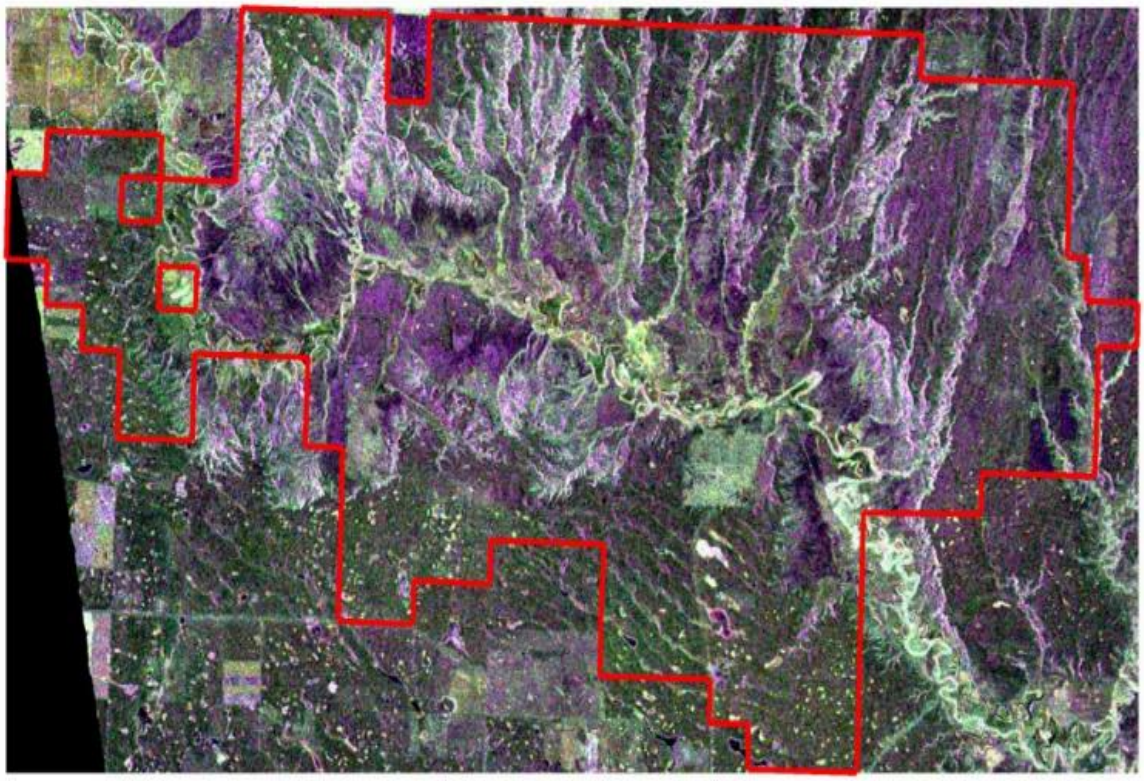

(k) July 9, 2014,FQ23

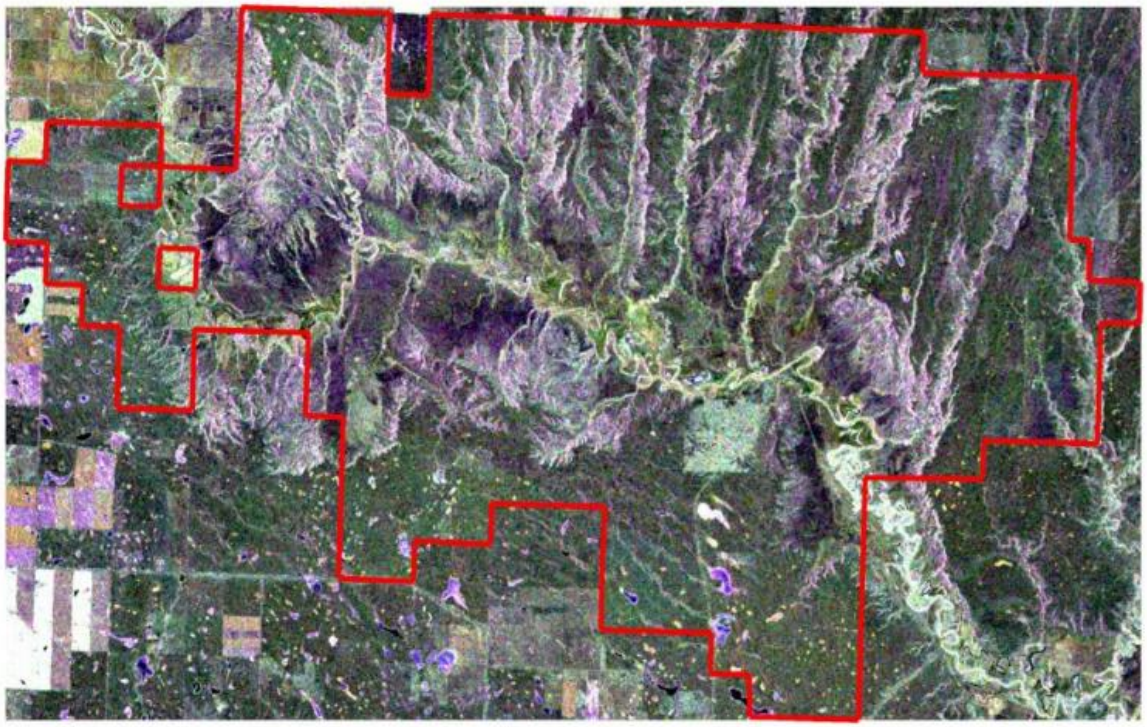

APPENDIX C: Landsat 8 OLI images

(a) June 10, 2016

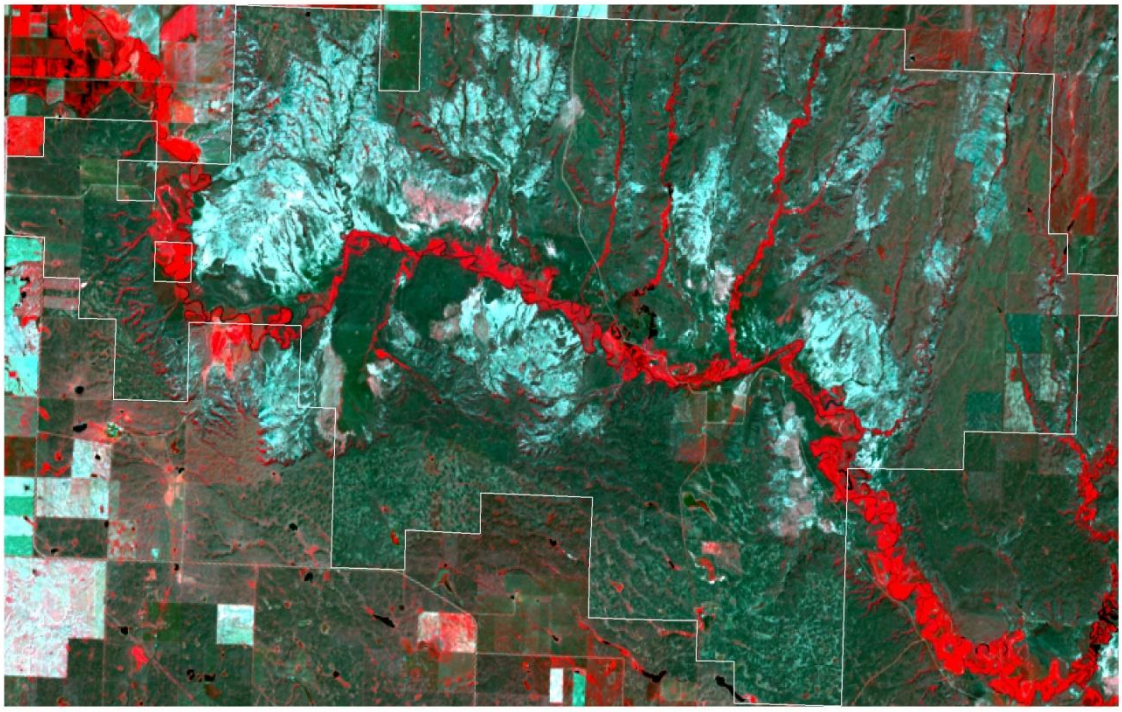

(b) June 17, 2016

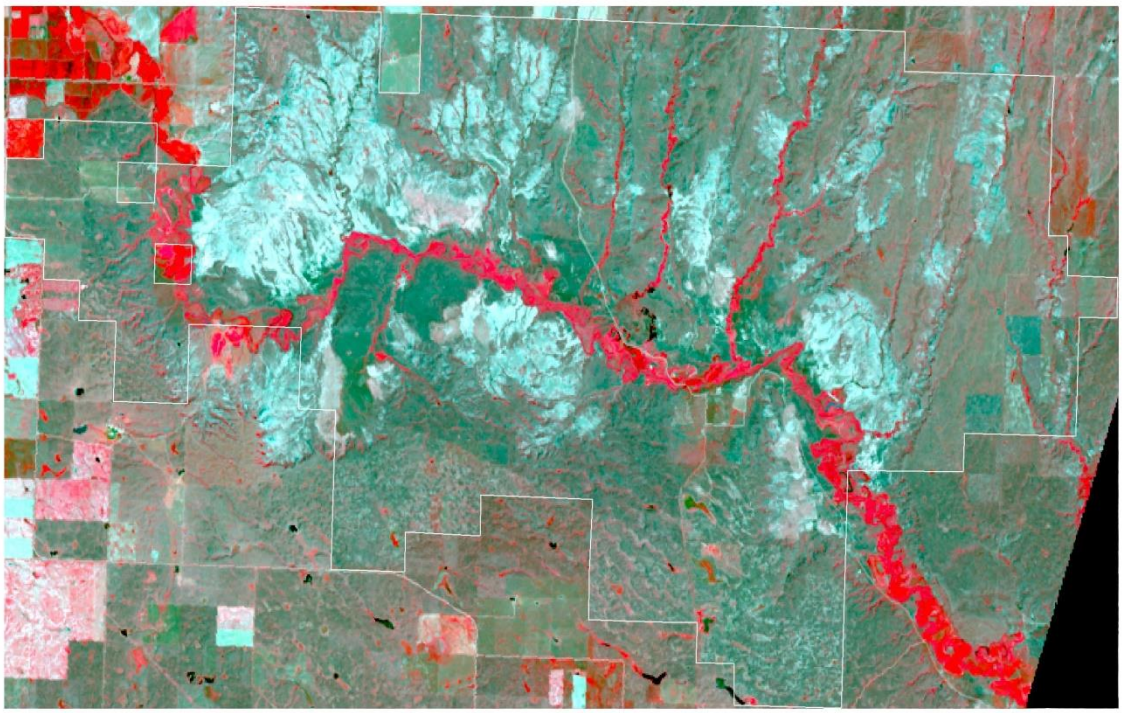

(c) July 3, 2016